IMPROVING ROADWAY DIAGNOSTICS USING NETWORK-LEVEL DATA

A Dissertation

by

CHARLES FELDER GURGANUS

Submitted to the Office of Graduate and Professional Studies of
Texas A&M University
in partial fulfillment of the requirements for the degree of

DOCTOR OF PHILOSOPHY

Chair of Committee,	Nasir G. Gharaibeh
Committee Members,	Jon A. Epps
	Timothy J. Lomax
	Robert L. Lytton
	Kumares C. Sinha
Head of Department,	Robin Autenrieth

August 2018

Major Subject: Civil Engineering

ABSTRACT

Large amounts of empirical data on transportation infrastructure assets continue to be collected at the network-level due to advancements in technology and in response to data-driven processes. These vast amounts of new data, combined with existing data, leave practitioners searching for ways to transform disparate datasets into effective information. This study expands the use of these data into new areas of application, namely roadway and roadside diagnostics. Providing diagnostics informs practitioners not only about the needs of an infrastructure project, but the causes of those needs. Using network-level data to diagnose fundamental causes improves the engineering aspect of early project development decision making. Mobile light detection and ranging (LiDAR) technology was used to create a new dataset by evaluating road and roadside surface geometry and drainage conditions. Temporal patterns in pavement condition data were mined to inform engineers about the health of the pavement. The geometric and drainage information was combined with information gleaned from mining the pavement condition data and publicly available soils data to provide improved diagnostic analysis of roadway projects. The study capitalizes on graph theory to convert network-level data into diagnostic information. The primary contribution of this study lies in developing new analytical methods that use network-level data to provide comprehensive diagnoses of roadway infrastructure projects and systems. Using these diagnostics early in project development has the potential to reduce late project problems that cost both time and money.

DEDICATION

To my wife, Elizabeth. Without you none of this, or anything I have accomplished, would have been possible. Thank you!

ACKNOWLEDGEMENTS

There are several people that have sacrificed and supported me to make this a reality. To my children, Coleman and Kathy, thank you for you encouragement and patience. To Nana (Kelly Bentley), your financial support and constant encouragement made this possible and I am forever grateful for all you have done. The encouragement and support provided by the rest of my family, James Todd, Belle Todd, my dad (Felder Gurganus), and stepmom (Kelley Gurganus) has helped me see this through. And for two family members no longer with me, Charlie Webb and Kathy Gurganus, your impact and endearing marks motivated me to get to this point.

Several individuals from Texas A&M University Civil Engineering and Texas A&M Transportation Institute (TTI) deserve recognition for their support. First, thank you to Dr. Nasir Gharaibeh for advising me and supporting me from the beginning. Without the support and advocacy of Dr. Gharaibeh, Dr. Yunlong Zhang, and Dr. Timothy Lomax, I would not have received the Graduate Merit Fellowship at the beginning of this process that jumpstarted this journey. Dr. Robert Lytton has offered hours of his time toward my success. Dr. Lytton is second to none as a student advocate and much of my success and the success of other students can be attributed to his tireless efforts.

Within TTI, Tom Scullion provided me with an opportunity to pursue research projects as the lead researcher. This support proved essential in both my dissertation work and my financial support. Dr. David Newcomb invited me to work on projects and offered

career, academic, and personal advice that helped see me through this task. Tom Freeman, Emmanuel Fernando, and Andrew Wimsatt have always been encouraging and supportive.

The kind words of a good friend, Bobby Bari, put my mind at ease. Advocacy letters from Kim Droege and Walter Smith helped secure financial support through fellowships. There are many more that have made this a reality. For those that I have forgotten to mention, thank you.

CONTRIBUTORS AND FUNDING SOURCES

This work was supervised by a dissertation committee consisting of Dr. Nasir Gharaibeh (advisor and committee chair), Dr. Robert Lytton, and Dr. Jon Epps in the Department of Civil Engineering, and Dr. Timothy Lomax in the Department of Landscape Architecture and Urban Planning, and Dr. Kumares Sinha of the School of Civil Engineering at Purdue University. Additionally, Dr. Stuart Anderson in the Department of Civil Engineering was kind enough to substitute for Dr. Epps during the preliminary exam. Finally, Dr. William Eisele graciously substituted for Dr. Lomax during the final exam.

The conversion of the student's pseudocode to working MATLAB code for analysis of network-level mobile LiDAR data was completed by Deepika Ravipati, Master of Science student in the Department of Computer Science and Engineering. Deepika's work was relevant to the data activation discussed in Section 5.7 thru Section 5.11. All other work conducted for the dissertation was completed by the student independently.

Graduate study was supported by various funding sources throughout the period of study. Fellowship funding included:

- Association of Former Students Graduate Merit Fellowship which included a one year living stipend and four years of tuition and fee assistance,
- Four consecutive FHWA Eisenhower Fellowships of various funding levels,
- Three consecutive Texas A&M Civil Engineering Joseph Orr Fellowships, and
- A one-time Texas A&M Transportation Institute Keese Wootan Fellowship.

Graduate study was also supported by a Teaching Assistantship during the 2014-2015 academic year. Lastly, TTI has allowed me to pursue research funding opportunities that has led to employment and essential financial contributions.

TABLE OF CONTENTS

Page

Page

Page

LIST OF FIGURES

FIGURE Page

FIGURE Page

LIST OF TABLES

1. INTRODUCTION

1.1 MOTIVATION AND PROBLEM STATEMENT

Vast amounts of empirical data on transportation infrastructure assets continue to be collected due to advancements in technology and in response to data-driven processes (e.g., asset management and performance management). These data continue to expand into multiple roadway and roadside asset classes, beyond the major classes of pavements and bridges (Woldesenbet et al. 2016). In addition to the expansion of data, existing data remain underutilized and inactive in the decision making process. A shift is needed within transportation agencies to better capitalize on all available data and to increase its utilization in operating procedures and processes (Smith and Fallaha 1992; Gurganus and Gharaibeh 2012; El-Akruti et al. 2013; Hawkins 2013; Dingess 2014; Melchers 2015). This study focuses on expanding the use of network-level asset management data to new areas of application, namely roadway and roadside diagnostics.

In the current data driven era, businesses are seeking ways to improve their competitive advantage by extracting useful information from large datasets (Haque et al. 2014; Bayrak 2015; Khalifa and Zabani 2016; Woldesenbet et al. 2016). The phrase data rich, but information poor applies to many industrial sectors, including transportation and construction. Identifying and exploiting information and trends ultimately improves business processes, regardless of sector. However, the identification and exploitation process proves challenging (Bayrak 2015; Jones et al. 2016; Kokina et al. 2017). State highway agencies (SHAs) are a prime example of an entity that has invested heavily in data

acquisition, but now find themselves searching for information within data to help drive decisions.

In a broader sense, the construction sector has lagged behind other sectors in activating available data in the decision making process (Woldesenbet et al. 2016). Specifically within the transportation sector, a recent national study called for the creation of analytical tools to assist SHAs in the roadway project scoping process (Anderson et al. 2016). These tools are needed to achieve more realistic work actions, schedules, and cost estimates that ultimately lead to better performing projects in terms of construction cost and project schedule (Kyte et al. 2004; Miller and Lantz 2010; Taylor 2012). Improvement requires capitalizing on existing network level datasets and combining it with new datasets to provide valuable diagnostic information on why a roadway is behaving in a certain way. Traditionally, project planning and fund allocation decisions are made devoid of detailed information, but network-level datasets that commonly exist or will commonly exist in the near future can inform these decisions. What is missing, however, is the theoretical framework and analytical methods needed to accomplish this goal. This dissertation investigates the combination of existing and new network-level datasets in a new way to contribute to filling this gap.

In order to fill this gap, the researcher developed diagnostic tools for roadway maintenance and improvement projects by integrating a new network-level tool and mining existing network-level data on roadway infrastructure. Three broad types of network-level information are used: a) roadway geometry, b) pavement condition, and c) publicly-available soil data. The diagnostic tools are built upon business analytic (BA) techniques,

specifically graph theory. Diagnostically, the created method within this study identifies the health of the overall project, four project systems, and 11 dimensionally heterogeneous indicators. The diagnostic tool contains a visualization component, a critical element in effectively telling the story of data to help better inform decision makers (Jones et al. 2016; Kokina et al. 2017).

The 11 indicators included in the diagnostic tool are not taken directly from network-level datasets, but require pre-processing of data, referred to as data activation. The 11 indicators are:

1. Fatigue (alligator) cracking deterioration rate,
2. Current rutting,
3. Temporal change in ride quality based on average International Roughness Index (IRI),
4. Roughest ride quality within the analysis period based on IRI,
5. Hydroplaning potential,
6. Traveled way width (includes travel lane and shoulder),
7. Roadside front slope steepness,
8. Ditch flowline slope steepness;
9. Ditch depth,
10. Dynamic loading based on the difference in wheel path ride quality using IRI, and
11. The American Association of State Highway Transportation Officials (AASHTO) soil classification.

Surface geometry affects surface drainage and safety within the right-of-way (ROW). Hydroplaning potential, width, front slope steepness, flowline slope, and ditch depth indicators consist of geometric elements and are included within the diagnostic framework. Data on these indicators are often not readily available in SHA's databases. The emergence of mobile Light Detection and Ranging (LiDAR) systems presented an opportunity to collect these data rapidly and safely and will likely become prevalent within the industry over the next decade. In anticipation of these data becoming more prevalent a portion of this study is dedicated to the creation of a surface geometry network-level dataset for inclusion in the diagnostic scheme.

Most existing network-level pavement management systems contain time-series data on pavement condition that span many years. Currently, these data are underutilized with regard to pavement diagnostics. Distress data within the Texas Department of Transportation's (TxDOT) pavement management system (PMS) was mined to identify the underlying causes of pavement symptoms (e.g., distress) and integrate that knowledge into the analytical diagnostic framework. Specifically, the alligator cracking deterioration rate, change in ride quality, roughest year, and dynamic loading indicators were derived from data within this system.

To advance the diagnostic process farther, readily available soil data was included in the process. Soil conditions are known to affect pavement performance (Huang 2004) and more broadly the performance of the roadway system as a whole. Simply inputting basic soil data into an analytic framework that combines pavement distress history and surface geometry information can improve an engineer's understanding of project health. The

AASHTO soil classification indicator was included in the diagnostic method to capture these data.

Finally, the rutting indicator used within this study was developed using mobile LiDAR measurements. While rutting is a measure commonly included in SHA's datasets, changes have been made to collection techniques within the Texas Department of Transportation (TxDOT) that make its historical data unreliable; therefore current rut measurements taken from mobile LiDAR data were used.

Ultimately, this study presents a diagnostic framework that integrates network level-data into a diagnostic process that helps engineers better manage road networks by understanding why pavements and roadsides are behaving in particular ways. This allows for the use of network-level data to provide engineering based decisions early in the process. Currently several iterations are required to arrive and final plan sets. The diagnostic tool created through this work has the potential to save time and costs in the project development stage. The techniques employed in the diagnostic process help move from a data rich, but information poor environment to a data rich, and information rich environment. The ability of the diagnostic framework to take disparate datasets and convert the data into indicators is akin to a doctor evaluating multiple symptoms across different biological systems to properly diagnosis a patient.

By building the process on network-level data, engineers and decision makers are more equipped to make more informed decisions earlier in the processes. Also, the inclusion of a new network-level dataset created a holistic diagnostic process that included information on the traditional roadway features (i.e. pavement distress), while expanding to

drainage features (e.g. ditch depth) and safety features (e.g. hydroplaning and width). The method provides a realistic perspective of the health of a roadway from ROW line to ROW line.

1.2 RESEARCH QUESTIONS AND GENERAL HYPOTHESIS

Based on the aforementioned observations, this research addresses the following specific questions:

- Can an analytical framework be developed to incorporate multiple network-level datasets to provide diagnostic information for a roadway from ROW line to ROW line?
- Can network-level surface geometry data be converted to diagnostic information?
- Can existing network- level pavement distress data be mined in an effective way to generate useful diagnostic information?
- Does the application of actual network-level data through the diagnostic method result in realistic diagnostics as judged against detailed engineering decisions?

The following general hypothesis is used in this study to answer the above questions:

The integration and proper mining of network-level datasets can inform engineers about the needs of roadway infrastructure by providing diagnostics about the health of the roadway from ROW line to ROW line.

1.3 RESEARCH OBJECTIVES

The aim of this research was the development of roadway diagnostic methods and tools that use existing network-level data or newly created network-level data. This entails the following specific objectives:

- Objective #1: Develop an analytical diagnostic framework for roadway maintenance and improvement projects.
- Objective #2: Develop a network-level method for evaluating roadway and roadside surface geometry attributes and performance using mobile LiDAR data for inclusion in the diagnostic method.
- Objective #3: Develop a data mining methodology to extract pavement health information from existing network-level datasets for inclusion in the diagnostic method.
- Objective #4: Test the realistic nature of the diagnostic framework against actual engineering decisions.

2. LITERATURE REVIEW

This chapter presents a review of the literature associated with data usage on infrastructure projects, techniques to exploit data collected by agencies and businesses, and roadway specific data. Geometric indicators play a critical role in the diagnostic method. Thus, attention is given to the conversion of mobile LiDAR measurements into these indicators. The literature shows that the penetration of mobile LiDAR is only growing and that practitioners can expect these data to become commonplace in the near future. The literature review is intentionally eclectic in nature, drawing on experience from multiple disciplines. With a focus on diagnostics, the researcher has borrowed from different sectors to develop a tool that is effective, accurate, and analytically rigorous.

2.1 THE USE OF DATA TO INFORM ENGINEERS OF PROJECT NEEDS

Infrastructure projects associated with built networks do not simply exist; rather they are created by an agency. The creation of a project requires choice about its robustness and desired effect. This choice is often made under the assumption that well-defined objectives exist, which is often untrue (Schraven 2011). The lack of defining objectives early in the process often leads to underestimation or poor scope selection (Kyte et al. 2004). While a uniform definition of scoping is illusive within the transportation industry, many researchers have noted inconsistency in the process, particularly as it relates to determining the needs of a project early in the process (Kyte et al. 2004; Miller and Lantz 2010; Taylor 2012; Anderson et al. 2016).

The typical repository for roadway data is an agency's PMS. AASHTO guidelines for PMSs state that a pavement management system is "designed to provided objective information and useful data for analysis so that highway managers can make more consistent, cost-effective, and defensible decisions related to the preservation of a pavement network" (American Association of State Highway and Transportation Officials (AASHTO) 1990). However, they are often not used in this way because they are viewed as having a plethora of data, but little in the way of useful information (Federal Highway Administration (FHWA) 2007).

Current PMSs contain data on the relative behavior of the pavement, but often fall short in providing information to assist in defining the most appropriate treatment. The aggregated condition data found in PMSs often neglect the dominant distress, potentially leading to the selection of a less than optimal strategy. Additionally, undocumented maintenance actions are missed in condition reporting, yet these actions can inadvertently lead to an overestimation remaining pavement life (Hoffmann 2016). Other studies have indicated that current analytical tools within PMSs fail to mimic engineering judgement (Gharaibeh et al. 2012).

As PMSs evolve, research has continued to find ways to extract more information to assist in the decision making process. This includes evaluating temporal data rather than only capturing the current condition, but it also includes combining variables in different ways to better understand performance. TxDOT's PMIS was mined using ranking and classification algorithms to predict a pavement's structural condition index (SCI). This analysis used a five year distress window and analyzed the combination of many attributes

to determine which attribute correlated best to SCI, in hopes that the structural capacity of the pavement could be described at the network-level (Chi et al. 2014). Other studies have looked at extended time periods of pavement histories to determine if the pavement age should be reset or if it is an error in the data associated with the condition rating (Chen 2016). In Tennessee, a study was performed to capture historical pavement performance and include it in the current decision tree methodology. Multiple regression methods were used to determine the impact different parameters have on treatment performance models and draw conclusions on how pretreatment work affects posttreatment condition and deterioration (Dong et al. 2015). Others have sought to capitalize on PMS databases to assist road mangers with broader management and diagnostics. In order to accomplish this task, relationships among different engineering parameters must be identified, particularly when trying to capture the cause of damage at the macroscopic level (Pozarycki 2016).

Within Texas, a study was performed to create a screening and prioritizing tool to support the 4-year pavement plan. This tool focused on using current year data from TxDOT's PMS, while researchers suggested future work should explore the treatment selection decision making process. The researchers noted the need to capture several factors beyond pavement data in a future algorithm (Chi et al. 2013). Others researchers have begun to look at the collection of data on other assets. In one particular study, the performance and condition of roadside assets was studied. These assets included safety, drainage, cleanliness, and vegetation and the performance of these assets was noted as important for planning future maintenance and rehabilitation strategies (Gharaibeh and Lindholm 2014). While the previously mentioned studies focused primarily on hard assets, researchers have noted the

lack of economic relevance and the inability of transportation decision support tools to account for other factors. These same researchers proposed new performance-deterioration modeling, while at the end of the study noting that future research should include a wider range of objectives, such as road safety (Amador-Jiménez and Amin 2013)

Regardless of the process or type of project, new pieces of data are required to better communicate the needs to the decision maker (Zaghloul et al. 1998; H. Zhang et al. 2013; Jones et al. 2016). New Jersey explored the ability to include falling weight deflectometer (FWD) results in the project needs determination process within project planning (Zaghloul et al. 1998). TxDOT's *Project Development Process Manual* indicates that data within PMIS might be helpful in identifying project needs, but fails to provide guidance on how to extract or analyze the data (Texas Department of Transportation (TxDOT) 2014b). In a survey study performed in South-East Europe, the need for additional data to help inform decisions about improving road safety was highlighted. This need, particularly about accidents, was noted by policy and high-level decision makers (Laiou et al. 2017).

2.2 THE USE OF MOBILE LIDAR DATA IN INFRASTRUCTURE RELATED PROJECTS

The researcher leveraged mobile LiDAR data to include new information to better communicate the needs of a roadway project. These data allowed the researcher to develop a more holistic network-level tool than currently exists. Researchers have noted that asset data beyond the traditional pavement and bridge assets remain limited across the United States (Wiegmann and Yelchuru 2012).

The use of mobile LiDAR to measure and inventory roadway attributes is on the rise (Findley et al. 2011; Tsai and Li 2012; Tsai et al. 2013; Chang et al. 2014). However applying the results of mobile LiDAR measurements and incorporating the results into asset management systems and processes often requires tailor made techniques. NCHRP Report 748 (2013) suggests that applying mobile LiDAR to transportation related applications has the potential to revolutionize the industry, particularly if data are shared across agency silos from project planning to facility maintenance (Olsen et al. 2013).

The use of LiDAR for specific infrastructure applications is well-documented in the literature. A LiDAR study (2011) conducted on over 145 km (90 mi) of roadway in North Carolina evaluated LiDAR data against manually collected data and found that mobile data compared reasonably well to manual collection (Findley et al. 2011). Potential LiDAR application at the network-level includes the measurement of roadway cross slope with a device that generates over 10,000 laser points per second (Tsai et al. 2013). An algorithm referred to as the horizontal alignment finder (HAF) was created to inventory highway curves (Cook et al. 2015).

Studies related to storm water surface drainage infrastructure have also been performed. The use of LiDAR data within an Italian storm water study sought to overcome the challenge of not knowing the in-field condition because as-built data were often out of date or inaccurate (Cazorzi et al. 2013). Lantieri (2015) used mobile LiDAR data to determine water runoff conditions on the pavement surface and to understand how improper surface drainage can lead to pavement striping and delamination (Lantieri 2015). The Florida Department of Transportation (FDOT) has evaluated methods to analyze cross slope

from mobile data collection. The analysis of highway geometric conditions assists agencies in evaluating accidents related to surface geometry or surface drainage (Mraz and Nazef 2008).

2.3 ROADWAY INFORMATION NOT TRADITIONALLY USED AT THE NETWORK-LEVEL

For highway pavements, extensive damage can be caused by both surface and subsurface water entering lower, unbound layers more quickly than it can exit (Winterkorn and Fang 1975). When water becomes entrapped within the pavement structure, the strength of unbound layers and subgrade soils is greatly reduced. Loading a pavement with wet sublayers results in a loss of support (Huang 2004). The need to properly drain pavements using pavement geometry and roadside geometry to ensure the expected design life has been advocated for many years (Cedergren 1987; Birgisson and Ruth 2002). Though the problem has been noted for years, it continues to plague SHAs. Fig. 1 is a photo of water being pumped out of concrete pavement by passing traffic, taken by the researcher in 2016. This water was initially surface water that was not adequately drained away from the roadway.

Fig. 1. Water pumping through a pavement structure due to inadequate surface drainage and pavement distress

The impact of poor drainage on pavement performance and maintenance costs has been noted by many researchers. A case study on Route 656 in Hanover County, Virginia was undertaken to demonstrate the damage associated with poor subsurface drainage. This case study found that the subsurface water was primarily due to groundwater, rather than infiltration through surface cracks (Daoulas et al. 2011). Another case study evaluating premature rutting along I-20 in Louisiana concluded that water in underlying layers was the cause of the failures as the underdrain system was not functioning properly (King Jr. et al. 2015).

Highway drainage guidelines have often been geared toward the construction of new facilities, but addressing drainage impacts to the built environment can be integral for

sustainable network management (American Association of State Highway and Transportation Officials (AASHTO) 2007). Data about the geographic and geometric properties of the drainage area are integral to proper hydraulic analysis (Texas Department of Transportation (TxDOT) 2014 (Rev. 2015)). Programs developed to generate cross slope, profile grade, rut depth, and other surface features help engineers visualize the current state of the roadway, ultimately assisting in decision making (Mraz and Nazef 2008). These features do not typically exist within an agency's databases (Luo et al. 2014). However, the researcher believes the continued development of mobile LiDAR and its applications to roadway inventories will become common within the next 10 years. For this reason, the researcher sought ways to include these data in the diagnostic process.

To simulate surface drainage on the roadway and roadside, LiDAR readings must be linked together to form a grid that can be used in grid based algorithms. O'Callaghan and Mark created the deterministic eight-direction (D8) single-flow algorithm to extract data from digital elevation models (DEMs) in 1984 (O'Callaghan and Mark 1984). The use of grid based algorithms continued in a study used to capture manmade storm water infrastructure (Choi et al. 2011). TopoToolbox is a set of Matlab commands built upon the D8 algorithm to assist with hydraulic analysis of topographic data (Schwanghart 2010; Schwanghart 2014).

An important surface element for transportation decision makers is hydroplaning. Hydroplaning can be defined as the actual separation of the tire from the pavement surface, caused by a layer of fluid (Gallaway et al. 1979; Ong and Fwa 2007). Hydroplaning potential is a function of geometric conditions such as cross slope, longitudinal grade, and

pavement width. Surface textures also effect hydroplaning by directly impacting the fluid thickness between the tire and roadway. On pavements, this thickness is called the water film thickness (WFT) or water film depth (WFD) (Gallaway et al. 1971; Gallaway et al. 1979; Anderson et al. 1998; Ong and Fwa 2007; Yassin et al. 2013; Luo et al. 2014; Luo et al. 2016.

A study from 2014 used cross slope and profile measurements gathered from an inertial measurement unit (IMU) and texture data from a 1 mm (0.04 in.) three dimensional texture laser to calculate water film thickness. The equation used for water film thickness was taken from the PAVDRN model and mean texture depth was determined using the 1 mm (0.04 in.) three dimensional texture laser. A primary output of this study was the identification of potential hydroplaning areas (Luo et al. 2014).

Roadsides must function as an effective conduit to transport water away from the roadway. The challenge often comes in balancing the safety and drainage aspects of surface geometry (American Association of State Highway and Transportation Officials (AASHTO) 2011; Gurganus et al. 2017). A recent study evaluated the use of mobile LiDAR to preliminarily design a roadside drainage plan under multiple roadside constraints (Gurganus et al. 2017). Roadside constraints often include front slope steepness and ditch depth. A front slope is categorized in one of three ways: recoverable, non-recoverable, or critical. The TxDOT Roadway Design Manual notes that about 1/3 of all highway fatalities are associated with single-vehicle, run-off-the-road accidents (Texas Department of Transportation (TxDOT) 2014c).

During the course of this study, it was discovered that the desirable ditch depth is under-researched. A recent study from Nordic countries in Europe indicated that general practice was to have the bottom of the ditch at least 20 cm (8 in.) below the bottom of the pavement structure (Matintupa and Saarenketo 2012). Occasionally, in plans, designers include a typical ditch depth, commonly 60 cm (2 ft.) below the pavement surface. TxDOT's design manual recommends a ditch depth at least 15 cm (6 in.) below the crown of the subgrade (Texas Department of Transportation (TxDOT) 2014c). Iowa DOT uses a desirable ditch depth from the pavement surface of 90 cm (3 ft.) and an absolute minimum of 60 cm (2 ft.) (Iowa Department of Transportation 2012). New York recommends a typical depth of 75 cm (30 in.) below the surface of the edge of pavement (EOP) (New York State Department of Transportation 2016). Illinois' Bureau of Local Roads and Streets recommends a 60 cm (2 ft.) ditch depth with an absolute minimum of 45 cm (1.5 ft.) (Illinois Department of Transportation 2006).

2.4 ANALYTICAL TECHNIQUES AND TOOLS USED TO CAPITALIZE ON DATA

The previous sections of the literature review illustrate the many sources or data available to transportation decision makers. Those sections also showed strides made within the transportation sector to include more assets in the decision making process. However, recent work has indicated that the lack of informed decisions early in the process continues to plague the industry, prompting the call for new tools to help capitalize on the available data (Anderson et al. 2016).

Informed decisions in the financial sector have long been sought as market volatility can create deep concerns with investors. Research has been performed to study underlying signatures within market occurrences in hopes of identifying the driving forces behind the occurrence. Financial analysis often requires the use of financial time series data and the integration of multiple analytic techniques to help diagnose the reason for the volatility (Guharay et al. 2016).

The healthcare industry is another industry that relies heavily on data analytics. It has turned to data analytics to present information to decision makers drawn from significant volumes of data. These techniques are proving effective in analyzing and summarizing data from different sources and different dimensional spaces. Analytic frameworks often develop unique solutions to specific problems, such as analysis cubes used to feed dashboards that visualize the information for decision makers. The visualization of information comes after the identification, pre-processing, and analysis of key performance indicators (KPI). The ability of dashboard visualization, including the use of gauge charts, helps convey the output of analytical methods in an understandable way (Kokina et al. 2017). The effective conveyance of the information is integral in applying analytic techniques in ways that will shape the future of the healthcare industry (Haque et al. 2014; Jones et al. 2016).

In fact, effectively communicating complex ideas with graphics is its own field. The goal with graphics is to draw the viewer's attention to the data and effectively present quantitative information. The purpose of the graphic is to assist in thinking, helping the decision maker understand causality, make comparisons, and navigate through multivariate space (Tufte 2001; Tufte 2006). Dashboards have become popular across several sectors for

displaying indicators in an effective way (Kokina et al. 2017). A dashboard is defined as a visual interface that provides a quick view of relevant data for a business process. When structured properly, the graphics within a dashboard portray information clearly and concisely, proving effective because the human brain processes numbers and images as discrete chunks (Wolf 2016).

Diagnostic analytics is a term currently being used within BA research (Khalifa and Zabani 2016; Kokina et al. 2017). Diagnostic analytics is one of several types of analytical methods within BA, including descriptive analytics, predictive analytics, and prescriptive analytics. Diagnostic analytics seeks to answer why something has happened and within the hierarchy of analytic techniques falls between descriptive analytics and predictive analytics. Descriptive analytics seeks to describe the data, diagnostic analytics seeks to use the data to answer why, predictive analytics uses the data to answer what next, and prescriptive analytics seeks to determine alternatives (Bayrak 2015; Khalifa and Zabani 2016; Kokina et al. 2017). The effectiveness of predictive and prescriptive analytics hinges on the effectiveness and accuracy of diagnostic analytics, the primary emphasis of the study within.

A data analytics problem presents with a lack of structure fed by various datasets containing the KPI (Chen et al. 2016; Maceda-Veiga et al. 2017; Wang and Wu 2017). Applying different analytic techniques to multivariate datasets requires dedicated pre-processing techniques (Aggarwal 2013; Chen et al. 2016). Dimensionality reduction can occur at multiple phases within the data analytics processes. Within some techniques it might be necessary to place the data on an indexed scale. It has been noted across all sectors, including the transportation sector, that a key component of multi-criteria decision making is

the ability to place all components on equal footing with regards to scale (Sinha and Labi 2007). A recent study developed an index called the Highway Infrastructure Data Integration (HIDI) index using a five-point scale (Woldesenbet et al. 2016). Another study from the accounting field used the five-point Likert scale for data processing (Kokina et al. 2017).

The use of n-point scales, or more specifically five-point scales, is common with roadway data. TxDOT has five condition score thresholds with very poor, poor, fair, good, and very good descriptors (Texas Department of Transportation (TxDOT) 2014a). TxDOT uses the same five descriptors to describe ride quality using various IRI ranges (Texas Department of Transportation (TxDOT) 2003). Finally, for rutting, TxDOT has rut depth ranges associated with no rutting, shallow rutting, deep rutting, severe rutting and failure rutting descriptors (Texas Department of Transportation (TxDOT) 2016). A project developing sustainability assessments used both 1-5 point scales and dashboards with gauge charts and other graphics to communicate a project's sustainability index. The sustainability index included six indicators (Umer et al. 2016). The use of n-point scales finds its origins in the 1930s when Rensis Likert used them as tool to assess attitudes. Within the research world, these scales are expanding into the multi-criteria and multi-expert arena and now include cardinal data, not only qualitative data (Stoklasa et al. 2017).

2.5 GRAPH THEORY AND EIGENVALUE TECHNIQUES

Of the many tools and techniques with the BA field, the researcher borrowed primarily from mathematics. The diagnostic tool developed by the researcher used graph theory and particularly the eigenvalue techniques associated with matrices.

Within graph theory, networks are used to describe a collection of points joined together by lines. The network structure simplifies a complex system by only representing the fundamental connection between elements. When a system can be structured as a network, calculations about that network provide useful information about the overall system (Newman 2010). Graphs are considered directed when the edges point from one node to another node. Graphs can further be defined as acyclic if no cycles exist. A directed and acyclic graph is referred to as a DAG and can fundamentally be defined by its incidence matrix (Newman 2010; Chelvam et al. 2010).

The edges within a DAG can contain weights, thus the incidence matrix becomes a weighted edge incidence matrix. Typically, weighted edge incidence matrices are asymmetric. Users of graph theory have dealt with the asymmetry of matrices by creating a Laplacian Graph or a "generalized" Laplacian. Formally, the Laplacian Graph is calculated by subtracting the adjacency matrix form a diagonal matrix filled with the degree of each node. However, when the orientation of a graph is fixed, the incidence matrix can be multiplied by its transpose to create a generalized Laplacian (Cvetkovic et al. 1997; Biyikoglu et al. 2007; Newman 2010).

Laplacian graphs have been used to deal with multidimensional datasets and reduce those datasets without the loss of local information (Belkin and Niyogi 2003; Shi et al. 2013). With a symmetric generalized Laplacian, real, non-negative eigenvalues exist. The eigenvalues produced with the generalized Laplacian are characteristic of the network on which the graph and weighted edge incidence matrix was built. The largest eigenvalue is called the index and is the most commonly used value to describe a matrix. The descriptive

nature of eigenvalues comes from the mathematical formula used to solve for the eigenvalues. The eigenvalues are the roots to the characteristic polynomial equation of a symmetric matrix (Cvetkovic et al. 1997; Biyikoglu et al. 2007; Cioaba and Murty 2009).

Laplacian eigenvectors are commonly used in heuristics to solve combinatorial problems (Biyikoglu et al. 2007). The use of eigenvalue calculations or the creation of Laplacian eigenmaps has been used by other researchers for dimensional reduction and in combination with other techniques in classification heuristics (T. Zhang 2010; Shi et al. 2013).

3. DATA

This chapter describes the data types and sources used in this study along with a brief introduction to some of the methods used to convert these data into information. These data consist of:

- Surface geometry data collected through single laser mobile LiDAR.
- Pavement condition history data extracted from an existing pavement management database.
- Soil data obtained from public databases.

3.1 SURFACE GEOMETRY DATA

In this study, a single-laser mobile LiDAR system (MLS) was used to collect roadway and roadside surface geometry to evaluate the geometric performance as it relates to design compliance, roadside drainage and hydroplaning potential. This data represents the creation of a new dataset. While creating a new dataset in what is already a data rich environment might seem like the introduction of a challenge, new datasets are often required to advance or improve current analytical techniques. The collection of this type of data at the network-level is currently evolving with the emergence of MLSs and post-processing softwares. Prior to this study, little has been done to evaluate how these data can be collected and integrated into broader network-level management techniques. The researcher believes the rapid emergence of LiDAR technology and penetration into the industry will make these data as prevalent as pavement condition data within a few years.

The common components of MLSs include the hardware technology mounted to the vehicle, the in-vehicle software interface for data collection, and the software package for post-processing. The MLS used in this study included the Road Doctor CamLink camera, a single SICK laser scanner, a NovAtel global positioning system (GPS), a NovAtel inertial measurement unit (IMU), a 3D accelerometer, Road Doctor CamLink 7.0 in-vehicle software, and Road Doctor 3 post-processing software. The laser scanner package was constructed by Roadscanners Oy of Finland (Roadscanners). Two primary pieces of data are generated by the laser: the reflectivity of the target object and the straight-line distance to the object in relation to the angle of the laser. The IMU functions as an accurate gyroscope with pitch, roll, and yaw measurements taken on frequent intervals during data collection. Algorithms in the software use the IMU measurements to make corrections to the straight line distance measurements improving accuracy. These corrections were discovered as beneficial on roadways with poor ride quality. Fig. 2 illustrates the geometry associated with MLS measurements.

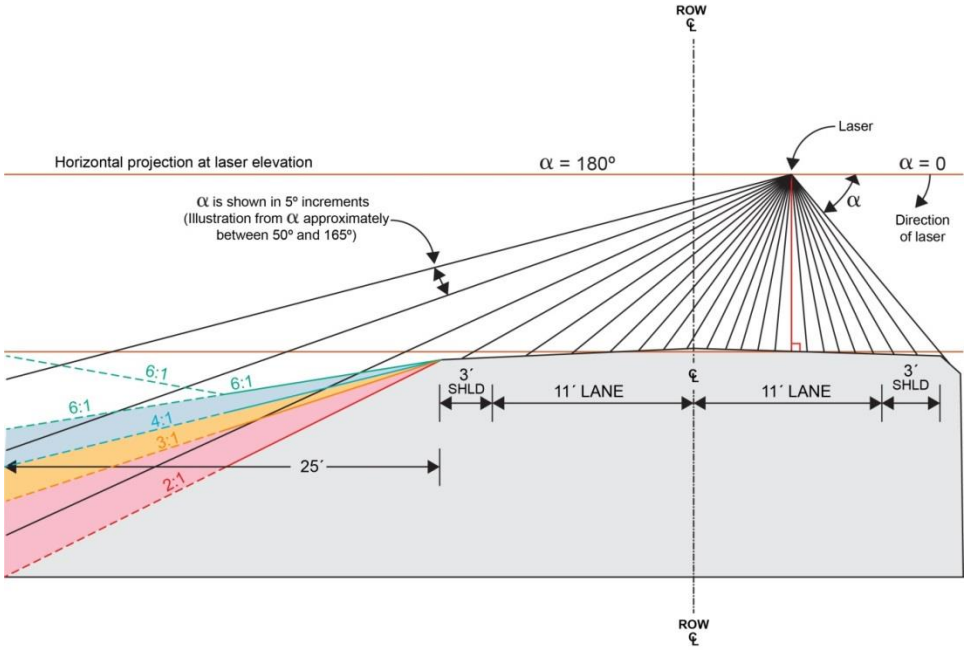

Fig. 2. Laser scanner geometry

Within Fig. 2, α represents the angle between the horizontal projection of the laser and the laser shot. The α angle is controlled by the laser's angular resolution. The angular resolution, 0.6667° within this study, is defined as the angular movement in the laser between measurements (SICK: Sensor Intelligence 2011). The angular resolution increment spacing does not change so more data points are collected in close proximity to the laser source. This can be seen in Fig. 2, which includes laser lines on approximately 5° increments.

Point density is the number of LiDAR measurements (i.e., points) per unit area. Point density changes in relation to laser proximity and the speed of the MLS vehicle. Within a 161 m (0.1 mi) data collection section, the mobile LiDAR unit in this study had a point density of approximately 190,000 points per lane mile at 72.5 kph (45 mph). At 113 kph (70 mph), the point density reduces to approximately 127,000 points per lane mile.

Within this study, validation of the accuracy of mobile LiDAR readings occurred through a multi-step approach using sections of known geometry. The raw accuracy of the laser and other MLS components are established by equipment manufacturers and assumed to be valid. Appendix A includes tables and figures with information on the accuracy of the mobile LiDAR device used. In summary, the device is capable of providing post-processed length data to within 0.15% of the actual length. The MLS accuracy of the cross slope in the data collection lane is typically between 0.05% and 0.10% (i.e., 2% ±0.10%). As data processing moves into a gridded analysis, some accuracy can be lost. This accuracy loss is marginal, as 0.305 m (1 ft.) x 0.305 m (1 ft.) gridded data yielded collection lane cross slope accuracy of within 0.20% and often remained within 0.10%.

Ditch offsets can be identified 100% of the time. When using 0.9144 m (3 ft.) x 0.9144 m (3 ft.) gridded data, the comparison between MLS processed ditch offset and actual measured offsets resulted in MLS offsets always falling within a 0.9144 m (3 ft.) window on the right roadside. For example, if the actual ditch flowline fell 5 m (16 ft.) from the EOP, the gridded data always showed the ditch location within the 4.57 m (15 ft.) to 5.49 m (18 ft.) grid. Ditch depths are also accurately measured, but roadside vegetation will indicate a shallower ditch than actually exists. Care was taken to collect data shortly after the annual mowing cycle or after the first frost when the grass becomes dormant for roadside data consistency. Roadside vegetation also results in roadside slopes that are flatter in MLS data than in reality. Although the roadside slopes are slightly flatter, they are within 0.5H:1V accuracy along the right roadside.

The MLS used in this study measures rut depth to within 0.254 cm (0.10 in.) and often measurers rut depth to within 0.127 cm (0.05 in.).

The indicators extracted from surface geometry included:

- Rutting: measured as the deepest wheel path rutting, mm or in., at any location within a data collection section,
- Hydroplaning: measured as the potential for hydroplaning to occur based on the difference, in kph or mph, between the posted speed limit and a simulated hydroplaning speed for the 50-year, 15-minute storm event,
- Traveled way width: measured as the distance from the centerline striping to the EOP, m or ft.,
- Roadside front slope: measured as the slope from the edge of pavement to the toe of slope at the flowline of the ditch or the ROW line, expressed as a ratio between the horizontal distance, m or ft., and a 0.3048 m (1 ft.) vertical drop,
- Ditch depth: measured as the depth from the edge of pavement surface elevation to the flowline of the ditch when a ditch is detected on the ROW, expressed in m or ft., and
- Ditch slope: measured as the percent fall from the highpoint to the low point of roadside drainage basin.

Design standards, hydraulic calculations, and simulations were used to convert geometric data into useful diagnostic information. The uses of these standards, calculations, and simulations are discussed in more detail in the Indicator Selection and Data Activation chapter.

3.2 PAVEMENT CONDITION DATA

The pavement condition data were obtained from TxDOT's Pavement Management Information System (PMIS). These data consist of annual time series values for the past 10 years (2007-2016) for the following pavement condition indicators:

- Fatigue (alligator) cracking: measured as the percent of the data collection lane area with fatigue cracking over a 805 m (0.5 mi.) data collection section,
- Average ride quality: determined as the average of the left and right wheel path IRI over a 805 m (0.5 mi.) data collection section, and
- Difference between left and right wheel path ride quality: determined as the absolute value of the difference between the right and left wheel path IRI values from a 805 m (0.5 mi.) data collection section

These pavement condition indicators were chosen because of their inclusion in the final rules associated with the Moving Ahead for Progress in the 21st Century Act (MPA-21) and the Fixing America's Surface Transportation (FAST) Act (Federal Highway Administration (FHWA) 2017). PMIS data were utilized because of its historical use within TxDOT dating to 1993 and TxDOT's annual audit program to ensure proper pavement ratings. Data from the TxDOT Austin, Bryan and Tyler districts were used within this study.

Using alligator cracking as the distress type, a comparison of rated sections to their respective audit sections from the past 10 years revealed that alligator cracking ratings can be considered reliable. Table 1 shows the reliability of the data by illustrating that 90% of all audit sections from the previous 10 years were within at least 1% of the annual rating.

Table 1. Ten year comparison of audit sections with alligator cracking

District	Number of Alligator Sections with an Audit	Mean Difference between Annual Rating and Audit (% Section Area)	Standard Deviation for Difference (% Section Area)	Median Difference between Annual Rating and Audit (% Section Area)	90th Percentile Difference between Annual Rating and Audit (% Section Area)
Austin	2490	0.44	3.62	0	1
Bryan	3791	0.13	1.85	0	0
Tyler	4811	0.58	4.49	0	1

The researcher treated temporal alligator cracking as a process to effectively determine the deterioration rate within a project. By considering the manifestation and growth of a distress as a process, the researcher capitalized on the cumulative sum technique from process control theory to mine the pavement data for diagnostic information.

Ride data used in this study were collected by TxDOT using annually calibrated pavement profilers. Unfortunately, TxDOT's current data collection plan does not require ride quality to be collected on the same lane year to year, only from the same roadbed, where the roadbed is defined as the contiguous structure of a roadway regardless of the direction of traffic. Therefore, the temporal analysis of ride data focused on the dynamic nature of the ride quality within a roadbed. Finally, TxDOT's database separately stores ride quality information for both the left and right wheel path, allowing the researcher to include dynamic loading as an indicator by capturing the difference in wheel path ride quality.

The length of pavement projects varies and represents the actual way pavements are managed. Often, project lengths are submitted by a decision maker with intimate knowledge of the network. Therefore, the analysis and data mining technique remain district specific to

capture the perspective of decision makers submitting potential projects. The projects used to apply the diagnostic tool include multiple data collection sections within PMIS, typically 0.8 km (0.5 mi) in length. The projects used for diagnostic application and to evaluate the realistic nature of the tools are listed in Table 2.

Table 2. Projects used for diagnostic method application

Project Hwy.	TxDOT District	County	Project Length, km (mi.)	Begin RM	End RM	No. of Sects.	General Construction Description
FM 1696	Bryan	Grimes	14.7 (9.1)	642	651	18	Rehabilitating existing roadway
FM 1660	Austin	Williamson	5.4 (3.3)	429	432.7	8	Rehabilitating existing roadway
FM 908	Bryan	Milam	2.5 (1.5)	581	582.5	3	Rehabilitating existing roadway
OSR	Bryan	Madison	24.5 (15.2)	634	649	28	Rehabilitating existing roadway
FM 50	Bryan	Washington	8.5 (5.3)	447	452	10	Rehabilitating existing roadway
FM 1844	Tyler	Gregg	6.3 (3.9)	702	706	8	Widen, repair, & resurface
FM 2661	Tyler	Smith	5.1 (3.2)	290	293	6	Widen for safety
FM 2054	Tyler	Anderson	5.5 (3.4)	328	331.4	7	Widen for safety
RM 690	Austin	Burnet	7.4 (4.6)	402	406.5	9	Widen
SH 138	Austin	Williamson	10.2 (6.4)	526	532.4	13	Add shoulders & rehabilitate

3.3 SOIL DATA

Pavements often fail due to the weakening of subsurface layers caused by water infiltration (Winterkorn and Fang 1975). To better account for the susceptibility of pavements to water infiltration, soil type was obtained from the United States Department of Agriculture (USDA) Natural Resources Conservation Services (NRCS) Web Soil Survey (WSS). The WSS is a quality controlled database with representative samples from over 95% of the nation's counties. Most of the soil data within the survey has been collected within the last 25 years and was done so by soil scientists (Covar and Lytton 2001; Natural Resources Conservation Service (NRCS)).

The researcher built shape files using the open source GIS software, QGIS™, to load into the WSS survey. The shapefiles were 3.22 km (2 mi) in length and 30.5 m (100 ft.) wide with the roadway in the center of the shape. Importing the shape file into WSS generated soil maps and associated soil reports. The soil property used by the researcher in development of the diagnostic method was the AASHTO classification.

The AASTHO system uses seven groups, listed as A-1 through A-7. With regard to subgrade quality, soils classified as A-1 through A-3 are typically considered excellent to good, while soils classified as A-4 through A-7 are fair to poor (Budhu 2015). Fig. 3 is an example of a 3.22 km (2 mi) soil map of FM 1696 showing the soil labels at different locations along the roadway. Table 3 has the AASHTO soil classification at different depths for the same portion of the FM 1696 project as the soil map in Fig. 3. Table 3 also has the percent of the area of interest (AOI) of each soil type within this portion of the project that was used to develop a weighted classification for each 3.22 km (2 mi) section of a project.

Fig. 3. Example of soil map for FM 1696

Table 3. Example of AASHTO soil classification for FM 1696

Reference Markers	Map Symbol	Depth, cm (in.)	AASHTO Class	% AOI
642 to 644	BfB	0-33 (0-13)	A-4	
		33-117 (13-46)	A-7	14.2%
		117-152 (46-60)	A-6, A-7	
	SlC	0-38 (0-15)	A-2-4	
		38-102 (15-40)	A-4, A-6	0.3%
		102-122 (40-48)	A-2-4, A-4, A-6	
		122-165 (48-65)	A-1-b, A-2-4, A-4	
	ZaC	0-15 (0-6)	A-4	
		15-56 (6-22)	A-7-6	26.4%
		56-81 (22-32)	A-7-6	
		81-122 (32-48)	A-4, A-6	
	ZuA	0-23 (0-9)	A-4	
		23-104 (9-41)	A-7-6	19.2%
		104-152 (41-60)	A-7-6	
	ZuC	0-15 (0-6)	A-4	
		15-89 (6-35)	A-7-6	39.9%
		89-152 (35-60)	A-7-6	

3.4 BUSINESS ANALYTICS

Many sectors are actively researching ways to capitalize on readily available data. BA, also referred to as Business Intelligence (BI) or Big Data (BD) is a field of active research focused on methods used to transform data into actionable information. Analytics most appropriately describes the work within this study because this term captures the techniques from fields like computer science, math, and industrial processes and applies them with engineering knowledge to transition from data rich to information rich (Haque et al. 2014; Bayrak 2015; Seret et al. 2015; Kokina et al. 2017).

The researcher chose graph theory as the primary tool to convert data to information. Many systems across many sectors are modeled as networks built upon graph theory (Newman 2010). The use of graph theory allowed the researcher to develop a mathematical framework for the health indicators within a project. The mathematical framework was exploited to gather descriptive information about the health of each of the indicators, systems comprised of multiple indicators, and for the project as a whole.

4. ANALYTICAL FRAMEWORK OF THE DIAGNOSTIC METHOD

To acquire diagnostically useful information from network-level data, the researcher represented roadway projects as a network. Projects were used because it allowed the researcher to investigate multiple data collection sections grouped together. Managing agencies develop roadway projects that function similar to management sections, but are in reality the combination of several adjacent data collection sections. Therefore, the phrase roadway project is used to describe the combination of management sections, but in reality the method could be applied to any roadway length of interest containing multiple data collection sections. A network consists of a graph, G, with nodes, N, and edges, E, and uses functions to weight the edges between nodes. Within a roadway project, a naturally occurring hierarchical network exists with data collection section measurements at the bottom of the hierarchy and the project at the top of the hierarchy. For diagnostic purposes, the researcher inserted health indicators into the hierarchy, along with health systems.

Conceptually, the network looks like Fig. 4 for a project with eight data collection sections.

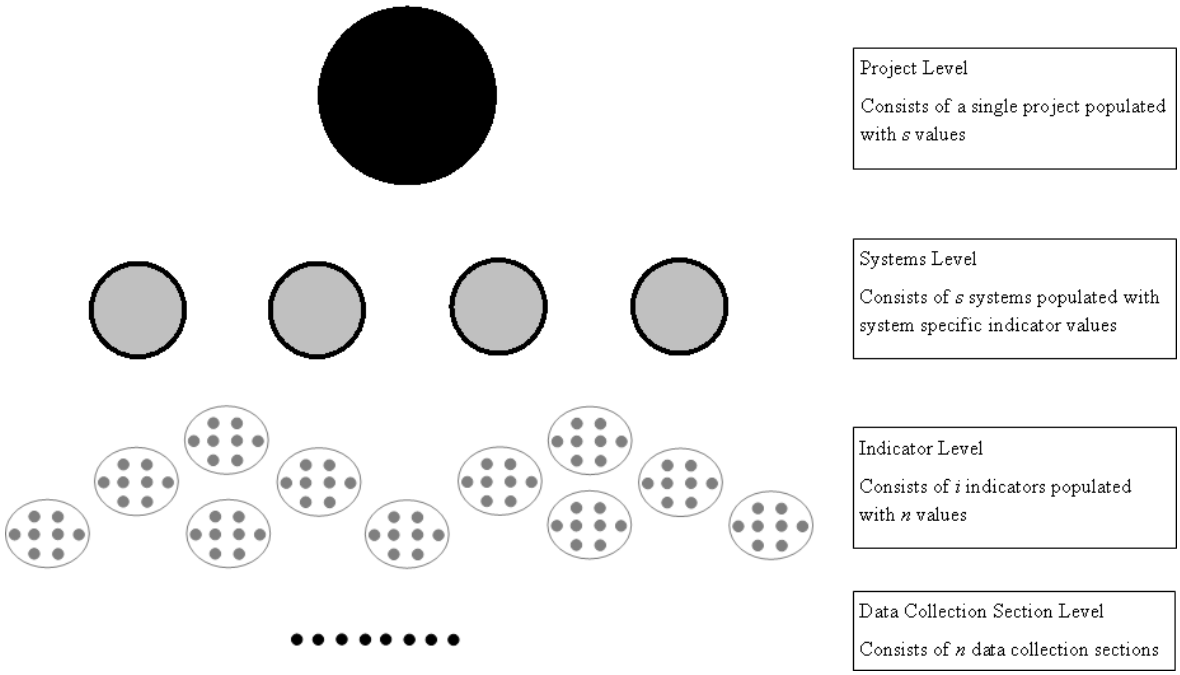

Fig. 4. Conceptual representation of a roadway project as a network

Restrictions on the number of data collection sections, indicators, or systems do not exist within the diagnostic method developed by the researcher. The roadway project diagnostics within the researcher's work consist of four systems and 11 indicators, with projects consisting of varying amounts of data collection sections. The initial step in developing project diagnostics focused on calculating a single health value for the project. Subsequently, this value was dissected to determine diagnostically useful information for each indicator that can then be recombined to determine the health of various systems within the project.

4.1 FRAMEWORK FOR OVERALL PROJECT HEALTH CALCULATION

Determination of the health of the entire project represents the value at the top of Fig. 4. The researcher constructed a weighted directed acyclic graph (DAG) to represent a roadway project and enable the calculation of mathematically descriptive values. Because the graph contains information specific to a particular project, the researcher utilized the mathematical characteristics of the graph to glean diagnostic information. The DAG used by the researcher is shown in Fig. 5.

The graph in Fig. 5 is directed because movement in the graph always moves from the outside ring inward. The graph is acyclic because no cycles exist in the graph; in fact movement within the graph terminates at the large middle node. The DAG is weighted because the edges between the nodes have weights upon them, applied through an activation function or a matrix function. The small points contained within the outer ring are the basic building block and represent the attribute measurement collected at the network-level. Through activation or indexing functions across the edges between the outer ring and the overarching indicator nodes, the data becomes useable within a matrix. The overarching indicator nodes consist of a vector of activated data. The size of this vector corresponds to the number of data collection sections within the project or length of interest. Each indicator has a vector, that when aggregated becomes the weighted edge incidence matrix. The vectors sit upon the edges between the indicator nodes and the overall project diagnostic node. The weighted edge incidence matrix is represented by the lighter interior circle. The weighted edge incidence matrix is populated with characteristic values that describe the physical phenomena within a project or length of interest. Calculations associated with the

weighted edge incidence matrix provide the diagnostics for the project as a whole and ultimately for various project systems and all of the indicators.

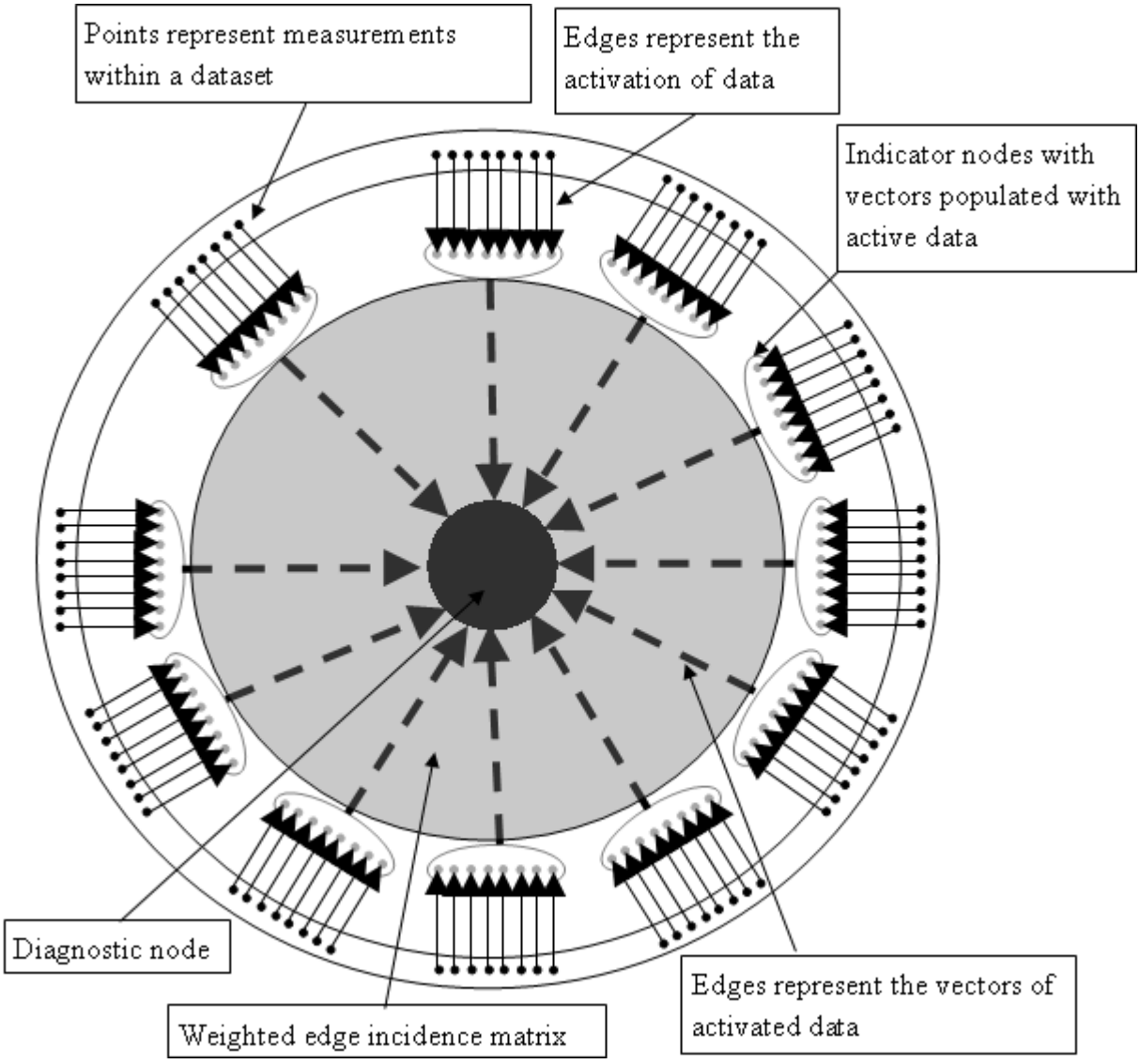

Fig. 5. Project representation as a weighted directed acyclic graph (DAG)

4.1.1 **Activation of Data**

The outer ring in Fig. 5 represents the data collection section level. The number of nodes in this outer band equals the number of data collection sections multiplied by the number of indicators, shown in the following equation:

$$N_{outer} = ni \tag{1}$$

where n is the number of data collection sections within a project, and i is the number of indicators.

The data collection section nodes contain raw network-level measurements for each roadway or project attribute within an indicator. For example, the researcher used deterioration rate as an indicator. This indicator required temporal alligator cracking data stored as percent alligator cracking at the data collection section level. Between this level and the next level, the researcher activated the raw data through various indexing functions. During the activation process, each indicator was placed on a 1 to 5 scale, with 1 indicating the healthiest measure and 5 indicating the unhealthiest measure. The indexing of each indicator is described in more in the Indicator Selection and Data Activation chapter.

The edges of the graph between the outer data collection section ring and the indicator level consist of the indexing function. Data stored at the data collection section level always flows or walks across the directed edge to the indicator level.

4.1.2 **Indicator Level Calculations**

The indicators are overarching nodes that consist of activated data from the data collection section nodes. Within the indictor node, activated data resides in a vector format. Each entry within the vector represents active data from the data collection section level that populated

a matrix. The matrix acts as a weighted edge incidence matrix. The large dashed lines between the indicator nodes and the project node are actually the combination of n directed lines storing activated data for each section. In graph theory and graph calculations, the activated data functions as weights attached to each edge, thus creating a weighted edge incidence vector for each indicator. When combined, all indicator vectors serve as the weighted edge incidence matrix for the project.

The weighted edge incidence matrix forms the mathematical foundation for the diagnostic method. The population of this matrix includes values specific to a particular project, therefore from a mathematical perspective describes the project's health. While numerically descriptive, the matrix still does not necessarily provide information, at least not directly to the end user.

For a project, the weighted edge incidence matrix,$[A]$, is of size, nxi or ixn depending on how the matrix is structured. From a calculation perspective, it does not matter if the indicators are the rows and the data collection sections are the columns or vice versa, the number of eigenvalues calculated totals the smaller of the two dimensions. However, the calculations require the dot product of two matrices and it helps understand that no loss of information occurred if the indicators are structured as the rows and the data collection sections as the columns. The outcome is the same regardless of structure, but this helps visualize the calculations.

Except when the number of indicators and number of data collection sections are equal, the weighted edge incidence matrix is asymmetric. To overcome the problem of asymmetry, the researcher created the equivalent of a Laplacian Graph or generalized

Laplacian. This new graph, L, functions similarly to an adjacency matrix for an asymmetric bipartite graph. In asymmetric bipartite graphs, the incidence matrix is multiplied by its transpose to create a symmetric matrix for additional calculations. Because the Laplacian Graph is symmetric and populated with real positive numbers, the eigenvalues for it are also real and positive. The calculations used to transition from an asymmetric matrix to a symmetric matrix and calculate the eigenvalues followed the following series of equations:

$[L] = [A][A^T]$ = symmetric Laplacian Graph (2)

where $[A]$ = asymmetric weighted edge incidence matrix.

λI = identity matrix multiplied by λ, representing the eigenvalues (3)

$P = [L - \lambda I]$ (4)

$determinant[P] = |P|$ = characteristic polynomial equation (5)

$|P| = 0$, values of λ that solve this equation represent the eigenvalues for $[L]$ (6)

The researcher developed the diagnostic method off of the premise that if the determinant of the Laplacian graph formed the characteristic polynomial equation that if these characteristics could be defined, information and knowledge could be gained that are particular to the population of the Laplacian graph. Because the Laplacian graph is populated with active data for a specific project, the diagnostic method used the descriptive nature of the characteristic equation to define the health of the project. The eigenvalues solve the characteristic polynomial equation and thus provide the basis for calculating a descriptive value for each project.

The calculation succeeds in maintaining its descriptive nature without compromising the amount of detail in the original matrix or convoluting the original matrix by multiplying

by its transpose by using the λI calculation. The rows represent activated data for the indicators, while the columns represent data collection sections. To make the matrix symmetric, all of the first row in $[A]$ is used with all of the first column in $[A^T]$. Take a small 3x4 matrix as an example:

$$[A] = \begin{bmatrix} w_{1a} & w_{1b} & w_{1c} & w_{1d} \\ w_{2a} & w_{2b} & w_{2c} & w_{2d} \\ w_{3a} & w_{3b} & w_{3c} & w_{3d} \end{bmatrix} \tag{7}$$

$$\left[A^T\right] = \begin{bmatrix} w_{1a} & w_{2a} & w_{3a} \\ w_{1b} & w_{2b} & w_{3b} \\ w_{1c} & w_{2c} & w_{3c} \\ w_{1d} & w_{2d} & w_{3d} \end{bmatrix} \tag{8}$$

$$[L] = [A][A^T] =$$

$$\begin{bmatrix} w_{1a}w_{1a} + w_{1b}w_{1b} + w_{1c}w_{1c} + w_{1d}w_{1d} & w_{1a}w_{2a} + w_{1b}w_{2b} + \cdots & w_{1a}w_{3a} + w_{1b}w_{3b} + \cdots \\ w_{2a}w_{1a} + w_{2b}w_{1b} + w_{2c}w_{1c} + w_{2d}w_{1d} & w_{2a}w_{2a} + w_{2b}w_{2b} + \cdots & w_{2a}w_{3a} + w_{2b}w_{3b} + \cdots \\ w_{3a}w_{1a} + w_{3b}w_{1b} + w_{3c}w_{1c} + w_{3d}w_{1d} & w_{3a}w_{2a} + w_{3b}w_{2b} + \cdots & w_{3a}w_{3a} + w_{3b}w_{3b} + \cdots \end{bmatrix} \tag{9}$$

The diagonal in $[L]$ consists of indicator values multiplied by themselves. Continuing the calculation using the identity matrix, as shown below, λ only applies to the diagonal.

$$[I] = \begin{bmatrix} 1 & 0 & 0 \\ 0 & 1 & 0 \\ 0 & 0 & 1 \end{bmatrix} \tag{10}$$

Therefore, the solutions to $|P| = [L - \lambda I]$ provide values for λ, specifically associated with diagonal values in $[L]$, where the diagonal values are essentially the square of themselves. In summary, while the calculations are the same regardless of structure, structuring the weighted edge incidence matrix with the indicators as the rows clearly shows that no loss or confusion of data occurs by multiplying the weighted edge incidence matrix by its transpose.

The eigenvalues, λ, solve the characteristic polynomial equation and thus provide the basis for calculating a descriptive value for each project. While the eigenvalues are descriptive, on the surface it provides little information to the end user. Therefore, the researcher continued the development of the diagnostic process by bringing meaning and perspective to the eigenvalues.

4.1.3 **Comparison Analysis to Make Eigenvalues Diagnostically Relevant**

In order to gain perspective into the descriptive nature of the eigenvalue, the researcher developed a comparative technique. The first step in the comparative technique was to formulate the project in its unhealthiest possible state. Each data collection section had its data activated by indexing it to the unhealthiest value that then populated the indicator vectors and became the weighted edge incidence matrix.

The comparative technique was structured to help determine how much of the available health a project had used. For example, if a project presents with all values of the unhealthiest order, the entire health of that project has been used. On the other hand, if a project presents with all values of the healthiest order, none of the project's health has been used. The assumption that the unhealthiest possible project has consumed all of the project health created a scenario where each potential health option was compared to the unhealthiest option. Again, a 3x4 matrix is used to illustrate the comparative analysis. For the method designed by the researcher, populating the matrix with the unhealthiest activated data means that each data collection section at the indicator level had a 5 on the 1 to 5 scale. This is shown in the matrix format below.

$$A = \begin{bmatrix} w_{1a:unhealthiest} & w_{1b:unhealthiest} & w_{1c:unhealthiest} & w_{1d:unhealthiest} \\ w_{2a:unhealthiest} & w_{2b:unhealthiest} & w_{2c:unhealthiest} & w_{2d:unhealthiest} \\ w_{3a:unhealthiest} & w_{3b:unhealthiest} & w_{3c:unhealthiest} & w_{3d:unhealthiest} \end{bmatrix}$$

$$= \begin{bmatrix} 5 & 5 & 5 & 5 \\ 5 & 5 & 5 & 5 \\ 5 & 5 & 5 & 5 \end{bmatrix} \quad (11)$$

As with the standard eigenvalue calculations described in the previous section, the matrix must first be transposed and the transpose multiplied by the original to create a symmetric matrix, referred to as the Laplacian graph. Using the symmetric matrix, eigenvalues were calculated for the unhealthiest scenario. Because the matrix is filled with the same value at each location, only one eigenvalue, referred to as the maximum eigenvalue, was produced. Therefore, all comparisons with regard to health consumed used maximum eigenvalues when more than one eigenvalue could be calculated. The calculation of the unhealthiest scenario maximum eigenvalue used the following equation:

$$\lambda_{max:unhealthiest} = in5^2 \quad (12)$$

Where, i equals the number of indicators and n equals the number of data collection sections. When the weighted edge incidence matrix is populated with all of the same value, a more general form of the equation can be expressed as:

$$\lambda_{max} = inx^2 \quad (13)$$

Where x represents the health value that populates the entire matrix. Within the method developed by the researcher, five potential health scenarios existed where the weighted edge incidence matrix could be populated by the same value. All of these scenarios were compared to the unhealthiest scenario where the project was said to have consumed all of its available health. Conceptually, this comparison looked like:

$$\frac{\lambda_{x:scenario}}{\lambda_{unhealthiest}} = \frac{inx^2_{scenario}}{inx^2_{unhealthiest}} \quad (14)$$

Because i and n were the same in the numerator and denominator, the health comparison simplified to a ratio of squared indexed values. Table 4 shows these comparisons for the method used by the researcher. Plotting these comparisons generated the health curve show in Fig. 6. Because the eigenvalue comparison simplified to a ratio, the power law equation fit the curve in Fig. 6. The equation is shown in Fig. 6 and below Fig. 6 in the text.

Table 4. Health scenario comparisons

Indicator Health Description	Indicator value, *r*	λ Ratio	λ_{max} Comparison
Unhealthiest	5	25/25	100%
↑ Deteriorating Health	4	16/25	64%
	3	9/25	36%
	2	4/25	16%
Healthiest	1	1/25	4%

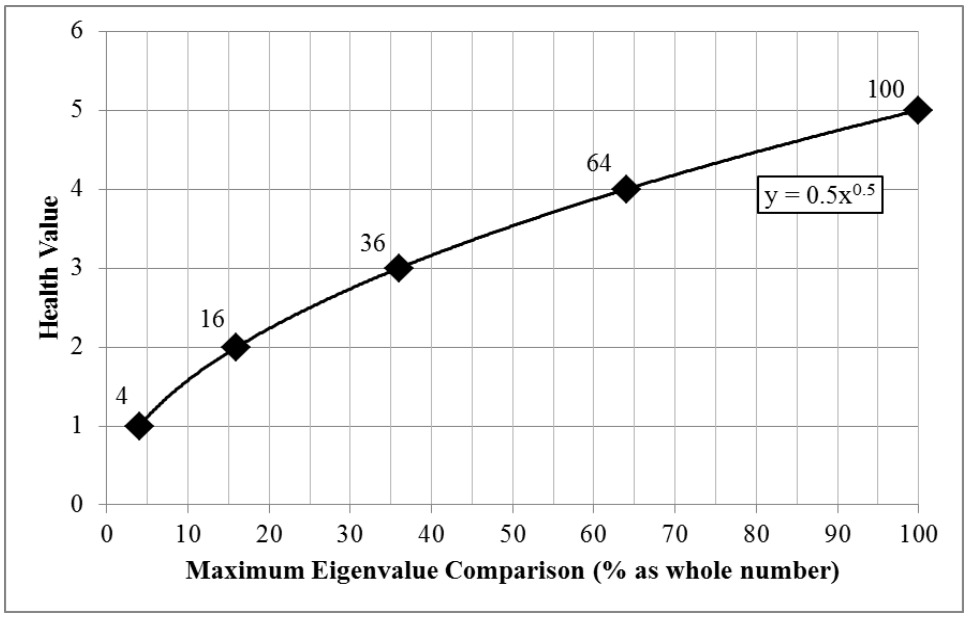

Fig. 6. Health curve

$$Health\ Eqn. = \frac{1}{2}\left(\frac{x^2_{scenario}}{x^2_{unhealthiest}} * 100\right)^{1/2} = \frac{1}{2}X^{1/2} \quad (15)$$

To use the curve for future calculations and to assist in the creation of the visualization tool within the diagnostic method, the researcher used the area under the health curve to define the amount of health available to a project. In order to determine this area, the health curve was integrated as shown in the following equations:

$$\int_{g_1}^{g_2} \frac{1}{2}X^{1/2}dX = \frac{1}{3}g_2^{3/2} - \frac{1}{3}g_1^{3/2} \quad (16)$$

Where, g_1 was the lower limit of the integration and $g_2$was the upper limit. Within the researcher's diagnostic method, g_1, was always 4%, represented as the whole number four in the equation. The upper integration limit, g_2, represented the maximum eigenvalue comparison of a scenario with the unhealthiest scenario. When calculating the total health available for a project, g_2 was 100%, with 100 used in the equation. Integrating the curve

produced Fig. 7, color coded based on health regions that are used to qualitatively describe the health. The color coding and overall appearance of Fig. 7 provided the foundation for the visual aid created within the diagnostic method. Table 5 contains the values associated with the integrated health curve as well as showing the region boundaries in terms of both area and indicator value.

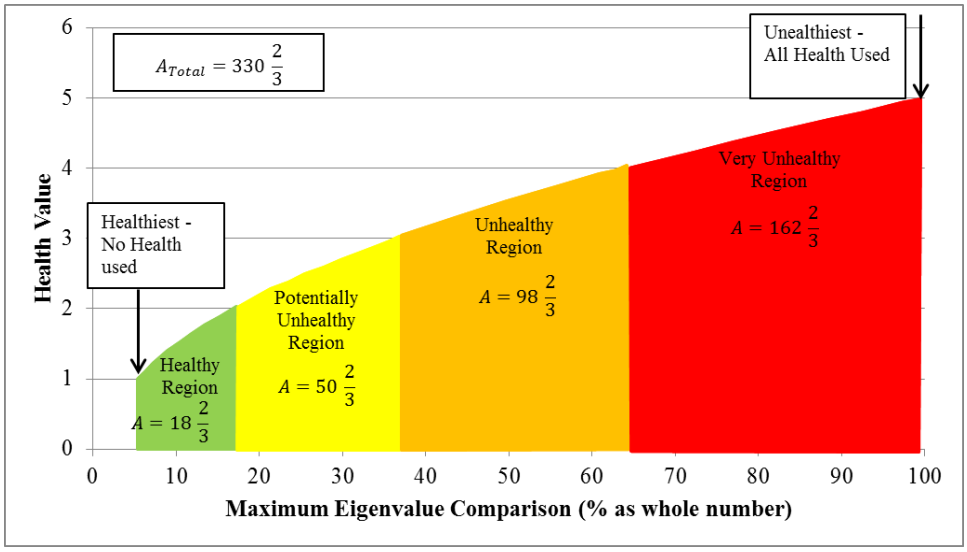

Fig. 7. Integrated health curve with health regions

Table 5. Health curve values

	Healthy Region	Potentially Unhealthy Region	Unhealthy Region	Very Unhealthy Region
Begin Indicator Value	1	2	3	4
End Indicator Value	2	3	4	5
Begin Area	0	18.67	69.34	168.01
End Area	18.67	69.34	168.01	330.68
Total Area	18.67	50.67	98.67	162.67
Cumulative Area	18.67	69.34	168.01	330.68

In the healthiest scenario, all data collection sections within all indicators have been assigned a one, creating the beginning of the health curve. At the healthy region to potentially unhealthy region, all indicators were populated with a two. For the potentially unhealthy region, the indicators are completely populated with a two at the left edge of the region and with a three at the right edge of the region. This continues through the unhealthy region and very unhealthy region with the unhealthiest scenario consisting of all data collection sections within each indicator populated with a five.

In reality, a project likely consumes a portion of available health, but is not in the healthiest or unhealthiest state. Because the health scenarios used to build the health curve consisted of weighted edge incidence matrices of the same value and only the maximum eigenvalue existed, the maximum eigenvalue of a project was compared with the unhealthiest option. This comparison allowed the researcher to determine the amount of consumed health for a project. While this value provides diagnostically useful information to decision makers about the overall health of a project, it remains somewhat vague as to

individual diagnostics. The researcher further developed the diagnostic method to provide drilled down information on the health of the project at different levels.

4.2 INDICATOR DIAGNOSTICS

To this point, graph theory has been used to determine the overall health of the project using a weighted edge incidence matrix, the calculation of eigenvalues, and the comparison of eigenvalues. To calculate diagnostically useful information for each of the indicators, the researcher employed a similar comparative analysis technique as the one described for the entire project.

4.2.1 Indicator Comparison Analysis

Initially, the researcher populated the weighted edge incidence matrix with a single indicator at the unhealthiest state and all other indicators as healthy as possible. Using this scenario, the eigenvalues were calculated, and as in the previous section a matrix populated in this way only produced a maximum eigenvalue. This calculation provided the researcher with the unhealthiest potential for a particular indicator and formed the value to compare other health options against. The different health options for an indicator were calculated in the same as they were calculated for the project as a whole. This is displayed below using a 3x4 matrix example and the indicator in the first row.

$$A = \begin{bmatrix} 5 & 5 & 5 & 5 \\ 1 & 1 & 1 & 1 \\ 1 & 1 & 1 & 1 \end{bmatrix} \text{ and } A = \begin{bmatrix} 4 & 4 & 4 & 4 \\ 1 & 1 & 1 & 1 \\ 1 & 1 & 1 & 1 \end{bmatrix} \text{ and } A = \begin{bmatrix} 3 & 3 & 3 & 3 \\ 1 & 1 & 1 & 1 \\ 1 & 1 & 1 & 1 \end{bmatrix} \text{ and } A = \begin{bmatrix} 2 & 2 & 2 & 2 \\ 1 & 1 & 1 & 1 \\ 1 & 1 & 1 & 1 \end{bmatrix}, \text{ and } A = \begin{bmatrix} 1 & 1 & 1 & 1 \\ 1 & 1 & 1 & 1 \\ 1 & 1 & 1 & 1 \end{bmatrix} \quad (17)$$

The calculation of the eigenvalues for these matrices and the comparison of each against the unhealthiest potential for an indicator resulted in the same health curve as shown in Fig. 6 and Fig. 7. But, once again, the actual indicator health within a project likely falls between the healthiest and unhealthiest scenario. Therefore, the actual indicator values are placed in the weighted edge incidence matrix, with the other indicator values held at their healthiest potential. This was done for each indicator and the eigenvalues for each indicator were calculated and corrected to maintain a mass-balanced network.

4.2.2 **Correction in the Indicator Calculation**

For the method to maintain consistency and coherent data movement across the edges in the graph, the researcher ensured the method consisted of a mass-balance structure in regards to the diagnostic information. For this to occur, the maximum eigenvalues for each indicator would need to sum to the maximum eigenvalue for the project as a whole. With a method built in this fashion, a manager, engineer, or decision maker could look at the project as represented by a network and see that the eigenvalues at one level can be summed to determine the eigenvalue at the next higher level. This also would allow for the consolidation of indicators to create systems of interest within a project. The health of these systems could then be reviewed to inform decision makers about specific needs within a project.

During the indicator comparison analysis, the researcher discovered that when an indicator was populated with the unhealthiest potential, the maximum eigenvalue for the weighted edge incidence matrix contained residual that must be removed to achieve the eigenvalue balance at each level. The residual came from the fact that the matrix consisting

of a single indicator (i.e. vector) of the unhealthiest values, also has non-zero vectors containing the healthiest value. The non-zero values contribute to the eigenvalue calculation. This contribution was calculated for removal and was termed as an absolute correction. For the weighted edge incidence matrix populated with all of the same value, the formula for the maximum eigenvalue was:

$$\lambda_{max} = inx^2 \tag{18}$$

When only considering a single indicator at the unhealthiest level and all others at the healthiest, the researcher developed the following formula to account for the absolute correction:

$$\lambda_{indicator:corrected} = \lambda_{indicator:calculated} - (i-1)n \tag{19}$$

Within the formula above, an eigenvalue was calculated for the weighted edge incidence matrix with a completely unhealthy indicator, noted as $\lambda_{indicator:calculated}$. The absolute correction removed the contribution of the other indicators, populated in the matrix as healthy as possible. The absolute correction took place by subtracting $(i-1)n$, where i is the number of indicators and n is the number of data collection sections. By subtracting one from i, only the indicators other than the unhealthiest indicator are included in the absolute correction.

When stepping through the comparison of the unhealthiest to healthiest possibility for a particular indicator, the maximum eigenvalue calculation simplifies to:

$$\lambda_{indicator:comparison} = nx^2 \tag{20}$$

However, corrected indicator eigenvalues required an additional correction when populating the weighted edge incidence matrix with actual project health values. When

calculating the eigenvalue for each indicator, the researcher discovered that after the initial absolute correction, additional residual remained between the summation of the indicator eigenvalues and the overall project eigenvalue. The sum of the indicator eigenvalues always exceeded the overall project eigenvalue. The researcher first determined the residual value requiring correction by:

$$\Delta = \sum_{i=1}^{i=i_f} \lambda_{indicator:calculated} - (i-1)ni - \lambda_{project:max} \quad (21)$$

Where, Δ is the residual value, the summation includes the maximum calculated eigenvalue for each indicator populated with project data, the term $(i-1)in$ accounts for the absolute correction across all indicators, and $\lambda_{project:max}$ is the maximum eigenvalue for overall project health.

When each data collection section within an indicator consisted of the same value, only one eigenvalue was produced and Δ after accounting for the absolute correction was zero. However, when an indicator consisted of a vector of differing values, Δ was not zero and the additional residual was removed from $\lambda_{indicator}$. The researcher determined the amount of correction to be applied to each indicator by evaluating the magnitude of the second eigenvalue. The size of the second eigenvalue related to the complexity of the matrix and indicator vector. The more complex the weighted edge incidence matrix or indicator vector, the larger the second eigenvalue. Case in point, when the weighted edge incidence matrix or indicator vectors were populated with all of the same value, only one eigenvalue was created. The simplicity of these matrices resulted in no additional eigenvalues and no additional correction beyond the absolute correction was required.

Upon discovering this nuance in the remaining residual, the researcher allocated the residual to correct $\lambda_{indicator}$ based on the second eigenvalue contribution to the summation of second eigenvalues. Therefore, the estimated correction applied to each indicator based on the complexity of each indicator was calculated as:

$$c = \frac{\lambda_{2nd:indicator}}{\sum_{i=1}^{i=i_f} \lambda_{2nd}} \Delta \tag{22}$$

Where, c is the estimated correction, $\lambda_{2nd:indicator}$ is the second eigenvalue for the indicator in question, the denominator is the summation of all second eigenvalues, and Δ is the residual after accounting for the absolute correction.

The final corrected indicator eigenvalue used within the mass balance structure of the network was calculated using the following formula:

$$\lambda_{indicator:final} = \lambda_{indicator:calculated} - (i-1)n - c \tag{23}$$

With the mass balance structure of the eigenvalues, the structure of the network allows future calculations to simply sum from one level to the next and use the comparison technique to determine the amount of health used. Fig. 8 shows this structure where the overall maximum eigenvalue for the project totals the sum of all corrected indicator eigenvalues. Fig. 8 also shows the inclusion of systems between the indicator and project levels. With the mass balance structure, these system can be interjected and contain whichever indicators are appropriate for that system. Indicators can belong to more than one system or function as a system by itself. For this reason, the mass balance occurs between the indicator level and whatever level falls above it within the analysis, but not necessarily from the system level to the project level. Using the equations already discussed, the

comparison can be made between the actual maximum eigenvalue and the unhealthiest potential value to integrate over the health curve.

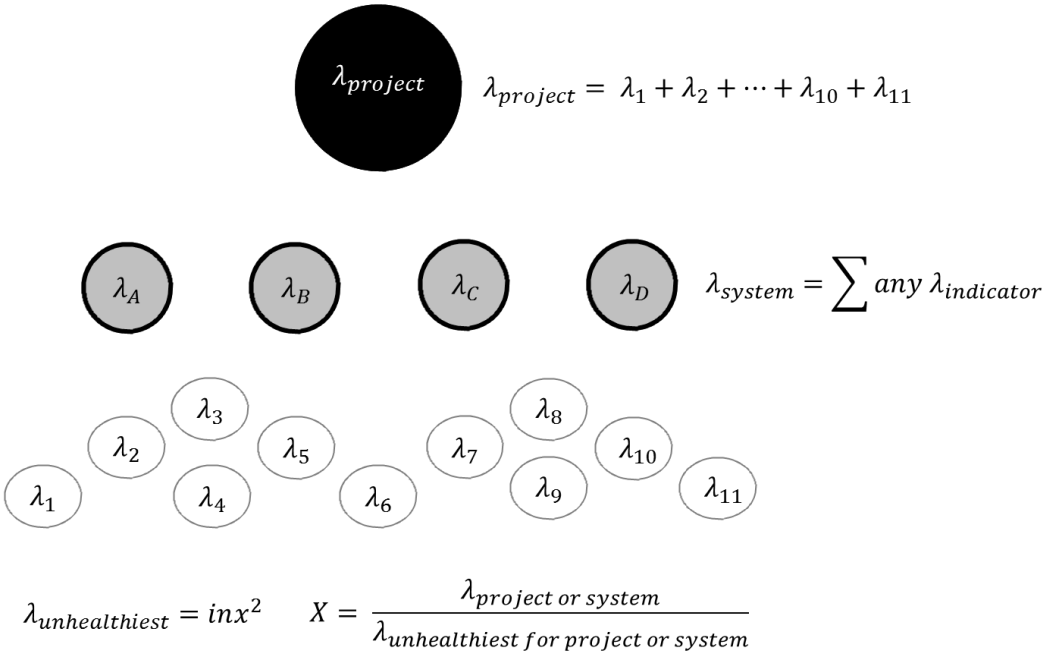

Fig. 8. Mass balance structure of the network

The four systems developed by the researcher to create a holistically diagnostic approach include:

- Pavement structural system
- Pavement surface system
- User safety system, and
- Roadside system.

The four systems represent an expansion of the use of network-level data by expanding into the safety and roadside arena. The specific development of these systems and the indicators

within each system are discussed in the Application of the Diagnostic Method chapter. For the work developed in this study and the application of the method, all indicators and subsequently all systems were assumed to have equal weight. The researcher suggests weighting indicators after producing diagnostic information. A central purpose of the method was to generate diagnoses that capture the actual health of the project. In future work, as the method is expanded for use in decision making, the different indicators or systems can be weighted depending on managing agency needs. The mass-balance approach created in the new diagnostic method helps with post-facto weighting because values are more fundamental after the diagnosis and can then be weighted as necessary.

Within the method developed by the researcher, integration over the health curve was consistent across all calculations because of the activation of the data from raw measurements to indexed values on a 1 to 5 scale. This activation simplifies the process and is highly encouraged and common in business analytic techniques, but is not required. While more complicated mathematically, it is possible for all indicators to use different scales. The mathematical structure holds and the power law to the ½ power remains constant, but the leading coefficient changes. The estimated correction also requires additional care because the second eigenvalues vary based on matrix complexity and relative to the size of the scale. Therefore, it behooves managing agencies to consider activating the data in the way the researcher chose and discussed in the Indicator Selection and Data Activation chapter.

4.3 SECTION BY SECTION DIAGNOSTICS

The two preceding sections describe the calculations required to determine the overall health of a project and the health of the individual indicators that comprise the overall health. In addition to these calculations the mass-balance approach developed by the researcher shows how health systems can be created within a project. These systems can be individually analyzed for diagnostically relevant information. The method developed is flexible enough to allow for the addition of other indicators or the construction of other systems. However, the method was built upon analyzing projects, meaning a decision maker has selected a particular pavement length for consideration. Once this occurs, diagnostically useful information can be developed, but decision makers might find the need to diagnostically drill down into a specific section. To continue the health analogy, a patient might be diagnosed with heart disease, a useful diagnosis for prescribing medicine and making lifestyle changes. However, additional testing might find that a particular artery requires a stint. To this point, calculations have been described that are similar to the overall diagnosis of heart disease, allowing for fairly detail prescriptive assumptions to be made. The follow discussion details the expansion of the method to drill down to the section level.

4.3.1 Matrix Structure for the Section Level

The researcher chose to expand the matrix structure to the section level. The expansion of the matrix structure allowed the researcher to maintain continuity in the mathematical structure by capitalizing on the descriptive nature of eigenvalue calculations. The matrix for each section consisted of rows populated with indicators and columns populated with systems. This structure created a matrix of size 11x4 for each section. While specific

indicators and structures were used by the researcher to develop a diagnostic technique, the analytical structure described below remains ambiguous. The ambiguity is intentional to show how the method could be expanded or adapted in future work.

Within a data collection section, each system represents a vector to populate the matrix. Each system vector includes an entry for each indicator, regardless of whether or not that indicator is included within the system. When an indicator is not included in the system, the vector location associated with that indicator receives a zero. The matrix representation of this structure assuming four systems ($a, b, c,$ and d) and 11 indicators (1 thru 11) is:

$$|S_k| = \begin{bmatrix} a_1 & 0 & 0 & 0 \\ a_2 & b_2 & 0 & 0 \\ 0 & b_3 & 0 & 0 \\ 0 & b_4 & 0 & 0 \\ 0 & b_5 & c_5 & 0 \\ 0 & 0 & c_6 & 0 \\ 0 & 0 & c_7 & d_7 \\ 0 & 0 & 0 & d_8 \\ 0 & 0 & 0 & d_9 \\ a_{10} & 0 & 0 & d_{10} \\ a_{11} & 0 & 0 & d_{11} \end{bmatrix} \quad (24)$$

Where, $|S_k|$ is the matrix for section k, and $a_i, b_i, c_{i,}$ or d_i are the activated value on a 1 to 5 scale for indicator i in healthy system $a, b, c,$ or d. Where an indicator exists in two or more systems, the indicator values will be equal. For example in Equation 24, a_2 and b_2 are the same value because indicator 2 is included in both system a and b. When an indicator is not included in a system, a zero is used.

Because $|S_k|$ is an asymmetric matrix, the researcher multiplied it by its transpose to create a symmetric matrix and calculate eigenvalues. Using the descriptive nature of eigenvalues and the same comparison technique developed for the project as a whole, the

researcher expanded the method to determine the overall health of a section and the health of each system within a section.

4.3.2 **Section Level Health**

When populating $|S_k|$ with all of the unhealthiest potential values, the researcher assumed a data collection section had consumed all of its available health. The researcher then populated $|S_k|$ with various other health options in the same way as it was done for the project as a whole. When comparing the maximum eigenvalues from each health scenario with the unhealthiest scenario, the researcher discovered that the same master health curve and equation shown in Table 4 and Fig. 6 continued to hold. Therefore, the researcher filled the matrix with actual data collection section values, calculated the maximum eigenvalue, compared that value to the unhealthiest option, and integrated the health curve between the healthiest option and the actual health to determine the overall health of a pavement section.

While the above calculation provided overall health information about each data collection section, the researcher realized that health information could be provided about each system within a data collection section. The systems are not rigid and the method developed can be expanded to include more systems or modify the systems used by the researcher. The health of each system was calculated by populating $|S_k|$ with actual indicator values for the data collection, a value of 1 (i.e. the healthiest potential value) for indicators in other systems, and the zeros remain constant. Where an indicator existed in multiple systems, the actual value was used to maintain consistency. An example matrix for system a is:

$$|S_k| = \begin{bmatrix} a_1 & 0 & 0 & 0 \\ a_2 & a_2 & 0 & 0 \\ 0 & 1 & 0 & 0 \\ 0 & 1 & 0 & 0 \\ 0 & 1 & 1 & 0 \\ 0 & 0 & 1 & 0 \\ 0 & 0 & 1 & 1 \\ 0 & 0 & 0 & 1 \\ 0 & 0 & 0 & 1 \\ a_{10} & 0 & 0 & a_{10} \\ a_{11} & 0 & 0 & a_{11} \end{bmatrix} \quad (25)$$

The maximum eigenvalue for the matrix shown in Equation 25 was compared with the maximum eigenvalue of the unhealthiest potential for system a. When the unhealthiest potential for a system was developed, the matrix in Equation 25 was populated with the value 5 where a_i values are currently shown. This method builds on the comparative technique used throughout the researcher's work and assumes the master health equation holds not only for the overall health of a data collection section, but for each system within a data collection section.

In reality, for systems at the data collection section level, the researcher discovered that the master curve serves as a good approximation but should not be viewed as an absolute calculation. The project level calculations were simplified because each row represented an indicator vector that could be held static and every other indicator could be set to a static value with no cross-over values or zeros. At the project level, when creating the comparisons, only maximum eigenvalues were generated. Furthermore, when calculating the actual indicator health eigenvalues, contribution of other indicators could completely be subtracted with the absolute correction and the additional residual generated

by the complexity of the matrix could be minimized using the relative size of the second eigenvalue.

At the section level, the cross-over of indicators between systems and the presence of zeros leads to the presence of four eigenvalues even when the matrix is simplified to the unhealthiest potential for a group of indicators within a particular system. Fortunately, populating the data collection section matrix with different health values for indicators within a particular system leads to a good approximation of the master health curve, assuming that the healthiest possibility for any systems is fixed at a comparison of 4%. Examples of the section by section diagnosis are provided in the Application of the Diagnostic Method chapter for the FM 1696, FM 1660, and FM 908 projects. Before applying the method, the actual indicators and the activation of network-level data to populate the indicators are described.

5. INDICATOR SELECTION AND DATA ACTIVATION

This chapter presents the method developed to activate the network-level data and populate the indicator level. The data collection section level consisted of raw data measurements, while the indicator level consisted of activated data indexed to a 1 to 5 scale. Several of the indicators incorporate network-level data not previously available, but believed by the researcher to become prevalent within industry. In anticipation of these data becoming available, the researcher has included it into the diagnostic method to create a more holistic tool. The inclusion of new data, not previously captured or measured, can be integral into the success of building new analytical tools (Liebowitz 2014). To continue the doctor/patient analogy, the methods described in this chapter are similar to new tests available that can shed more light on a patient's condition.

The indexing of data occurred within a process referred to as data activation. Raw network-level measurements were activated through data mining, additional calculations, application of design standards, and guidance from literature. The raw network-level measurements were direct attribute measurements taken from the network level. The indexing and activation of these measures converts the data into an active format for additional analytical processing. This initial step proves beneficial in transforming the data so that it may be combined in a matrix that ultimately permits the diagnostic method to acquire relevant health information about multiple indicators and systems within the project or length of interest. Indicators and systems function as more than attributes, rather they represent activated data that when passed through the diagnostic method offer practitioners

insight into the actual phenomena occurring within the project. The complexities of the activation varied from indicator to indicator and are discussed in the following sections.

5.1 ACTIVATION OF FATIGUE (ALLIGATOR) CRACKING MEASUREMENTS TO INFORM THE DETERIORATION RATE INDICATOR

Fatigue cracking, also referred to as alligator cracking, is a common distress measured by highway agencies and stored in PMSs. Often, decisions are made about the health of a pavement by looking only at the current measure of alligator cracking. This approach is akin to a doctor making a diagnosis without getting the necessary information on previous illnesses or family history. While the current measure of alligator cracking tells decision makers something about the pavement, it does not tell the entire story. Therefore, the researcher developed a method to determine the deterioration rate for data collection sections within a project based on the determined age of the entire project.

Pavement projects consist of multiple data collection sections that function similarly to products manufactured in a manufacturing process. In the manufacturing sector, processes are often evaluated for stability and compliance by comparing the measurements of manufactured parts with predefined limits. Typically, manufacturing processes have a normal distribution where the mean value serves as the target value and multiples of the standard deviation or standard error (SE) serves as limiting boundaries. The behavior of deterioration rate does not have a normal distribution across a network, nonetheless adaptations to process control methods allowed the researcher to develop a temporal data mining tool to determine the deterioration rate.

Similar to the body aging, deterioration of the pavement structure is expected and the deterioration rate is expected to increase as the age of the pavement increases. This is a departure from standard process control applications where the target value is typically static, but for pavements the target value shifts with the anticipated deterioration. As a comparison to process control methods, the target value for a data collection section would be at or below the expected deterioration curve, while warning limits are akin to rapid deterioration, and action limits are akin to very rapid deterioration. Before determining the deterioration rate, the current age of the pavement was determined.

The age in question was actually the age of the project, not necessarily each data collection section. The date of last work action is often lost within the institutional framework or remains hidden in filed as-built plans. Even if the date of the last work action was known it does not guarantee that the pavement behaves as expected. Similar to the human body, depending on multiple variables, a 50 year old body can function like it is in its 30s or 80s. For this study, the researcher was interested in the age at which the pavement project was behaving and then the stability of each data collection section within the project.

In order to calculate the age of the pavement, a recently calibrated pavement prediction model for alligator cracking for TxDOT pavements was used (Gharaibeh et al. 2012). During age establishment, the researcher assumed the last work action consisted of a heavy rehabilitation, essentially resetting the pavement life. Using this assumption, a 10-year analysis period of distress density, and the cumulative sum (CUSUM) technique from process control methods was used to establish the pavement age for each section within a

project. The median age determined for all pavement sections was then used as the age for the entire project that was used for deterioration rate determination.

The CUSUM chart and method are effective in accounting for past data, making it an attractive technique for pavement distress history. This method required calculating a target value and then creating a table to subtract the target from the observed value within a section and summing the result in a cumulative fashion to generate a score. The median percent alligator cracking for sections with alligator cracking present was used as the target value to determine a pavement section's age. The median value for alligator cracking displays stability over the 10-year analysis window as shown in Appendix B. Also in Appendix B is the detailed description of the data mining methodology.

Using the project age as the reference point to develop deterioration rate curves for the control chart, the researcher established four limit lines that divide the deterioration rate into five potential zones. The zones and the definitions for each zone are:

- Over-performing zone – zone where data collection sections have less alligator cracking than expected based on the age of the project and assuming the last work action was a heavy rehabilitation.
- Slow deterioration zone – zone where data collection sections fall below a curve that assumes the previous work action was a medium rehabilitation performed at the calculated pavement age and above the over-performing zone.

- Moderate deterioration zone – zone where data collections fall below a curve that assumes the previous work action was a light rehabilitation and above the slow deterioration zone.
- Rapid deterioration zone – zone where data collections fall below a curve that assumes the previous work action was a preventative maintenance action and above the moderate deterioration zone.
- Very rapid deterioration zone – zone above all other zones.

Various work actions were used to set the limit lines because these actions are defined in a way that determined the expected rate of deterioration within the prediction model. Lighter treatments are expected to deteriorate more rapidly than heavier treatments, thus permitting the researcher to establish different deterioration zones on the control chart. Fig. 9 shows an example control chart for the FM 1696 project.

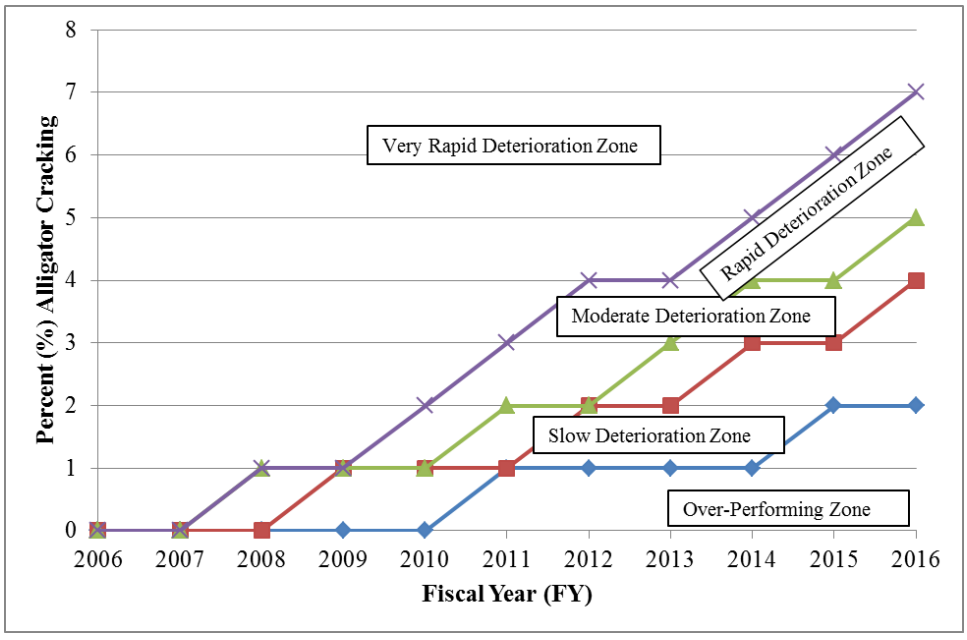

Fig. 9. FM 1696 project alligator cracking control chart

With five potential deterioration rate zones, the conversion to a 1 to 5 scale is obvious with 1 corresponding to the over-performing zone and 5 corresponding to the very rapid deterioration zone. The indexed values represent activated network level data and eventually populate a vector at the indicator level that falls within a weighted edge incidence matrix for additional diagnostic calculations. Table 6 shows the activated values for FM 1696, along with the deterioration rate for each data collection section. Appendix B contains age determination tables, control charts, and activated data tables for each of the projects used within the study.

Table 6. FM 1696 Activated alligator cracking values

Sect. No.	BRM	ERM	Deterioration Rate	Indexed Deterioation Rate
1	642	642.5	Rapid	4
2	642.5	643	Very Rapid	5
3	643	643.5	Very Rapid	5
4	643.5	644	Over Performing	1
5	644	644.5	Rapid	4
6	644.5	645	Very Rapid	5
7	645	645.5	Very Rapid	5
8	645.5	646	Very Rapid	5
9	646	646.5	Very Rapid	5
10	646.5	647	Moderate	3
11	647	647.5	Over Performing	1
12	647.5	648	Over Performing	1
13	648	648.5	Slow	2
14	648.5	649	Slow	2
15	649	649.5	Moderate	3
16	649.5	650	Rapid	4
17	650	650.5	Moderate	3
18	650.5	651.1	Moderate	3

5.2 ACTIVATION OF CURRENT RUTTING MEASUREMENTS TO INFORM THE RUTTING INDICATOR

Rutting represents a common pavement distress measured by SHAs. Network-level rutting data within TxDOT's PMIS was determined not to be reliable enough to perform a temporal analysis. With historically reliable rutting data and calibrated prediction models for rutting, a similar process control technique to the one used for fatigue cracking could be used. However, an attempt to do this will often find that the age calculation for rutting will not always match the age calculation determined for alligator cracking or other distresses.

The researcher decided to include current rutting in the diagnostic process by using mobile LiDAR measurements for rutting. Rutting measurements were made on 0.305 m (1ft.) increments moving in the direction of travel with measurements recorded approximately 7.5 cm (3 in.) apart in each wheel path.

The activation and indexing of rutting proceeded straightforwardly, using the discrimination points currently used by TxDOT to define rut severity. Table 7 shows the depth of rut and index values used to populate the rutting vector within the weighted edge incidence matrix.

Table 7. Rut depth indexing limits

Index Value	Rut Depth, mm (in.)	Rutting
5	Greater than 50.80 (2.0)	Failure
4	25.40 (1.0) to 50.80 (2.0)	Severe
3	12.07 (0.5) to 25.4 (1.0)	Deep
2	6.35 (0.25) to 12.70 (0.5)	Shallow
1	0 (0) to 6.35 (0.25)	None

5.3 ACTIVATION OF RIDE DATA TO INFORM THE DYNAMIC LOADING INDICATOR

The researcher chose to create a dynamic loading indicator for two reasons. First, to capitalize on ride quality data stored within a SHA's PMS. And second, to include an indicator in the diagnostic process that would provide an engineer with an understanding of how quickly the roadway might deteriorate due to disparate loadings. Dynamic loading occurs because of the profile differences in the right and left wheel paths, leading to an oscillating movement about the vertical axis. These surface induced loads can lead to premature failure or under prediction of distress manifestation and growth (Bilodeau et al. 2017).

TxDOT's PMIS contains many years of IRI measurements in each wheel path. In order to activate the stored data, the researcher exported 10 years of left and right wheel path IRI measurements. The researcher used the 0.095 m/km (6 in./mi) threshold provided in TxDOT's Standard Specification to compare wheel paths. Within TxDOT's Standard Specifications, 0.095 m/km (6 in./mi) is used to establish a threshold when referee testing is

required when comparing two profiles. When two profiles are within this range, TxDOT is willing to assume the profiles are the same. Therefore, when comparing the left and right wheel path IRI values, when the two profiles fall within ±0.19 m/km (±12 in/mi), the researcher assumes no dynamic loading occurs. The value is ±0.19 m/km (±12 in/mi) rather than ±0.095 m/km (±6 in/mi) because the left wheel path could be 0.095 m/km (6 in./mi) different than its actual profile, as could the right.

In order to finalize data activation, each section was analyzed over the 10 year period and the maximum dynamic loading value was used to populate the weighted edge incidence matrix. The worst case scenario was chosen to account for the potential maintenance applications that have been used to improve the roadway, but not solve the problem. The indexed values used to populate the weighted edge incidence matrix for this indicator are shown in Table 8.

Table 8. Dynamic loading indexing limits

Index Value	Difference in Wheel Path IRI, m/km (in./mi)	Dynamic Loading Description
5	Greater than ±0.76 (±48)	Very High
4	±0.76 (±48)	High
3	±0.57 (±36)	Moderate
2	±0.38 (±24)	Low
1	±0.19 (±12)	None

5.4 ACTIVATION OF PUBLICALLY AVAILABLE SOIL DATA TO INFORM THE SOIL INDICATOR

Soil data represents a source of publically available data that was combined with traditional SHA PMS data and newly created network-level data. Inclusion of network-level soil data provided a diagnostic feature that can guide engineers on the quality of the subgrade materials and the potential need for stabilization of modification.

Using open source QGIS™ software, the researcher used roadway shapefiles publically available through TxDOT to build new shapefiles that were exported into the WSS. Creating a 15.24 m (50 ft.) buffer on each side of the roadway centerline, 30.48 m (100 ft.) wide shapefiles were created. The researcher chose 3.22 km (2 mi) as the standard length of the shape file. This length was chosen through an iterative process to determine an appropriate length to capture changes in soil conditions without compromising the scale within the WSS.

The WSS provides an Engineering Properties Report that includes the AASHTO soil classification. The Engineering Properties Report is divided into various depths with an AASHTO classification at each depth. The AASTHO system uses seven groups, listed as A-1 through A-7. With regard to subgrade quality, soils classified as A-1 through A-3 are typically considered excellent to good, while soils classified as A-4 through A-7 are fair to poor (Budhu 2015).

In order to attach a single indexed value to a data collection section, the researcher took the average indexed value for each depth and weighted it for a particular soil type based on the percent of the area interest for that soil type. The weighted indexed value then

captured the variety of soil within a 3.22 km (2 mi) stretch of roadway and populated the weighted incidence matrix. The indexing values were:

- Soil classification A-1, A-3, or bedrock was indexed to a 1,
- Soil classification A-2 was indexed to a 2,
- Soil classification A-4 or A-5 was indexed to a 3,
- Soil classification A-6 was indexed to a 4, and
- Soil classification A-7 was indexed to a 5.

5.5 ACTIVATION OF RIDE DATA TO INFORM THE ROUGHNESS CHANGE INDICATOR

As discussed in the Pavement Condition Data section, temporal ride data within TxDOT's PMIS does not necessarily come from the same lane from one year to the next. However, the ride data does come from the same roadbed. Therefore, the researcher evaluated 10 years of ride quality data using the average IRI value for each pavement related project. The fundamental assumption during this data activation technique was that the roadbed should remain somewhat static from year to year. The researcher noted when the ride quality changed significantly from year to year, defining significant changes as those that varied by more than ±0.19 m/km (±12 in/mi). Again, this value was selected because of its inclusion in TxDOT's Standard Specifications as the threshold value to identify differing profiles.

The researcher mined 10 years of ride quality data for each data collection section within a project and indexed the roughness change as the worst change within the 10 year

period using the indexing shown in Table 9. This indicator provides the SHA or engineer with an understanding of how much the roadbed changes from year to year.

Table 9. Roughness change indexing limits

Index Value	Difference in Wheel Path IRI, m/km (in./mi)	Roughness Change Description
5	Greater than ±0.76 (±48)	Very High
4	±0.76 (±48)	High
3	±0.57 (±36)	Moderate
2	±0.38 (±24)	Low
1	±0.19 (±12)	Very low

5.6 ACTIVATION OF RIDE DATA TO INFORM THE ROUGHEST YEAR INDICATOR

During development of the process, only the roughness change indicator was included for diagnostic purposes. After performing diagnostics on multiple projects, the researcher noticed that it was possible for a project to have very poor ride quality, yet the roughness change and the dynamic loading appeared healthy. What was occurring was that a roadway project reached a state that both wheel paths were very rough, yet the ride quality did not change from year to year, it simply remained bad put appeared healthy within the method. The difference between wheel path ride qualities was also nonexistent with each simply being very rough, thus the dynamic loading indicator appeared healthy.

In order to address this shortcoming, the researcher included the roughest year over a 10 year period as an indicator in the diagnostic process. The average IRI value was used and the researcher indexed the values based on TxDOT's current criteria as shown in Table 10.

Table 10. Roughest year indexing limits

Index Value	Average IRI, m/km (in./mi)	Roughness Change Description
5	>2.666 (169)	Very Rough
4	2.052-2.666 (131-169)	Rough
3	1.500-2.051 (96-130)	Medium Rough
2	0.932-1.499 (60-95)	Smooth
1	0.016-0.931 (1-59)	Very Smooth

5.7 ACTIVATION OF MOBILE LIDAR DATA TO INFORM THE HYDROPLANING POTENTIAL INDICATOR

The Hydroplaning indicator and the Deterioration Rate indicator are the two indicators with the most thorough activation procedure. The Hydroplaning Potential indicator was built upon mobile LiDAR data. Incorporating the new geometric dataset from mobile LiDAR facilitated the creation of a more holistic diagnostic tool. The tool created by the researcher provides practitioners with information about more than current pavement condition performance. Safety and roadside diagnoses are available by incorporating and effectively including a new geometric network-level dataset. The mobile LiDAR data was used to extract surface geometric measurements which were used to define drainage basins along the roadway. In reality, hydroplaning potential is a function of surface geometry (i.e., cross-

slope, longitudinal grade, and pavement width), surface texture, rainfall intensity, vehicle characteristics, and vehicle speed. Surface geometry and surface texture are the only variables within the control of the SHA.

Mobile LiDAR measurements were used to determine the water film thickness (WFT) at the point of largest water accumulation in the wheel path. The researcher chose to use two separate hydroplaning speed models to transition from WFT to a comparison of the calculated hydroplaning speed. This comparison provides SHAs and engineers an understanding of the risk for a particular roadway.

Before the researcher could calculate the hydroplaning speed, mobile LiDAR measurements were used to determine the drainage basins within data collection sections. The researcher structured the LiDAR data into 0.3048 m (1 ft.) x 0.3048 m (1 ft.) grids. Grids of this size contained multiple LiDAR readings, thus the minimum elevation from each grid was selected to construct the drainage basins. Using TopoToolbox, the D8 algorithm was applied to the gridded data to determine the flow of water along the pavement. The algorithm and TopoToolbox determined the accumulation of water at each cell and grouped cells belonging to the same flow path into drainage basins (O'Callaghan and Mark 1984; Schwanghart 2014).

Within each data collection section, the cell with the largest accumulation and associated drainage basin was found. Knowing the grid size, the accumulation was easily converted into area, allowing for additional calculations using combinations of the Rational Method and the continuity equation. The details and order of these calculations are shown in Appendix B.

Two models were considered for computing HPS. One was developed in the 1970s by Gallaway, and a more recent one was developed by Ong and Fwa using finite element methods (Gallaway et al. 1979; Ong and Fwa 2007). Each model considers various vehicular elements to estimate hydroplaning speed. While the calculation of WFD and subsequently WFT primarily come from the researcher's methodology to define drainage basins with mobile LiDAR data, the research chose a Monte Carlo simulation to capture the effect of the other variables.

Within the Monte Carlo simulation, the daily traffic was used as the number of iterations and all other variables were assumed to have a normal distribution. The use of a Monte Carlo simulation generated an average hydroplaning speed that was representative of the number of vehicles and the cross section of vehicles traveling on a particular stretch of roadway. The details of the Gallaway equation and the Ong and Fwa FEM model are provided in Appendix B, along with the mean values and standard deviations of for the other variables required in the Monte Carlo simulation.

Previous work found that during rain events, motorists will slow below the speed limit by 4.83 kph (3 mph) to 9.66 kph (6 mph), but the primary cause of slowing is visibility, not hydroplaning risk (Yassin et al. 2013). In other words, motorists expect the roadway to function in a way that hydroplaning is not likely. The 50-year, 15-minute storm event used in the calculations would generate enough rain that visibility would be impacted, so prudent motorists will likely reduce their speed by approximately 8.05 kph (5 mph). Therefore, the indexing mechanism used to activate the hydroplaning potential data into the weighted edge incidence matrix used 8.05 kph (5 mph) indexing windows. If the calculated hydroplaning

speed was within 8.05 kph (5mph) of the posted speed limit, the hydroplaning potential for that data collection section was said to be healthy and received a 1 on the 1 to 5 scale. The indexing proceeded in 8.05 kph (5 mph) increments until the difference was greater than 32.20 kph (20 mph) when the indexed value became a 5.

The inclusion of a measure of hydroplaning potential has not readily been included in network-level applications. The use of mobile LiDAR for data collection and the development of preprocessing techniques as part of the researcher's work allowed for its inclusion. By using a Monte Carlo simulation, the researcher was able to simulate realistic vehicle features that effect hydroplaning. Of the two hydroplaning planning speed formulas, the Gallaway equation typically produced estimated speeds between 3.22 kph (2 mph) and 4.83 kph (3 mph) slower than the FEM equation. For final activation, the slower calculated HPS value was used for a conservative approach.

5.8 ACTIVATION OF MOBILE LIDAR DATA TO INFORM THE TRAVELED WAY WIDTH INDICATOR

Traveled way width represents a safety related indicator that is not often rated at the network-level. While some SHAs store width information, it often gets stored outside of databases in as-built plans and does not typically get measured annually during a rating cycle. Mobile LiDAR provided the opportunity to measure traveled way width at the network-level for each data collection section within pavement projects.

Within this study, mobile LiDAR reflectivity data were used to determine the location of pavement striping and the interface between pavement and roadside vegetation.

Predetermined α-based search windows were included in the algorithm to find changes in the reflectivity data that would indicate a material surface change.

The researcher developed the lane width indexing and activation using TxDOT's Roadway Design manual. Design lane widths are based on daily traffic, roadway functional classification, and the extent of the planned project. 4R design requirements are the most robust and include new location and reconstruction projects. 3R projects include rehabilitation and require less extensive design elements.

While 4R design standards represent the ideal, 3R standards provide guidance on what is acceptable for the existing system. For activation purposes, the ideal represents a perfect indexed value. The traveled way width data was activated for inclusion in the weighted edge incidence matrix using the curves in Fig. 10.

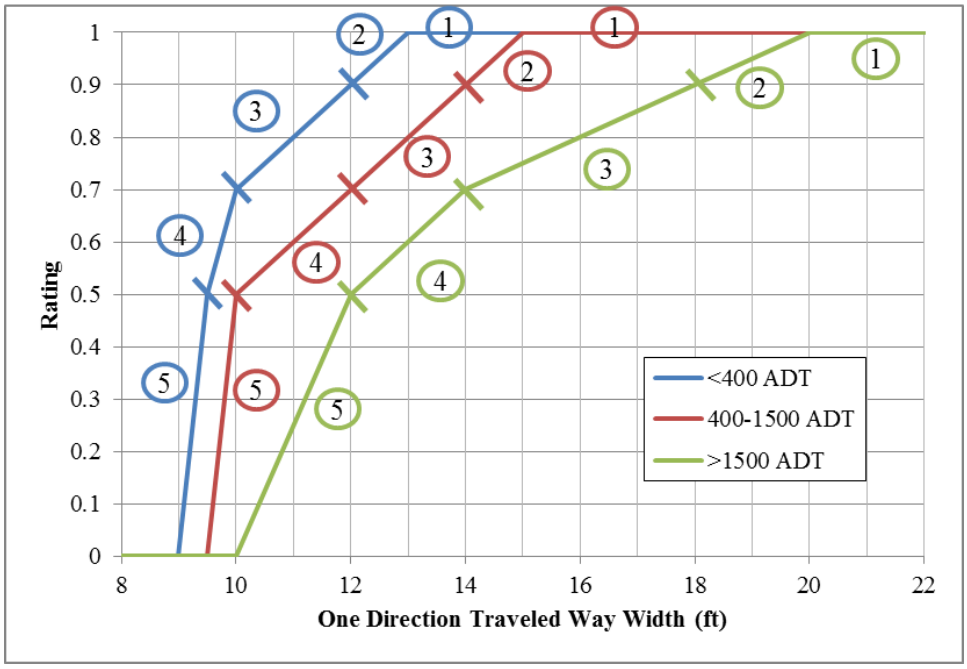

Fig. 10. Traveled-way width data activation curves

5.9 ACTIVATION OF MOBILE LIDAR DATA TO INFORM THE FRONT SLOPE INDICATOR

The front slope indicator represents a roadside indicator developed using mobile LiDAR data. The performance or health of front slopes at the network-level has not readily been included in roadway decision making until this study. However, as previously noted by the researcher, the likelihood of mobile LiDAR data becoming prevalent within industry will allow this type of information to become more involved in the decision making process. The use of it in this study serves as a proactive measure, setting the stage for its expanded use in the near future.

The front slope is the first portion of the roadside encountered by a vehicle that leaves the roadway. TxDOT's desirable front slope is 1m (1 ft.) vertical movement for every 6 m (6 ft.) horizontal movement (1V:6H) (Texas Department of Transportation (TxDOT) 2014c). A front slope is categorized in one of three ways: recoverable, non-recoverable, or critical. A recoverable front slope has a slope of 1V:4H or flatter. A non-recoverable front slope is traversable, but not recoverable. Slopes between 1V:3H and 1V:4H are often considered non-recoverable. Front slopes steeper than 1V:3H are considered critical because of the probability that a vehicle could overturn (American Association of State Highway and Transportation Officials (AASHTO) 2011).

Using 0.9144 m (3 ft.) x 0.9144 m (3 ft.) gridded LiDAR data for the roadside, the researcher extracted 176 front slope measurements within each 161 m (0.1 mi.) data collection section. The front slope measurements at each cross section were rated and the ratings were averaged for a data collection section. With 161 m (0.1 mi.) data collection

sections, the researcher chose to select the worst rated data collection section within an 805 m (0.5 mi.) data collection section to represent the 805 m (0.5 mi.) section in the diagnostic method.

The rating curve for front slope steepness was derived using design criteria. For slopes flatter than 1V:6H, no deduction was made because the flatness of this slope is desirable and flatter represents a safer condition. The indexing of the rating is shown in Fig. 11. The ratings allowed the data to be indexed (i.e. activated) to a 1 to 5 scale for inclusion in the weighted edge incidence matrix.

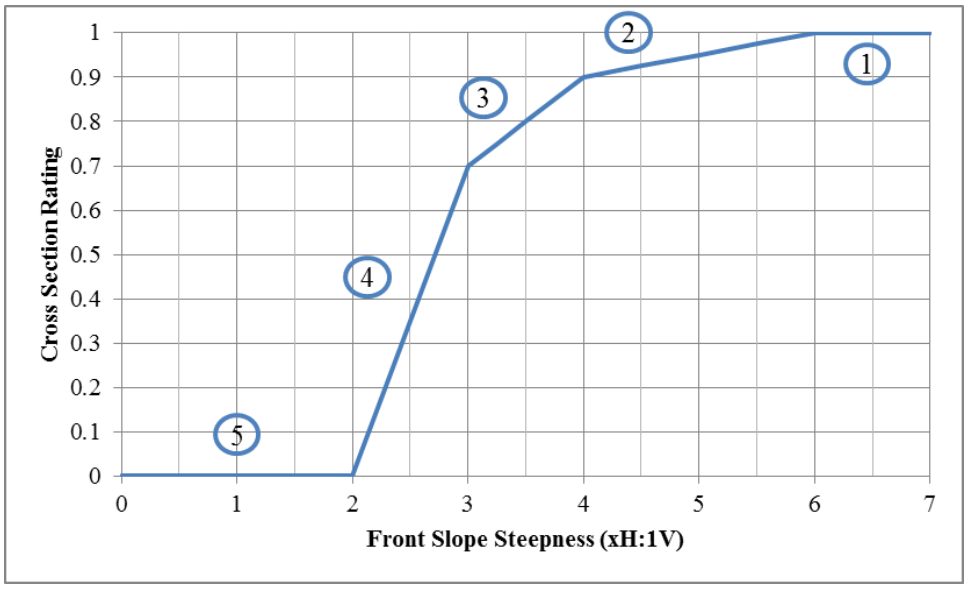

Fig. 11. Front slope indicator rating curve and indexing value

5.10 ACTIVATION OF MOBILE LIDAR DATA TO INFORM THE DITCH SLOPE INDICATOR

Similar to the front slope indicator, the ditch slope indicator and the data required to produce this indicator were not readily available at the network-level until this study. The use of mobile LiDAR measurements placed in 0.9144 m (3 ft.) x 0.9144 m (3 ft.) grids were used to generate the data needed.

The roadside consists of multiple drainage basins and for this study, the researcher was primarily concerned with drainage basins with flat slopes. Flat slopes lead to the silting-in of ditches, potentially raising the flowline upward toward the pavement structure. In a ditch with a flat slope and shallow depth, water could sit adjacent to the pavement for prolonged periods of time. The long sitting water could eventually be drawn into the pavement structure, weakening sublayers and accelerating deterioration.

The slope of the ditchline functions as a major contributor to water velocity. The researcher simulated water velocity under three different scenarios and discovered that water velocity begins to rapidly fall toward 0 m/s (0 ft./s) once the slope reaches 0.3%. Charts for the three scenarios are provided in Appendix B and included:

- Holding ditch geometry and Manning's *n* constant while varying water depth,
- Holding water depth and Manning's *n* constant while varying ditch geometry, and
- Holding water depth and ditch geometry constant while varying Manning's *n*.

The researcher activated the flowline slope measurements by indexing the values on the 1 to 5 scale. The mobile LiDAR data was originally processed in 161 m (0.1 mi.) data

collection sections. The researcher selected the worst flowline measurement from the five original data collection sections that were aggregated in the 805 m (0.5 mi.) data collection sections that were used for the project diagnostics. The researcher selected this approach to maintain a conservative perspective in the diagnostic process. In another conservative measure, the researcher selected 0.5% as the minimum acceptable slope rather than 0.3% to account for the difficulty in obtaining slopes to this level of precision in the field. The indexing values for data activation were:

- Slopes less than 0.5% receive a 5,
- Slopes greater than or equal to 0.5% and less than 0.7% receive a 4,
- Slopes greater than or equal to 0.7% and less than 0.9% receive a 3,
- Slopes greater than or equal to 0.9% and less than 1.0% receive a 2, and
- All slopes greater than or equal to 1.0% receive a 1.

5.11 ACTIVATION OF MOBILE LIDAR DATA TO INFORM THE DITCH DEPTH INDICATOR

The eleventh and final indicator included in the diagnostic method addressed ditch depth. Ditch depth represents another roadside feature included in the process to create a more holistic analysis than currently used. As with the other roadside features, front slope and ditch slope, ditch depth used mobile LiDAR data processed into 0.9144 m (3 ft.) x 0.9144 m (3 ft.) grids. For ditch depth, the gridded data created 176 depth measurements within a 161 m (0.1 mi.) data collection section. Eventually, the data had to be aggregated into an 805 m (0.5 mi.) data collection section. To do this, the researcher continued the conservative

approach and selected the worst value from the shorter data collection sections within the larger ones. With regard to ditch depth, the worst value was defined as the shallowest ditch.

TxDOT often includes a desired typical ditch depth in the typical sections within plan sets as shown in Fig. 12.

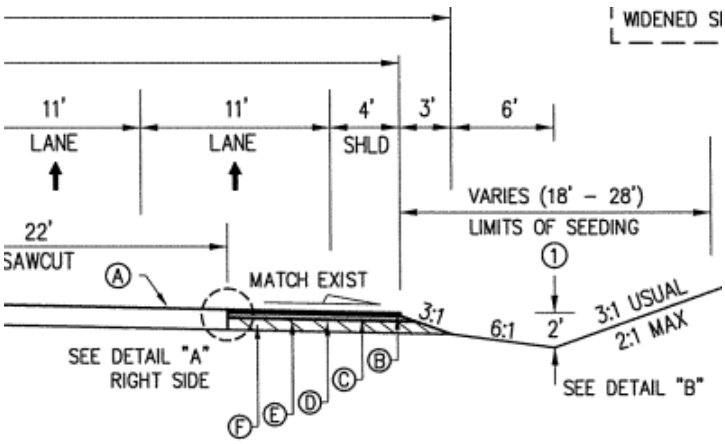

Fig. 12. Ditch depth shown in proposed typical section

Fig. 12 shows a measurement from the surface of the edge of pavement (EOP), a value easily measured using mobile LiDAR. Therefore, the ditch depth measurement used for diagnostic purposes was measured from the pavement surface and researcher had to account for the extra depth needed to get below the bottom of the pavement structure. Using feedback from TxDOT decision makers and guidance from literature, the researcher activated the ditch depth measurements by indexing them in the following way:

- Ditch depths greater than 1.07 m (3.5 ft.) received a 1 on the 1 to 5 scale,
- Ditch depths shallower than 1.07 m (3.5 ft.), but as deep as 0.76 m (2.5 ft.) received a 2,

- Ditch depths shallower than 0.76 m (2.5 ft.), but as deep as 0.46 m (1.5 ft.) received a 3,
- Ditch depths shallower than 0.46 m (1.5 ft.), but as deep as 0.30 m (1.0 ft.) received a 4, and
- Ditch depths shallower than 0.30 m (1.0 ft.) received a 5.

The activation scheme described above diagnostically drives toward having ditch depths deep enough to fall below the pavement structure. In the future, coupling ditch depth measurements with ground penetrating radar (GPR) measurements to determine layer thickness would allow the diagnostic process to activate data directly as it relates to the pavement structure in the field. This presents another potential advancement of this diagnostic work and illustrates the application of other technologies and how researchers can capitalize on other measures and include them in the diagnostic process created by the researcher.

5.12 DIAGNOSTIC INDICATORS SUMMARY

The 11 indicators used within the diagnostic method include indicators associated with the pavement structure, the pavement surface, user safety, the roadside. The integration of these indicators into a single diagnostic method represents an advancement of the use of network-level data by creating a holistic project tool. The different indicators required different analysis techniques in order to activate the data to a 1 to 5 scale for its use in the graph based diagnostic method. Existing guidance, current specifications, design standards, new data mining techniques, and simulations using new network-level measurements were used to

pre-process raw network-level measurements into useful data. The application of this method to actual pavement related projects in Texas is discussed in the next chapter.

6. APPLICATION OF THE DIAGNOSTIC METHOD

The researcher applied the diagnostic method to 10 pavement related projects from three different TxDOT districts. Three of the projects had detailed design plans available, while the other seven projects had a general description of work. All 10 projects are under construction or have been selected for construction during the 2018 fiscal year (FY). The application of the diagnostic method to actual construction projects allowed the researcher to investigate the realistic nature of the diagnostic method.

Within this section, it is shown that agreement exists between the diagnostic method and engineering plans. It is also shown that converting data into holistic diagnoses provides practitioners with information that has in the past been overlooked. Overall, the diagnostic method provides project developers, design engineers, and construction engineers with detailed information about the nature of the project using network-level data. This advancement allows managing agencies to get more out of network-level data currently being collected and streamline the scoping and design process. Finally the new method helps identify potential pitfalls that might be encountered during construction.

By comparing the information obtained from the diagnostic method to actual construction techniques designed by engineers, the researcher was able to determine if the diagnostic process identified the actual health needs of the pavement as it relates to the work prescribed by engineers. This type of comparison sheds light on whether or not the diagnostic process mimics engineering judgement and can provide engineers with a tool to better inform decisions earlier in the process with network-level data. This validation

functions differently than verification testing because no guarantee exists that engineering judgement and techniques provided in design plans are always correct. Therefore, in addition to comparing the method to design plans, other diagnoses were noted that offer engineers information that was not addressed in design plans.

The diagnostic method sought to capture foundational engineering knowledge that is nonexistent, hidden, or underexploited in network-level management systems. Future work can expand on these concepts within the diagnostic method to investigate verification of each indicator at a more fundamental level. The applications described below show that the researcher successfully created a diagnostic method that provides information about the health of pavement projects from ROW line to ROW line. These diagnoses coincide closely with items addressed in detailed design plans.

Table 2 in the Pavement Condition Data section of the Data chapter lists the projects used for application demonstration and method validation. The first three projects were those with detailed design plans.

6.1 CREATION OF SYSTEMS REQUIRING DIAGNOSTICS

In order to have a more holistic method, the researcher created a method by which a construction project's health, or any stretch of roadway requiring analysis, consisted of four systems informed by eleven indicators. Each system did not include all eleven indicators; rather many of the indicators are assigned to a single system, while some indicators fall into multiple systems. The four health systems included in the project health analysis were:

- Pavement structural system

- Pavement surface system
- User safety system
- Roadside system

The four pavement related health systems function similarly to the multiple biological systems within the human body. For an ill patient, current symptoms might indicate a cardiovascular problem; however additional diagnostics might reveal an additional respiratory issue. In order to properly treat the patient, each system must be diagnosed and treated appropriately. In fact, for the human body to function correctly and efficiently, up to nine different organ systems must work together on multiple complex tasks (Villa-Forte). For roadways, each system must also remain healthy for the greater good. An adequate pavement structure will only remain adequate if surface water effectively drains away from the surface and away from the roadside without entering the pavement structure. Additionally, deep ditches might provide good roadside drainage, but if the depth comes at the expense of a steep front slope the safety system will become compromised.

The construction of these systems from maximum eigenvalue calculations and the comparison technique was described in detail in the Analytical Framework of the Diagnostic Method chapter. The establishment of systems and the health of those systems helped to provide visual information in an effective way. Using the initial diagnostic chart, an engineer can understand if the primary area of concern within a project is structural, surface related, safety related, or roadside related. The gauge chart used for this visualization quickly and holistically informs the engineer about the health of the project.

6.1.1 **Pavement Structure System**

The pavement structural system includes the deterioration rate, rutting, dynamic loading, and soil indicators. Deterioration rate describes the pavement's behavior as it relate to fatigue cracking and relates to the horizontal tensile strain at the interface between a fairly stiff surface layer and less stiff unbound sublayer. While rutting obviously has a surface component, it is also a function of the vertical strain on the top of the subgrade, thus also being structural in nature (Huang 2004). If rutting and deterioration rate are related to the strain near the subgrade interface, it logically follows that the soil indicator should also be included in the structure system. Dynamic wheel loads are a function of pavement smoothness. When these loads become large, damage can increase quickly (Taheri et al. 2012). The potential for dynamic loading to accelerate deterioration led to its inclusion in the structure system.

6.1.2 **Pavement Surface System**

The pavement surface system includes the rutting, roughness change, roughest year, and hydroplaning indicators. The use of the IRI to classify pavement roughness has a long history of use (Bryce et al. 2013). Rutting by definition is a depression of the pavement surface and therefore exists in both the structure and surface systems. As described in the Activation of Mobile LiDAR Data to Inform the Hydroplaning Potential Indicator section, hydroplaning is a function of many variables, including the pavement surface and roadway geometry.

6.1.3 **User Safety System**

The user safety system includes the hydroplaning, traveled-way width, and front slope indicators. The inclusion of these indicators in the safety system are self-explanatory, particularly in light of the crash statistics associated with run-off-the-road crashes referenced in the Roadway Information not Traditionally Used at the Network-Level section of the Literature Review chapter.

6.1.4 **Roadside System**

The roadside system includes the front slope, ditch slope, ditch depth, dynamic loading, and soil indicators. The first three indicators are obviously associated with the roadside geometry. Dynamic loading was included because the lateral support provided by the front slope can directly affect the smoothness of the outside wheel path. The soil indicator was included because poor soils are typically poorly draining, thus impacting the drainage elements associated with the roadside system. While the diagnostic system created by the researcher proves accurate, future work can explore the inclusion or removal of indicators from various systems.

6.2 FM 1696 DIAGNOSIS

The researcher processed FM 1696, from the Bryan district, through the diagnostic tool, generating the diagnostic plots in Fig. 13 and Fig. 14.

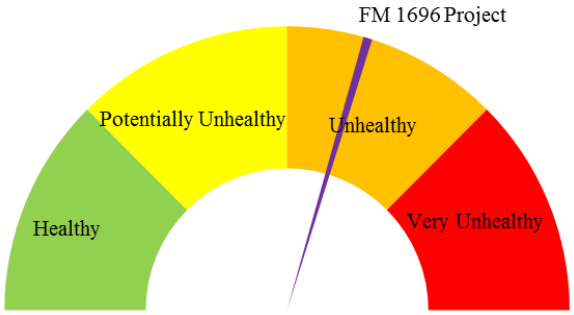

Fig. 13. FM 1696 project diagnosis

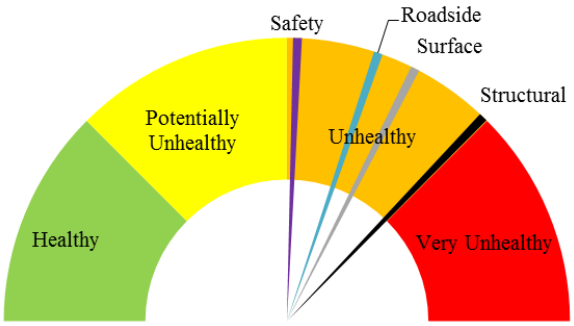

Fig. 14. FM 1696 systems diagnosis

FM 1696 presented as unhealthy and with all four project systems as unhealthy. The structural system exhibits almost very unhealthy diagnostic characteristics, while the safety system diagnostically falls within the unhealthy band, it only did so slightly. The diagnostic plot in Fig. 14 presents all four project systems on the same visual canvas, allowing decision makers to understand how each system presents with regards to health, but also how each system presents relative to each other. Fig. 14 indicates that more than just unhealthy structural issues along the roadway must be addressed within the project to appropriately solve the problems being faced.

6.2.1 **FM 1696 Systems Diagnoses**

Fig. 15 shows the FM 1696 structural system diagnostic plot. Fig. 14 intimated from a diagnostic standpoint that the structural system was the unhealthiest system, almost falling within the very unhealthy band. Fig. 15 provides insight as to why the structural system is unhealthy, driven predominantly by the very unhealthy behavior of the dynamic loading indicator and the soil indicator. On the other hand, the rutting indicator presents as potentially unhealthy, but the healthiest of all structural indicators. The deterioration rate falls within the unhealthy band, but the relative distance between deterioration rate and dynamic loading load was large. Fig. 15 allows the decision maker to visually see that dynamic loading and soil conditions must be addressed within the planned project.

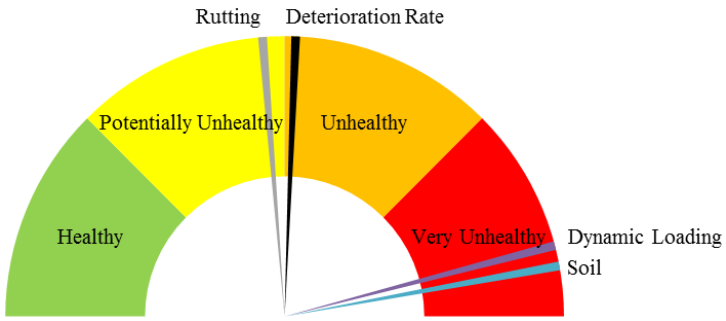

Fig. 15. FM 1696 structural system diagnosis

Addressing the dynamic loading issue and the soil issue with a specific work action begins to enter the scoping phase of a project, beyond the scope of the researcher's present work. Nonetheless, a decision maker's thought process quickly moves from diagnostics to potential treatments. Continuing the health analogy, doctors often have a potential treatment in mind based on initial diagnostics. The doctor might use the initial diagnostics to begin a

treatment while performing additional tests to verify the diagnosis and prescribe a final treatment that hopefully address the immediate and long term needs of the patient. The roadway diagnostic tool created within this work provides roadway decision makers similar techniques. For example, FM 1696 clearly has soil condition issues implying a project should include soil stabilization or soil alteration. Moving forward in the project development process beyond diagnostics, engineers can plan and budget for this work action while also planning for additional in-situ testing to determine if a stabilizer such as cement is more appropriate than an altering and stabilizing agent such as lime. To complete the analogy, if a patient presents as overweight, with high blood pressure, and chest discomfort, a cardiologist will likely implement a treatment to mitigate the potential for a heart attack while performing additional tests to verify the best treatment moving forward.

Fig. 16 shows the surface system diagnostic plot for FM 1696. Overall, the surface system was diagnosed as unhealthy in Fig. 14. Fig. 16 shows that hydroplaning, roughness change, and roughest year behave similarly with regards to health, falling near the upper limit of the unhealthy band. Rutting, considered a cross-over indicator between the structural system and the surface system, pulls the overall health diagnosis back toward the middle of the unhealthy diagnostic band by falling within the potentially unhealthy area.

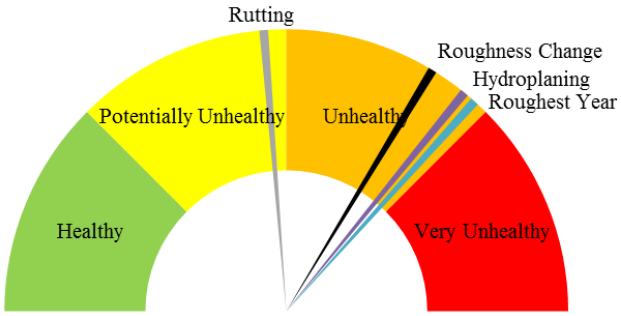

Fig. 16. FM 1696 surface system diagnosis

Considering the diagnostics presented in Fig. 16 with those in Fig. 15, the overall health of the project becomes more focused. Using the diagnostic plots, more informed conclusions can be drawn about the behavior of FM 1696. From Fig. 15, engineers know that high dynamic loading impacts the health of FM 1696. Dynamic loading refers to the difference in ride quality of the outside wheel path to the inside wheel path. The unhealthiness of this indicator is reinforced by the unhealthiness of the roughness change indicator included in the surface system and shown in Fig. 16. The roughness change indicator describes how the ride quality changes from year to year along the same roadbed. For FM 1696, if the outside wheel path is much rougher than the inside wheel path, it is not surprising that the loading impact of this can lead to large ride quality changes, particularly when soil conditions are poor.

The hydroplaning indicator is the first indicator associated with the new surface geometry rating tool developed by the researcher. The hydroplaning indicator falls close to the unhealthy/very unhealthy interface. From a project perspective, engineers might assume that if the scope includes repairing the pavement structure, the pavement surface will also be repaired, mitigating hydroplaning potential by improving the geometry. While potentially

true, from a diagnostic perspective it is important not to let potential scope undermine the diagnostic information. The diagnostic information indicates hydroplaning potential, while also indicating rutting is only potentially unhealthy. If the roadway was significantly rutted, high hydroplaning potential would not be surprising, but a lack of rutting indicates other elements are impacting the health of the hydroplaning indicator. These other factors could include posted speed limit or other surface geometric characteristics.

Fig. 17 shows the FM 1696 safety system diagnostic plot. Fig. 14 provides the knowledge that the safety system is the healthiest of all four systems along the proposed project. The safety system receives an unhealthy diagnosis, but the visual aid perspective created in Fig. 14 informs the engineer that while unhealthy, the safety system almost receives a potentially unhealthy diagnosis instead. All three of these indicators come from the LiDAR based network-level surface geometry tool created by the researcher as part of this work. Hydroplaning was discussed in the preceding paragraph and visually presents in the same location in Fig. 16 and Fig. 17. The researcher designed the diagnostic method so that indicators appearing in multiple systems visually present in the same location.

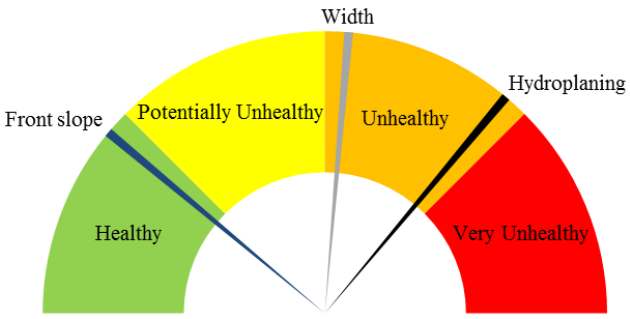

Fig. 17. FM 1696 safety system diagnosis

The width indicator of FM 1696 is unhealthy, but the front slope indicator is healthy. Healthy front slopes with unhealthy width and very unhealthy dynamic loading implies that widening could be beneficial for this project and might be accomplished within the existing ROW footprint. Healthy front slopes describe the actual conditions in such a way that the front slopes can be steepened without compromising the health of this indicator. Front slopes could be steepened by widening the roadway but keeping the ditch lines at the current configuration. Widening naturally improves the health of the width indicator, but might also improve the dynamic loading indicator by moving the outside wheel path inward away from the unconfined edge. This should improve the health of the dynamic loading indicator as long as the front slopes are not steepened to the point that lateral support becomes compromised.

While describing the safety system diagnosis, the researcher noted that width could be improved and that front slopes could likely be steepened by keeping the ditch lines at their current configuration. Within the diagnostic tool, the potential measures described above can be further analyzed by reviewing the diagnostic plot of the final system, the roadside system. Fig. 18 is the FM 1696 roadside system diagnostic plot.

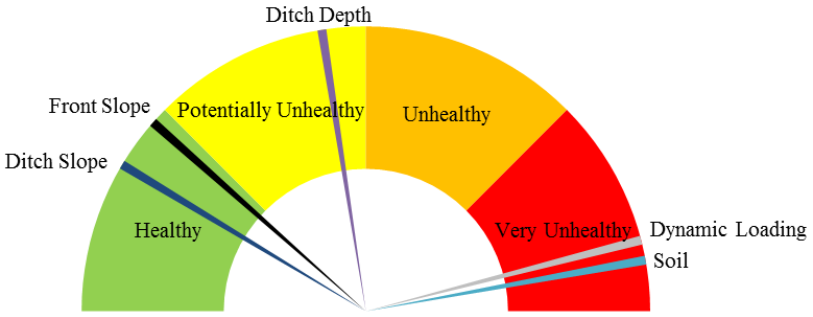

Fig. 18. FM 1696 roadside system diagnosis

Front slope, ditch slope, and ditch depth are all indicators created as part of the new network-level geometric dataset. All indicators but ditch slope and ditch depth have previously been described. Ditch slope presents as healthy, indicating the longitudinal fall parallel to the roadway is performing well. Ditch depth is potentially unhealthy and falls near the upper limit of the potentially unhealthy band. With this in mind, deepening the ditches might be advisable, but it could be offset by the amount of longitudinal fall within the flowline. With regards to diagnostic information guiding a preliminary scope, with the need to improve dynamic loading and width, healthy front slopes and good ditch flowline fall allow for roadway widening while leaving while leaving the ditch depths as they currently exist.

Overall, the FM 1696 project is an unhealthy project with the structural system the unhealthiest of all systems. The structural system is plagued by very unhealthy dynamic loading and soil indicators. The ride quality indicator was diagnosed as unhealthy and almost very unhealthy, along with the hydroplaning indicator. Width is slightly unhealthy.

6.2.2 **Comparison of FM 1696 Diagnoses with Construction Plans**

The description of work on the FM 1696 plan title sheet is "For the construction of rehabilitating existing roadway consisting of grading, structures, base, surface, signs and pavement markings." The overall work description describes a complete rehabilitation, an expected work action based on the diagnostic information provided using the new diagnostic tool.

Fig. 19 has the existing typical section for FM 1696 on top and the proposed typical section for the clay subgrade portion of FM 1696 on bottom. The existing typical section

shows that FM 1696 currently has a 7.32 m (24 ft.) paved surface over a 9.75 m (32 ft.) subgrade crown. The proposed section widens the paved surface to 9.14 m (30 ft.) over a 9.75 m (32 ft.) lime treated subgrade in the clay areas. The usual front slope increases from 6(H):1(V) in the existing section to 4(H):1(V) in the proposed section. Each of these elements agrees with the diagnostic information produced using the new diagnostic method. Widening the paved surface and treating the subgrade addresses the very unhealthy indicators, dynamical loading and soil. It also likely addresses roughest year and roughness change indicators that have a current health close to the very unhealthy line.

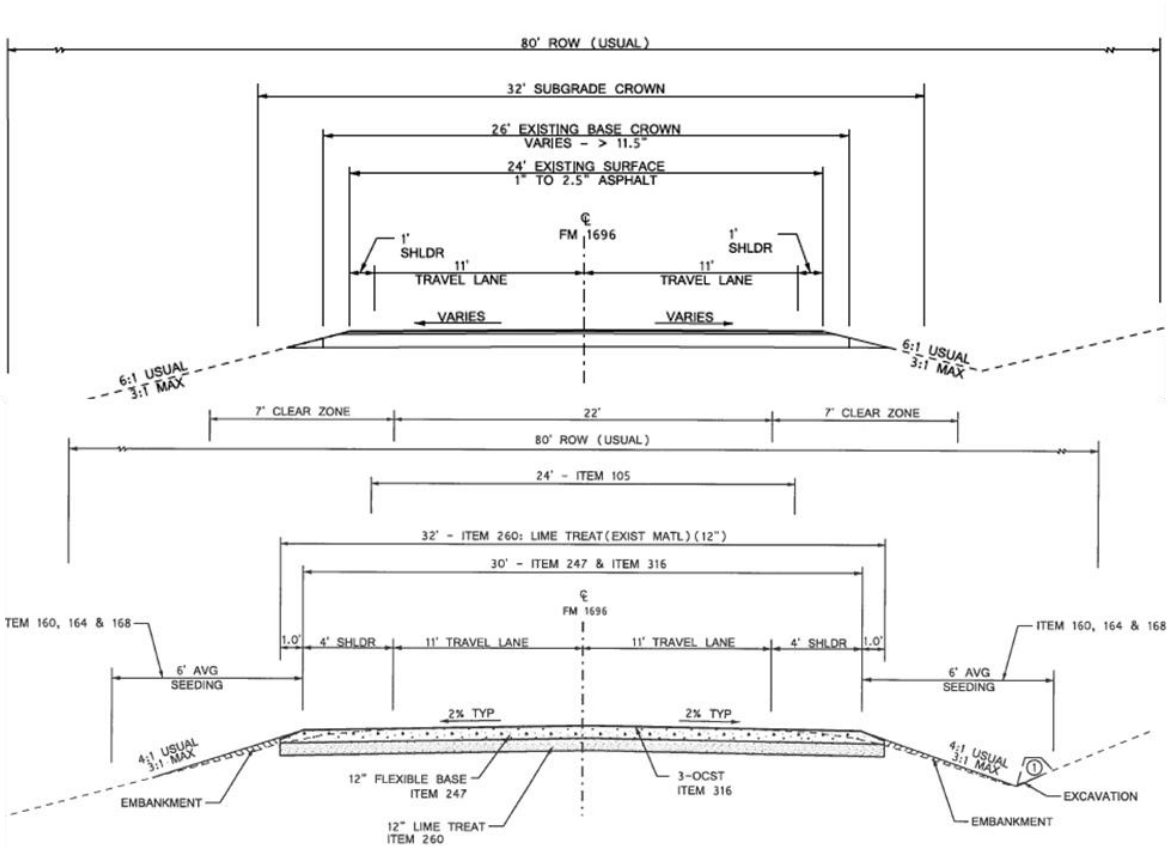

Fig. 19. FM 1696 existing and proposed typical section

What remains unknown from a review of Fig. 19 is whether or not the health of the hydroplaning indicator will be improved from the proposed construction. The title sheet for the project shows a design speed of 48 kph (30 mph) for FM 1696. A slow design speed is not surprising on a rural FM facility whose original construction likely dates to the mid-20th century or early, however the posted speed limit for the majority of the project is 112 kph (70 mph). The researcher constructed the hydroplaning health indicator by comparing the potential hydroplaning speed generated with a Monte Carlo simulation with the posted speed limit. In the case of FM 1696, the average hydroplaning speed for the entire project was 88 kph (54.97 mph) with a minimum hydroplaning speed of 82.75 kph (51.40 mph). Only one 0.1-mile data collection section had a hydroplaning speed above 112 kph (70 mph), while all others were below 96 kph (60 mph). Therefore, based on the geometry associated with a 48 kph (30 mph) design speed it will be difficult to mitigate the hydroplaning health without altering the geometry or lowering the speed limit. The plan and profile sheets within the plans show modifications to the vertical profile of the roadway profile grade, but no adjustments are made to the horizontal profile. The vertical alignment adjustments might improve hydroplaning health, but it cannot be known with certainty without applying the diagnostic method after construction. If a post construction diagnosis continues to indicate poor hydroplaning health, engineers can also review crash data to determine if the speed limit should be lowered. As a final note associated with hydroplaning health, the final surface on FM 1696 will be a seal coat, providing significant macro-texture if constructed properly. An increase in macro-texture also improves hydroplaning health, but the choice of a seal coat surface for FM 1696 likely had little to do with improving hydroplaning.

However, the fact that hydroplaning health can be included in the diagnostic process allows engineers to consider what surface should be placed to positively impact the hydroplaning indicator.

Fig. 19 provides proposed information for the clay subgrade portion of the project, consisting of the eastern 2930 m (9620 ft.) of the project. The remaining 10,640 m (34,900 ft.) of the project consists of a sandier subgrade and calls for the cement treatment of 200 mm (8 in.) of subgrade. Again, this reinforces the diagnosis of unhealthy soil and dynamic loading indicators, both of which can be effectively treated by treating the subgrade, regardless of the stabilizer selected. The change in subgrade type and stabilizer selection along FM 1696 shows that within a project health indicators can change. For FM 1696, the change was associated with the selection of stabilizer and does not impact the overall diagnosis, but it is possible that additional diagnostic analysis at a more micro-level can prove beneficial to engineers.

6.2.3 **FM 1696 Micro-Level Diagnostics**

The researcher developed a similar weighted edge incidence matrix technique to analyze the health of each data collection section. The technique used a generalize Laplacian to calculate maximum eigenvalues that could be used for comparison to determine individual section health. In addition, the health of each system within each section was estimated using the maximum eigenvalue and comparison technique.

The health of each section for the clay subgrade portion that received lime treatment of FM 1696 is shown on the left of Fig. 20, while the health of the cement treated portion is shown on the left. Overall, the health of the cement treated portion is slightly better, not a

surprising fact and one that helps validate the diagnostic method. Each section within the project was also diagnosed. The system diagnosis for section 642 is on the left of Fig. 21 and the diagnosis for section 645 is on the left. These two sections represent the unhealthiest and healthiest sections within the project. The diagnoses in Fig. 21 show that while safety was the healthiest system within section 642, it was the unhealthiest within section 645.

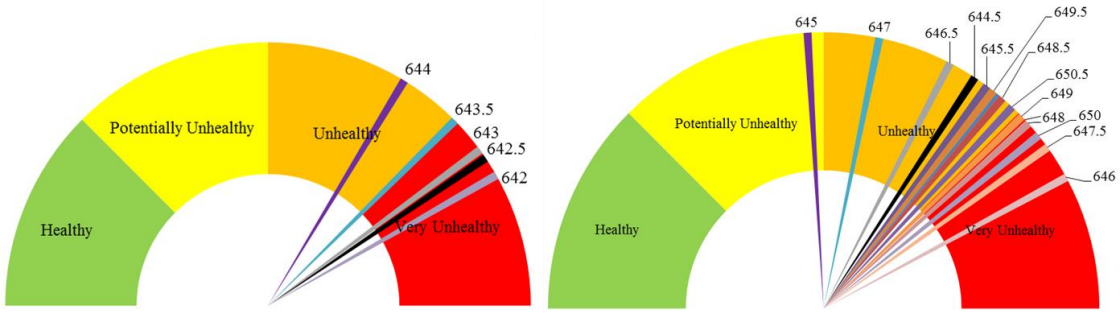

Fig. 20. FM 1696 section by section diagnosis

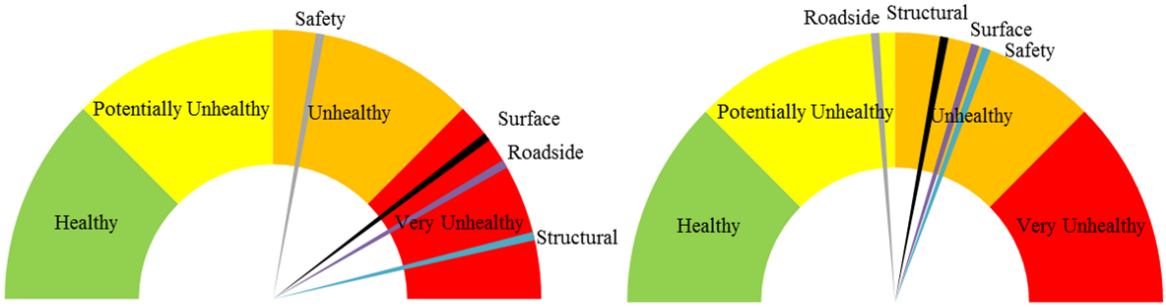

Fig. 21. FM 1696 healthiest and unhealthiest section diagnosis

The section by section diagnostics can help engineers dig deeper into project needs using only network-level data. The diagnostic information could be used to determine where additional testing or surveying is required. Additionally, the section by section diagnostic information could be used by maintenance supervisors to identify localized areas to perform

maintenance work. The expansion of the method to maintenance work shows its potential for other applications beyond analyzing already selected pavement projects.

The diagnostics for every section of FM 1696 are located in Appendix C. Also located in Appendix C is a radial style chart developed by the researcher to visually display the activated data for each indicator within each section. These charts do not require the mathematical rigor to create the graphical representation of the diagnostic information as the gauges charts required, but the charts represent the fundamental data within each node of the larger network. The representation of this data is valuable because it represents the active data used to create a weighted edge incidence matrix that becomes the building block for all other diagnostic calculations.

6.3 FM 1660 DIAGNOSIS

The researcher processed FM 1660 from the Austin district through the diagnostic process. The description of work for FM 1660, shown on the title page of the construction plans, was "For the construction of the rehabilitation of an existing road. Consisting of grading, structures, cement treat base, signing, pavement markings, and delineation." The diagnostic method produced the overall project diagnosis and system diagnoses shown in Fig. 22.

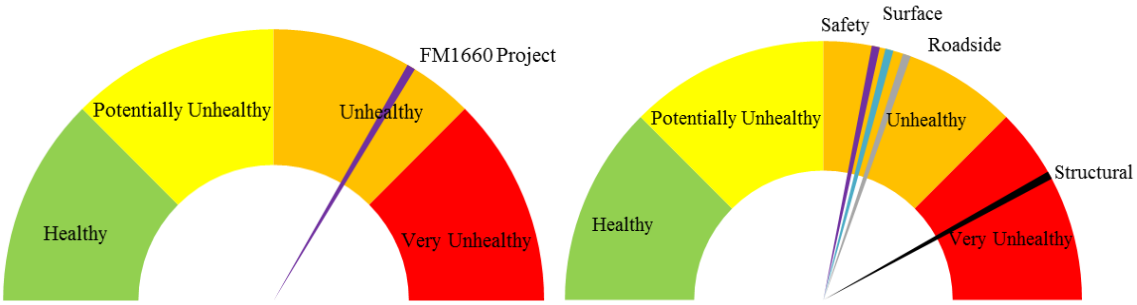

Fig. 22. FM 1660 project diagnosis and FM 1660 system diagnoses

6.3.1 **FM 1660 System Diagnoses**

The structural system for FM 1660 is the unhealthiest system by a large margin. While the surface, safety, and roadside systems are each diagnosed as unhealthy, the health gap between these systems and the structural system is large. The other three systems present in the lower half of unhealthy band. Drilling down into each system expands the diagnosis. The structural system diagnosis is shown in Fig. 23.

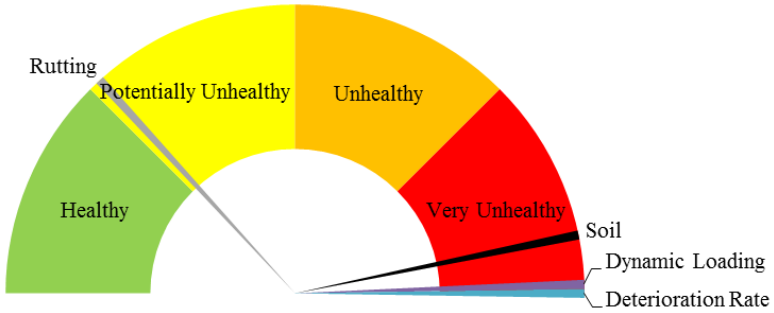

Fig. 23. FM 1660 structural system diagnosis

Structurally, FM 1660 has three very unhealthy indicators, deterioration rate, dynamic loading, and soil. A very unhealthy deterioration rate indicates that fatigue cracking has manifested and grown more rapidly than expected. In fact, deterioration rate is in the

unhealthiest possible state, informing the engineer that every section within the project was as unhealthy as possible. Very unhealthy dynamic loading and soil indicators exacerbate the deterioration rate problem by having weak subgrades that experience excessive pounding, likely accelerating deterioration. If the soil indicator was not also very unhealthy, it might be possible to simply reconstruct the pavement structure without the need to stabilize subgrade soils; however this was not the case.

Fig. 24 is the diagnostic plot for the surface system within the FM 1660 project. The ride quality indicators, roughest year and roughness change, both fall within the very unhealthy category.

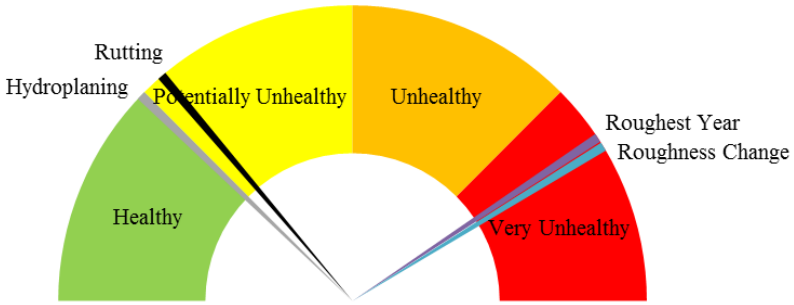

Fig. 24. FM 1660 surface system diagnosis

The safety system presented as the healthiest of the four systems within the project diagnosis. Fig. 25 shows that the width indicator is as unhealthy as possible. Initially, this might seem concerning for the diagnostic method because the safety system was the healthiest of all the systems, yet has an indicator in the unhealthiest state. While the safety system was the healthiest system, it was still within the unhealthy band. The overall health of the safety system was improved by the hydroplaning potential indicator falling very near

the healthy threshold and the front slope indicator residing just inside of the potentially unhealthy band. For this reason, the researcher developed the diagnostic method to build upon indicators in way that they could be dissected and visually displayed for engineers to drill down into the actual health of the project.

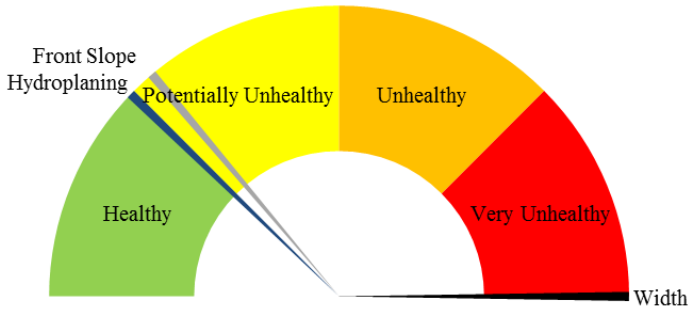

Fig. 25. FM 1660 safety system diagnosis

Fig. 26 shows the roadside diagnosis with the cross-over indicators from the structural system, soil and dynamic loading, as the only indicators that present as very unhealthy. The other three indicators were much healthier with ditch slope appearing to be very healthy. A healthy ditch slope indicates adequate longitudinal fall to move the water parallel with the roadway. The relative health of the ditch depth and front slope indicators allow for the movement of the ditch toward the ROW line to accommodate the pavement widening, which is need to address the poor width health.

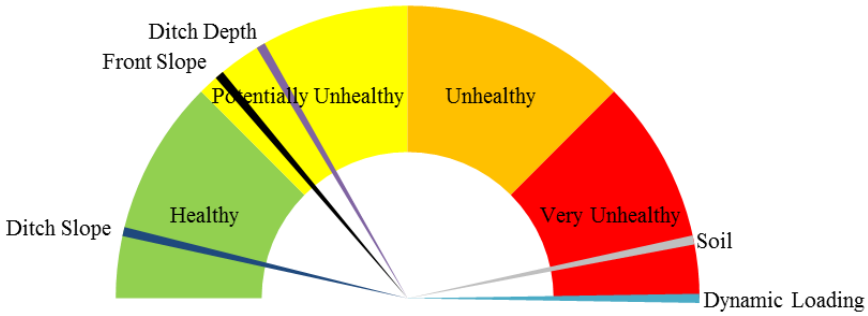

Fig. 26. FM 1660 roadside diagnosis

6.3.2 **Comparison of FM 1660 Diagnoses with Detailed Construction Plans**

Fig. 27 shows the existing typical section of FM 1660 on top and the proposed typical section on bottom. A pavement structure detail accompanies the proposed typical section in Fig. 27. The pavement structure detail indicates the construction project will cement stabilize a mixture of existing roadway material and new base material. Designing a more rigid pavement structure addresses the very unhealthy deterioration rate indicator. Widening the roadway from 6.7 m (22 ft.) to 9.8 m (32 ft.) addresses the very unhealthy dynamic loading indicator by adding a shoulder to the roadway, thus increasing lateral support for the outside wheel path and moving the outside wheel path away from the unconfined edge. The dynamic loading indicator also improves with the stiffening of the pavement structure. The very unhealthy soil indicator was not addressed in the construction project. A very unhealthy soil indicator suggested the need to stabilize subgrade layers which was not designed for FM 1660. A detailed pavement design might have shown that the cement treating the flexible base layer was structurally sufficient without treating the subgrade layers. Without full knowledge of the design process, this cannot be known for sure. However, the diagnostic method build by the researcher would allow engineers to use

network-level data to diagnosis the need to stabilize layers early on in the design process. This same data can provide this type of information on the network as a whole, regardless of whether or not a project has been planned by the agency.

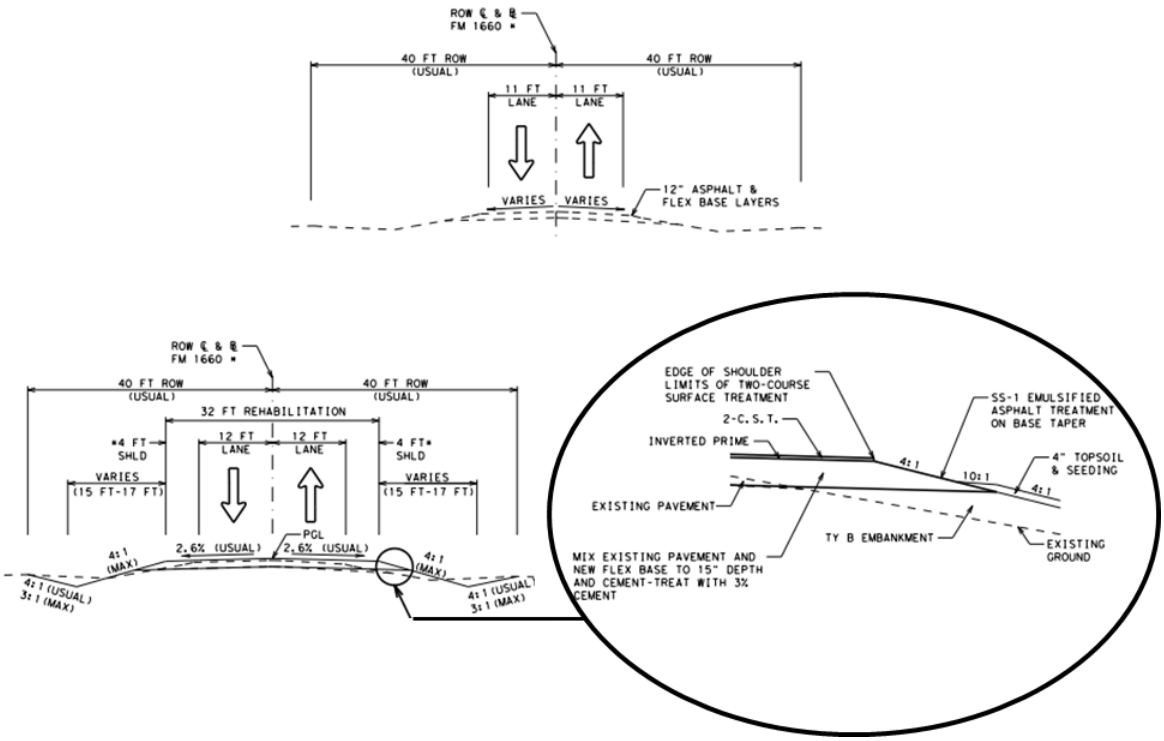

Fig. 27. FM 1660 existing and proposed typical sections

6.4 FM 908 DIAGNOSIS

FM 908, located in the Bryan district, was a construction project let for construction in September 2017. The FM 908 project spans just under 2.5 km (just over 1.5 mi), consisting of three data collection sections. The description of work provided in the plan set was, "For the construction to rehabilitate existing road consisting of grading, structures, base, surface, signs and pavement markings."

The project was diagnosed as unhealthy with two of the four systems diagnosed as unhealthy and two as potentially unhealthy. Fig. 28 has the overall diagnosis and has the systems diagnoses. Fig. 28 shows that the structural system and roadside system are both unhealthy, with the structural system nearing the very unhealthy threshold. Both the surface and safety systems are potentially unhealthy with the safety system presenting as the healthiest of the four systems.

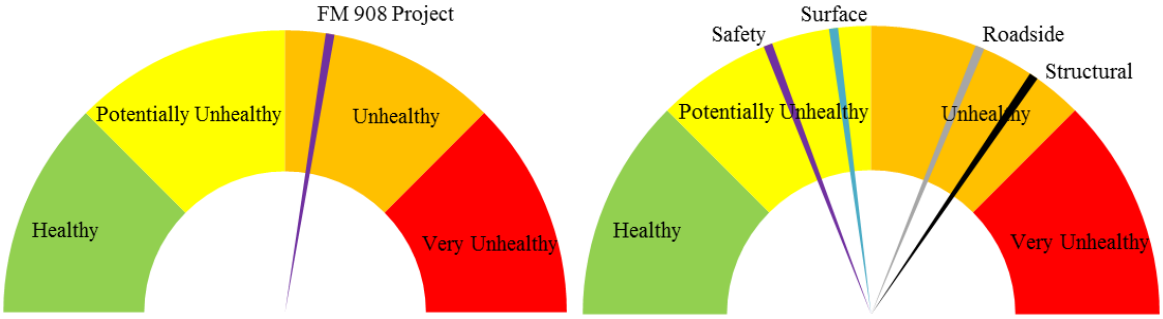

Fig. 28. FM 908 project diagnosis and FM 908 systems diagnoses

6.4.1 **FM 908 System Diagnoses**

The structural system on FM 908 is the unhealthiest of the systems, driven by a dynamic loading indicator that is as unhealthy as possible. The four indicators within the structural system are shown in Fig. 29. The diagnoses for the other systems follow in Fig. 30, Fig. 31, and Fig. 32. With the cross-over of dynamic loading and soil indicators between the structural system and the roadside system, it is not surprising that these two systems are the unhealthiest on FM 908.

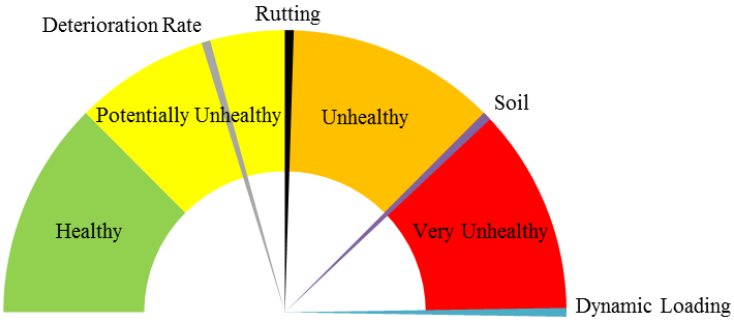

Fig. 29. FM 908 structural system diagnosis

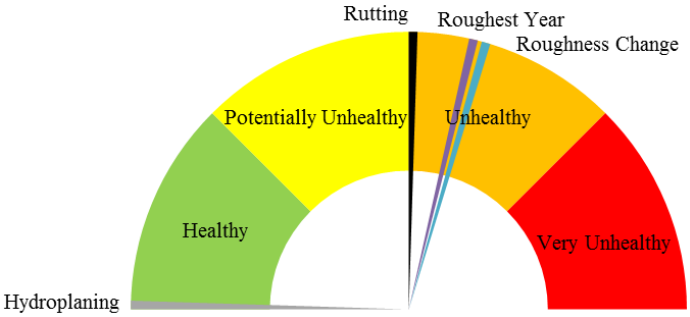

Fig. 30. FM 908 surface system diagnosis

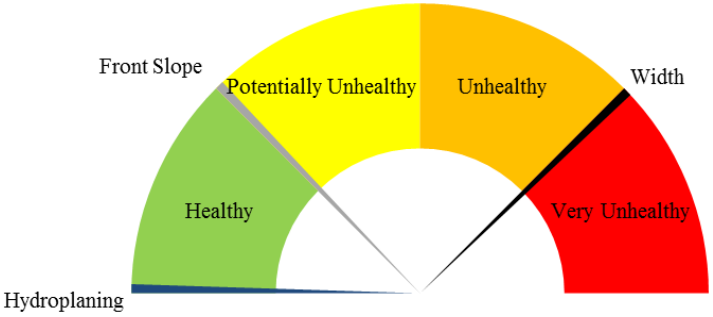

Fig. 31. FM 908 safety system diagnosis

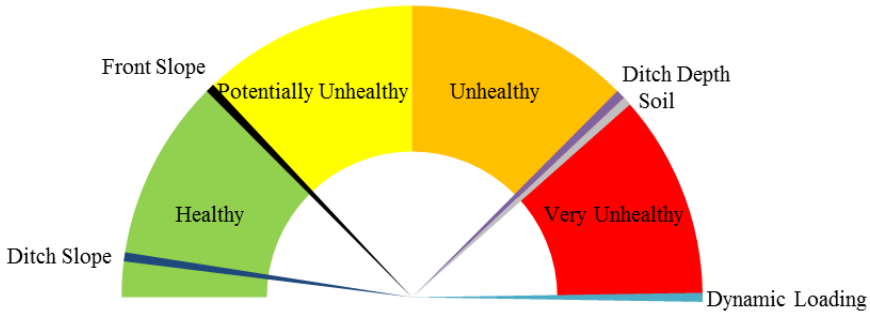

Fig. 32. FM 908 roadside system diagnosis

Fig. 30 shows that the roughest year and roughness change indicators are unhealthy, not surprising since the dynamic loading indicator was in the unhealthiest condition. Also concerning was the health of the width indicator, diagnosed at the very unhealthy threshold, shown in Fig. 31. The ditch depth indicator was diagnosed close to the very unhealthy threshold and shown in Fig. 32. Fortunately for the roadside system, the ditch slope indicator was healthy by a large margin and the front slope indicator was diagnosed at the healthy threshold. These diagnoses imply that the roadside has good longitudinal fall for the water with gently front slopes. Deepening the ditches might prove beneficial and will help the ditch depth indicator healthy and with the current health of the front slope indicators the deepening can be done within the existing footprint. Obviously widening the roadway would complicate this suggestion.

6.4.2 **Comparison of FM 908 Diagnosis with Construction Plans**

The existing typical detail and proposed detail for FM 908 are shown in Fig. 33. The existing detail is on top and shows a roadway with only a 6.71 m (22 ft.) roadway surface. The proposed typical section not only shows widening the roadway to a 9.14 m (30 ft.)

surface, but it shows cement treating the subgrade and creating more ditch depth where required.

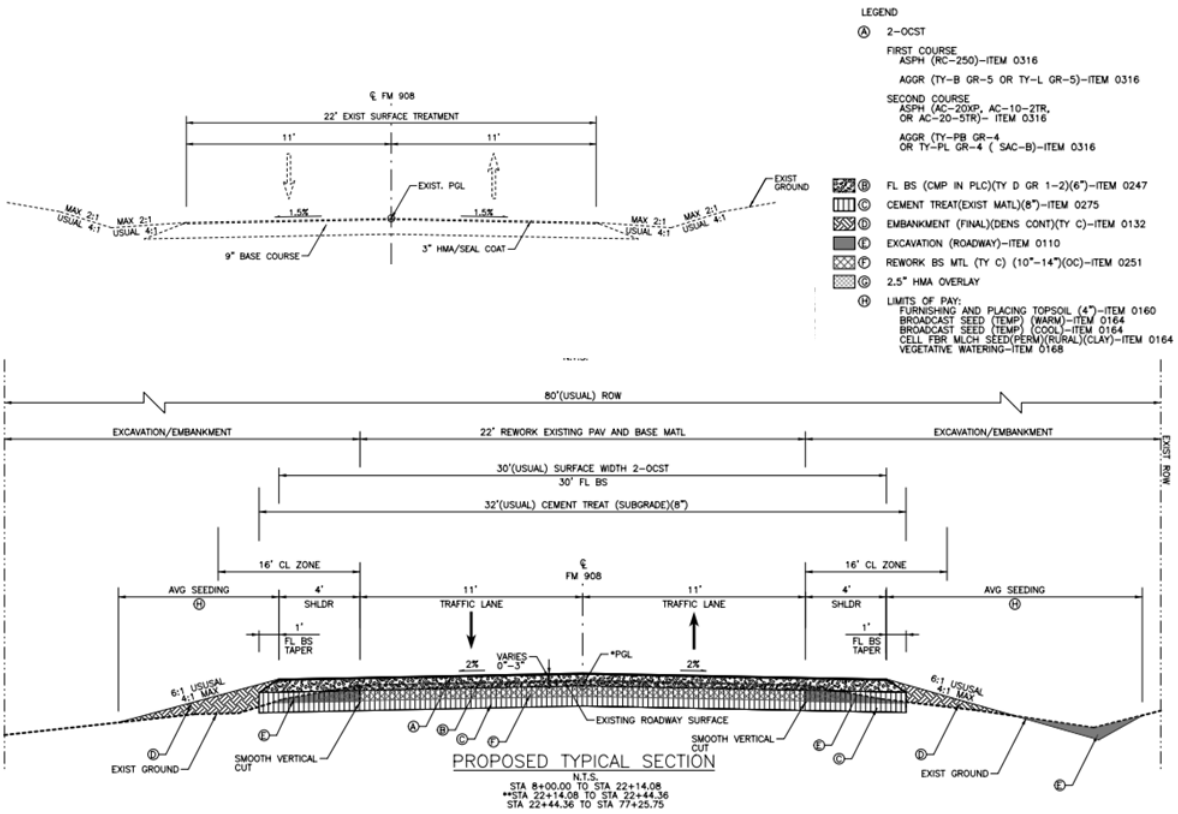

Fig. 33. FM 908 existing and proposed detail

The roadway widening, complete reconstruction, and treatment of the subgrade will improve the health of every system and if done properly will transform the structural and surface systems to perfect health. This conclusion can be drawn because hydroplaning was diagnosed in the healthiest state, thus the current geometry of the roadway provides adequate surface drainage against hydroplaning. This was not the case on FM 1696, where

hydroplaning was unhealthy and the construction plans did not necessarily guarantee the symptoms were addressed.

Increasing the ditch depth improves the health of the roadside system, but the typical section indicates a 24.38 m (80 ft.) ROW. While the diagnostic method tends to agree with deepening the ditches, the current health of the front slopes at the potentially unhealthy threshold indicates front slopes are already steeper than desirable and likely within the 1V:4H range. Using the diagnostic method, engineers can have a better understanding that while widening the roadway and deepening the ditches is needed, it will be done at the expense of the front slopes within the existing ROW footprint. Therefore, the researcher does not think the 6H:1V usual/4H:1V maximum for front slope steepness shown on the typical section is obtainable. As discussed in the Activation of Mobile LiDAR Data to Inform the Front Slope Indicator section, 1V:3H is acceptable. Within the diagnostic method, this would place the front slope indicator into the unhealthy band because 1V:3H front slopes are traversable, but not recoverable. Additionally, they are more difficult for maintenance to mow and avoid erosion. Nonetheless, with the high cost of ROW this might be a decision engineers are comfortable with pursuing. Using network-level data and the diagnostic plan, this knowledge would have been known at the beginning of the process. It also would have allowed engineers to perform a site visit to ensure guardrail was not require to protect front slopes steeper than 1V:3H.

6.4.3 **Section by Section Diagnostics of FM 908**

A section by section diagnostics approach was performed on FM 908 because of the short nature of the project. The project length was less than 2.5 km (1.5 mi.) and only

included three data collection sections. The section by section diagnostic charts are located in Appendix C. These charts show that over the three sections, the middle section of the project was the unhealthiest, diagnosed at the unhealthy/very unhealthy interface. Further diagnostics using the individual nodes showed that the deterioration rate in the middle section was as unhealthy as possible, whereas it was healthy in the other two sections. This diagnostic knowledge helps engineers know that special care should be taken in this area to ensure adequate pavement structure. This might also represent a location where additional geotechnical testing should be performed in the design phase to ensure underlying structural causes are addressed. The detailed section by section diagnosis also revealed that ditch depth was unhealthy in every section, thus roadside improvements are needed throughout the project.

6.5 OSR PROJECT DIAGNOSIS

The OSR project exists within the Bryan district and spans approximately 24.5 km (15.2 mi.) with a logical division point in the town of Normangee, TX. The researcher divided the OSR project into two analysis sections on each side of Normangee, TX. The diagnostics showed that this division ultimately provided insight into the health of each potential project that might have been masked by looking at the area as a whole. This fact often drives SHAs to have local managers with "boots on the ground" knowledge of the network provide limits for potential projects. The method created by the researcher operates flexibly enough to accommodate projects of any length. Future work using the researcher's method could look at ways to optimize project limits using the diagnostic method across an entire network.

For the OSR project and the remainder of the projects, the diagnostic visual aids are provided in Appendix D.

6.5.1 **OSR Part 1 Diagnosis**

The general construction description programed by TxDOT calls for the rehabilitation of OSR. The first portion of the project (i.e. west of Normangee, TX) had an overall diagnosis of potentially unhealthy, but approaching the unhealthy threshold. A rehabilitation for a project that presents as only potentially unhealthy might initially appear as too robust. The system diagnoses have the roadside and structural systems approximately a quarter of the way into the unhealthy band. The surface and safety systems are both in the potentially unhealthy band, with the former near the unhealthy threshold and the latter near the healthy threshold.

Drilling into the diagnostics, it was the soil, dynamic loading, and roughest year indicators that were all very unhealthy. With the roughest year diagnosed as very unhealthy and roughness change not, OSR part 1 is an example of a roadway that has very rough ride quality year after year. This continual roughness with poor soils likely led to selecting a rehabilitation project.

Using the diagnostic information, engineers would know early in the process that the hydroplaning potential indicator was healthy, indicating geometric changes were not required and the construction of a similar surface to the existing surface should perform adequately. In addition to healthy hydroplaning potential, ditch slope was healthy. Ditch depth and front slope were potentially unhealthy, along with width. With the roadside features within either the healthy or potentially unhealthy band, if widening is not included

in the project, engineers can reasonably assume the roadside will continue to function with a relatively high degree of health.

6.5.2 **OSR Part 2 Project Diagnosis**

While part 1 of the OSR project falls within the potentially unhealthy band, the part 2 was diagnosed as unhealthy. Three of its four systems were unhealthy. The structural system was diagnoses as unhealthy with the dynamic loading indicator at its unhealthiest and the soil indicator also very unhealthy. The surface system was also unhealthy, but near the threshold with potentially unhealthy. Similar to part 1, roughest year was diagnosed as very unhealthy. The third system diagnosed as unhealthy was the roadside system. With the cross over indicators from the structural system of dynamic loading and soil, it is not surprising this system is also unhealthy. However, the roadside system also has the ditch depth and ditch slope indicators diagnosed as unhealthy.

From a holistic health perspective, OSR part 2 was diagnosed in poorer health than OSR1. The rehabilitation description for this project was not surprising because of the obvious long-term ride quality issues and poor soil conditions. The diagnostics also show that the roadbed along this project moves, causing other ride quality issues and dynamic loading unhealthiness.

The safety system was diagnosed as potentially unhealthy, but the width indicator was diagnosed as very unhealthy. This diagnosis, along with the poor health of ditch indicators along the roadside, created problems for engineers. While the project is described as rehabilitation, the researcher does not know if widening will occur. Widening is needed from a health perspective; it will improve the health of the width indicator, but would help

with dynamic loading by moving the wheel path away from the edge. Unfortunately, the diagnostics also indicate the ditches need to be improved. Widening the roadway, while also deepening and steepening ditches would adversely affect the front slopes within the existing ROW footprint. Fortunately, the front slope indicator was diagnosed very near the unhealthy/potentially unhealthy threshold indicating some steepening could take place before becoming very unhealthy. Section by section diagnostics could be used to identify vulnerable areas if widening and roadside work is included in the project.

The discussion with OSR part 2 illuminates the diagnostic method's ability to help engineers capture a holistic view of a project's health. Existing methods might have told engineers something about poor ride quality, but they would fail in alerting engineers to the width and roadside needs. Also, a simple inclusion of basic soils data justifies a complete rehabilitation to address poor soil health.

6.6 FM 50 PROJECT DIAGNOSIS

FM 50 was a rehabilitation project in the Bryan district spanning approximately 8.5 km (5.3 mi.). The project was diagnosed as unhealthy, but sitting at the potentially unhealthy border. While the project was diagnosed as just inside of the unhealthy region, three of the four systems were within the unhealthy band width the structural system half way through the unhealthy band.

Similar to the OSR project, the FM 50 project has very unhealthy dynamic loading and soil indicators. The diagnostic method also diagnosed the width indicator as very unhealthy and roughest year and hydroplaning indicators as unhealthy. With the need to

improve the health of the width indicator, the affect it might have on roadside indicators becomes more important. Ditch slope was diagnosed as healthy as possible, while front slope fell just beyond the healthy/potentially unhealthy band. Finally, ditch depth was diagnosed as potentially unhealthy, falling approximately half way through the band.

With regard to applying the diagnostic method and the diagnoses coinciding with the prescribed rehabilitation project, this work description matches other rehabilitation projects because of the very unhealthy soil and dynamic loading indicator. The diagnostic method provided additional information on the need to widen the roadway and that doing so within the existing ROW footprint is likely feasible because of the general good health of roadside indicators.

6.7 FM 1844 PROJECT DIAGNOSIS

FM 1844 was diagnosed in overall unhealthy with the structural system and roadside system in an unhealthy state and the surface system and safety system in a potentially unhealthy state. The construction description assigned by TxDOT was "widen, repair, and resurface."

With regard to widening, the width indicator was diagnosed as very unhealthy, sitting at the threshold with unhealthy. The overall health of the safety system, which includes the width indicator, was potentially unhealthy. The reason for this overall diagnosis was the perfect health of the hydroplaning indicator and the diagnosis of the front slope indicator approximately half way through the potentially unhealthy band. While the overall system diagnosis tells the engineer something about the overarching health of a particular system, the indicator diagnoses help in drilling down into specific concerns. This was a

primary driver in the creation of the diagnostic gauge charts. This quick visualization tool helps engineers draw conclusions about the project's needs with succinctly aggregated network-level data that has been converted into information.

The repair aspect of the project coincides with the very unhealthy diagnosis of the deterioration rate. The resurfacing aspect coincides with the unhealthy roughness change and roughest year indicators.

The ditch depth indicator was diagnosed as unhealthy, implying deepening the ditches would improve health. Widening the roadway and deepening the ditches work against each other in the way that other indicators are affected. The front slope indicator is the most vulnerable to roadway widening and ditch deepening. The use of section specific diagnoses can help engineers use the diagnostic method and its output to further identify project needs or modifications.

6.8 FM 2661 PROJECT DIAGNOSIS

The FM 2661 project was programmed for TxDOT as widening project for safety purposes. This description implies that overall health of the roadway should be fairly good. After processing the FM 2661 data through the diagnostic method, it was diagnosed as unhealthy overall, but near the potentially unhealthy threshold. Three of the four systems were diagnosed as unhealthy, while only the surface system was diagnosed as potentially unhealthy.

The unhealthiness of the structural system was driven by the very unhealthy dynamic loading indicator and the unhealthy soil indicator. The widening project will not improve the

soil indicator, but could have a positive impact on the dynamic loading indicator by moving the outside wheel path away from the unconfined edge of pavement. The safety system was diagnosed as unhealthy, primarily affected by the very unhealthy width indicator. Unfortunately, the ditch depth indicator was also diagnosed as unhealthy, thus widening the roadway and deepening the ditches was required based on the diagnostics. Carrying out both of these operations without acquiring additional ROW could lead to the front slope indicator becoming unhealthy. The diagnostic process allows engineers to consider how the outcome of project will affect the holistic health of the project.

The diagnostic method's identification of poor health for the width indicator matches the described construction technique. The diagnostic method offers engineers additional information on the health of the roadside that might not have been considered during project development. Neglecting the roadside could lead to premature pavement related issues after the project or might lead to poorer roadside health and additional risks to motorists that leave the roadway.

6.9 FM 2054 PROJECT DIAGNOSIS

FM 2054 was listed as a widening for safety project. It was diagnosed as potentially unhealthy, but sitting at the unhealthy threshold. The roadside system was the unhealthiest of all of the systems, followed closely by the safety system, which was followed closely by the structural system. The surface system was by far the healthiest system and was diagnosed as potentially unhealthy, but at the healthy threshold point.

The structural and roadside systems' health was controlled by the soil and dynamic loading indicators with very unhealthy diagnoses. While the soil and dynamic loading indicators were in poor health, the surface system was relatively healthy, implying the ride quality indicators were also healthy. In fact, the roughness change indicator was in the healthy band, informing the engineer that little change occurred on the roadbed from year to year in terms of ride quality. The roughest year indicator was diagnosed as more than half way through the potentially unhealthy band, mostly likely dictated by the difference in wheel path ride quality that was impacting the dynamic loading health. Therefore, widening the roadway will likely improve the dynamic loading indicator by moving the wheel path away from the edge and engineers might decide no subgrade work is required because the roadbed is not moving from year to year.

With regard to the safety system, hydroplaning was diagnosed as healthy and front slope was barely diagnosed outside of the healthy band. However, the width was diagnosed in the unhealthiest possible condition. This diagnosis coincides with the overall construction description to widen for safety.

Diagnostically, the ditch depth was diagnosed as unhealthy and ditch slope was diagnosed well into the potentially unhealthy band. With unhealthy soils, the diagnostics indicate that improving the roadside health is advisable. Improving the roadside health will ensure the water is below the pavement structure and has plenty of fall to move away from the roadway. Once again, as has been pointed out with other widening projects, doing so in a confined ROW footprint places the front slope health in jeopardy. Fortunately, the front slope health for FM 2054 was diagnosed just beyond the healthy threshold, allowing

engineers to understand that room remains to steepen the slopes before getting into the unhealthy zone or worse.

The diagnostic method clearly coincides with the general construction description to widen for safety. The diagnostic method provides additional information using activated network-level to help inform the design process during the early stages of project development.

6.10 RM 690 PROJECT DIAGNOSIS

RM 690 was diagnosed as potentially unhealthy, approximately midway through the potentially unhealthy band. The general construction description for this project was simply to widen the roadway. The safety system, the system in which the width indicator resides was diagnosed as potentially unhealthy, but only about a quarter of the way into the unhealthy region. In fact, the safety system was diagnosed as the healthiest of the four systems. The hydroplaning indicator in the safety system was as healthy as possible and the front slope and width indicators were in the potentially unhealthy band.

The unhealthiest system within was the roadside system that was diagnosed at the potentially unhealthy/unhealthy threshold, followed closely by the structural system. As with other projects, the structural and roadside systems often mimic each other because of the cross-over of dynamic loading and soil indicators. For RM 690, the dynamic loading indicator was in the unhealthiest possible state, though soils were diagnosed as healthy. With an unhealthy dynamic loading indicator, one might expect that the ride quality indicators were unhealthy. The roughest year indicator was unhealthy, but the roughness change

indicator was healthy. These diagnoses inform the engineer that while the project has been rough, the movement of ride quality from year to year was nonexistent.

The unhealthy diagnosis of the ditch depth indicator allows engineers to plan for ditch improvements during construction, but also raises a red flag with the planned widening and the need to deepen ditches. This combination might compromise the health of the front slope indicator that was diagnosed approximately a quarter of the way into the potentially unhealthy band.

Widening the roadway will likely improve the dynamic loading indicator, but overall, the width was not diagnosed as unhealthy. The difference in diagnosis and construction description varies the most for the RM 690 project. It is possible that engineers have selected widening for this project to address other needs. For example, maybe there have been several run off the road accidents that widening will address. This project also sits adjacent to a large lake; therefore maybe engineers want to provide more width for recreational traffic that might be pulling boats or other trailers. The diagnostic method developed by the researcher can include these types of variables if the data can be captured.

The construction description to widen this roadway provides the least agreement between the diagnostic method and the chosen construction technique of any of the method applications. The researcher postulates that other variables in the decision process led to the project selection.

6.11 SH 138 PROJECT DIAGNOSIS

SH 138 was diagnosed at the potentially unhealthy/unhealthy threshold. The construction description for this project was to add shoulders and rehabilitate. With regard to adding the shoulder, the width indicator was diagnosed as very unhealthy. The width indicator resides in the safety system which was diagnosed with the same degree of unhealthy as the structural system. The surface system was also diagnosed as unhealthy, while the roadside system was diagnosed as potentially unhealthy.

While width was the only indicator diagnosed as very unhealthy, thus coinciding with the add shoulders part of the work, three of the four indicators in the structural system were diagnosed as unhealthy. The dynamic loading, deterioration rate, and soil indicators were all diagnosed as unhealthy. The unhealthy diagnosis of the deterioration rate tells engineers that fatigue cracking has manifested and grown faster than expected. The unhealthy nature of the deterioration rate matches the engineer's decision to rehabilitate the roadway.

Hydroplaning was diagnosed slightly into the unhealthy band, while rutting was diagnosed three quarters of the way into the potentially unhealthy band. It is likely the rehabilitation will improve the hydroplaning healthy, but the engineer suggests performing diagnostics post-construction to verify the improved health. Section by section analysis of the project might also help engineers identify hydroplaning susceptible locations and make adjustments to the design.

Overall, the diagnostics, particularly the very unhealthy width indicator and the overall poor health of the structural system with unhealthy deterioration rate coincide with the description to add shoulders and rehabilitate.

7. SUMMARY, CONCLUSIONS, AND RECOMMENDATIONS

7.1 SUMMARY

The researcher created a diagnostic method to provide engineers with a holistic technique to understand the health of road segments from right-of-way (ROW) line to ROW line. A holistic diagnostic technique that includes both roadway and roadside elements did not exist prior to this work. The diagnostic method more effectively used data stored in a pavement management system and combined it with geometric and soils data, not typically used at network-level analysis. The geometric data represented a new network-level dataset created during the researcher's work. The new dataset consisted of mobile light detecting and ranging (LiDAR) measurements, a technique likely to become common within the next several years. The burgeoning use of mobile LiDAR makes the developed diagnostic method proactive and deployable as these measurements become more available. The network-level soils data used in this method was extracted from a publically available dataset.

The diagnostic method was constructed on graph theory and exploited mathematical techniques used to describe matrices. The graphs created for each pavement project contained a weighted edge incidence matrix that could be manipulated into a square matrix, referred to here as a Laplacian graph. Using the square matrix, the researcher utilized eigenvalue calculations to determine characteristic values associated with the weighted edge incidence matrix. The use of the eigenvalues permitted the researcher to establish the project as a network that functioned with a mass-balance nature. The maximum eigenvalues at the

indicator level could be summed to produce the overall project maximum eigenvalue. The mass-balance nature allowed the researcher to group indicators into systems to provide summarized diagnostic information about projects. The mass-balance nature and the structure of the diagnostic method allow for the inclusion of new indicators and the creation of new systems with future use.

The researcher used a comparative technique to compare the project's health eigenvalues with various scenarios. For example, how does the project's health compare with the unhealthiest scenario? The comparative technique was used to establish a project health curve. Integrating the curve produced the diagnostic values that were visualized in gauge charts. The gauge charts functioned as a quick tool that could be used by engineers to understand overall project health, systems' health, indicator health, and the relative nature of each of these.

Application of the diagnostic method coincided well with the construction techniques outlined in actual construction projects. The ability of the method to mimic engineering judgement bodes well in gaining the confidence of practitioners. However, agreement with construction projects only served as an approximate reality check for the method. The diagnostics produced were able to provide additional useful information for engineers, particularly as it relates to roadside health and the health of features such as traveled way width and hydroplaning.

The diagnostic method offers engineers a more holistic view of the health of pavement projects. By utilizing techniques to extract information from network-level data, the method focusses on providing details on underlying causes rather than current

performance metrics. The work represents a step forward by converting network-level data into information, overcoming the data rich, but information poor conundrum.

7.2 CONCLUSIONS

7.2.1 Diagnostic Method Output Compared with Detailed Construction Plans

The diagnostic method generated holistic project diagnoses that coincided well with actual detailed construction plans. The ability to produce diagnostic information with network-level data assists in identifying both needs and potential solutions early in the project development process. For the three projects with detailed design plans available for comparison, the following conclusions were made:

- The method is highly effective at identifying the need to widen a segment of roadway within a project as illustrated by diagnosing width as unhealthy or very unhealthy for FM 1696, FM 1660, and FM 908. All three of the proposed typical sections for these projects included widening the roadway.
- The method is highly effective at identifying the need to improve the pavement structure as illustrated by the unhealthy or very unhealthy structural system diagnoses for FM 1696, FM 1660, and FM 908. Each of these projects included either subgrade stabilization or the stabilization of an unbound layer.

The two conclusions discussed above illuminate the method's strength to provide diagnostics on individual indicators and overall project systems. The widening conclusion specifically addresses a single indicator and the method's effectiveness in identifying and conveying the need to improve its health. The second conclusion specifically addresses an

entire system, made up of four indicators. Other conclusions gained from comparing the diagnostics to actual plans sets include:

- The front slope change and the inevitable steepening of the front slope due to pavement widening within the same footprint was captured in the FM 1696 typical section. Fortunately, the diagnostic method indicates the existing front slope condition is healthy, providing the engineer with knowledge that some steepening can occur without compromising the health of the indicator.
- The need to improve ditch depth was noted by the diagnostic method and identified in the FM 908 plan set.

In addition to these conclusions and observations, the more effective mining of historical network-level fatigue cracking assisted in better diagnostics.

- FM 1660 was diagnosed with a very unhealthy structural system that included as unhealthy as possible fatigue cracking. The process control technique used to analyze fatigue cracking data prior to including it into the diagnostic method helped determine that FM 1660 was deteriorating at a very rapid rate.

7.2.2 **Potential Health Issues Noted by the Method but not in Detailed Plans**

While project needs identified by the method coincide nicely with issues addressed in detailed design plans, the method also identifies needs not specifically addressed in design. It appears the method identifies project health concerns that are missed or overlooked, even during detailed design. For example, FM 1696 was diagnosed with an unhealthy safety system, mainly because of an unhealthy width and hydroplaning indicator. The widening

portion of the diagnosis was discussed above, but the plans do not directly address the poor hydroplaning health. While reconstruction and a new surface will positively impact hydroplaning health, there is no guarantee the health will completely improve. This fact was validated when it was discovered the design speed for the roadway geometry was 48 kph (30 mph).

7.2.3 **Micro-Level Diagnostics**

The method was created to help drill-down into network-level analyses. When data collection section specific diagnostics are performed, very detailed diagnostics were provided. Examples of these details include:

- The detailed plans associated with FM 1696 include a portion of the project requiring cement treatment of the subgrade and a portion of the project requiring lime treatment of the subgrade. The division between these two treatment types also had distinct health changes as the portion of the project requiring cement treatment presents as more healthy than the lime treatment section. This is visualized in Fig. 20.
- FM 908 was a short project, involving only three data collection sections. The application of the method on a section by section level showed that the middle of the project was very unhealthy, while the sections flanking each side were relatively healthy. This type of specific diagnostic information can help practitioners isolate specific areas requiring additional attention.

7.2.4 **Additional Diagnostic Conclusions**

In addition to FM 1696, FM 1660, and FM 908 the method was applied to seven other projects with general construction descriptions, but no detailed plans. The diagnostic methods identified the need to work on these segments of roadway with techniques generally described in the construction description attached to the project. However, the diagnostic method provided additional useful information such as:

- The OSR project was a long project and while a clear geographic separator was obvious, the method discovered that the width indicator and roadside system were unhealthier for the eastern section of the project.
- The FM 50 project diagnosis coincided with the rehabilitation description, while also alerting engineers to the need to widen the roadway and helping to understand that widening could be done within the existing ROW footprint due to the relative health of the roadside.
- The widening project described fro FM 2661 was easily identified using the diagnostic method as the width indicator was diagnosed as very unhealthy. However, the method also indicates that three of the four systems are diagnosed as unhealthy, providing more information to consider in the final development of the project.
- The FM 2054 description to widen for safety was easily captured using the diagnostic method.
- The RM 690 project had the least agreement between the project description and the method diagnosis. The project description indicates a widening project;

however the width indicator was not diagnosed as unhealthy. The method does note unhealthy ditches, offering pause associated with a widening project. Widening a roadway and deepening ditches can have an adverse effect on front slope health, information now readily available because of the diagnostic technique developed in this work.

- The SH 138 project description was to add shoulders and rehabilitate. The method identified the width indicator as very unhealthy and the structural system as unhealthy, agreeing with the overall construction description. Hydroplaning was also diagnosed as unhealthy, potentially alerting engineers to the need to perform a micro-level analysis to gauge high risk locations for hydroplaning.

7.2.5 **Overall Conclusions**

Highway agencies currently have or can obtain vast amounts of network-level data. Converting this data into information rarely occurs, particularly from a holistic perspective. This research helps fill the gap of converting network-level data into information by:

- Structuring different types of network-level data into a directed acyclic graph,
- Using the weighted edge incidence matrix associated with the graph to create a matrix structure,
- Unlocking the ability to characteristically define the nature of the matrix by creating a generalized Laplacian graph,
- Describing the characteristics of the generalized Laplacian graph through a comparative technique that created a characteristic health curve for a segment of roadway, and

- Using the characteristic health curve to provide relative diagnostic information about the project as a whole, each health indicator, and the combination of multiple indicators into systems.

As it relates to prescribed work actions, the diagnostic method easily captured the need to widen roadways or stabilize subgrades by incorporating new network-level datasets into the diagnostic process. The diagnostic process also used network-level data to identify ditch and front slope changes within projects. The diagnostic method also showed the capability of informing engineers about competing elements within the design process. For example, the diagnostic method might successfully diagnosis the need to widen the roadway, but it might also indicate ditches should be deepened. When the roadway is widened and the ditches are deepened, the health of the front slope will suffer. The diagnostic method and visualization help inform engineers on how these different indicators might be impacted from a health perspective.

The use of graph theory provided an effective means to build a diagnostic tool. The tool remains flexible for the inclusion of additional indicators or systems. The activation of data to a consistent scale simplifies the matrix calculations required to produce diagnostically useful information. The consistent scale is not required; however the researcher showed that using a consistent scale assisted in deriving a general health curve for projects, systems, and indicators. It also assisted in developing a mass-balance network as it relates to maximum eigenvalue calculations. The mass-balance formulation permits the creation of whatever systems the user desires and these systems will comply with the generalized health curve.

7.3 RECOMMENDATIONS

Further development of the method should come from validation processes and field trials. Validation should include the following:

- Diagnose segments of roadways and perform detailed field measurements to ensure proper diagnoses. This could include:
    - When a roadway is diagnosed as needing widening, field measure the location of the widening and determine the final surface elevation at that point. Subsequently measure the future ditch depth and front slope steepness to determine future conditions. Compare the existing and future conditions to diagnoses produced by the method to ensure agreement.
- Identify segments of roadways where other data can help to validate the method. For example, when a segment is diagnosed with poor hydroplaning health, use wet weather crashes to determine if the diagnosis is accurate. Additionally, site visits should be made during rain events to determine if the surface water flow creates the poor health conditions identified by the method.

Field trials using this method could take many forms, a few of which include:

- Work with a managing agency (i.e. TxDOT District) to perform the diagnostic method prior to preliminary project development. Allow the method to guide project development and identify the needs to be addressed in detailed design. Develop a set of design plans and follow the project through to construction to determine if using the method led to a noticeable improvement. Noticeable improvement could be measured in one of the following ways:

    - Shorter detailed design duration,
    - Fewer change orders during construction,
    - Fewer quantity overruns during construction, or
    - Feedback from experienced practitioners on the performance of the method.
- Work with a managing agency (i.e. TxDOT District Maintenance Office) to identify network-level problems that should be addressed in long-term planning (i.e., four-year plans). Use the method to narrow the limits of work to more precisely address the needs of the network. Feedback from experienced staff will help in determining if this is an effective use of the method. In addition to feedback, long-term monitoring of performance metrics could help determine method effectiveness. Monitoring improvement of performance metrics will require patience and several years to determine the effectiveness of the method in this way.

The effectiveness of the method should also be determined and validated by comparing the pre-construction diagnoses with the post-construction diagnoses. This analysis will help in understanding how projects impact the results of the method. Based on these results, the method might need to be adjusted to ensure the proper health improvement is captured after construction. However, the method might continue to provide diagnostically useful information and the managing agency might need to decide if the project adequately addressed the needs to the project. This validation can only occur by using the method both pre-construction and post-construction.

The pre- and post-construction comparison will allow for the comparison of eigenvalue change. For post-construction, the eigenvalue should be lower than pre-construction. Evaluating the magnitude of this change as it pertains to the cost of the construction project will lead to an understanding of project benefit. Understanding the benefit from different types of projects will assist in linking the diagnoses to construction costs required to mitigate poor health. This link will greatly improve preliminary estimates generated during the early stages of project development.

As the changes in eigenvalues become more understood, the method should transition into project prioritization and optimization. Project prioritization and optimization are essential within asset management systems. The diagnostic method created captures a more holistic picture than previous methods available. The holistic picture helps practitioners prioritize based on overall health and on the health of various systems. The mass-balance approach will let practitioners filter based on projects with the unhealthiest roadside system or user safety system or any combination of the systems used. With this type of information, managing agencies can tailor make different solutions. For example, maintenance supervisors might be most interested in roadside health as a ditch maintenance contract is developed. The diagnostic method can be used to hone in on unhealthy roadsides and the eigenvalues can be used to prioritize the work.

The previous example of roadside health, lends itself to worst-first approach. However, the method would not restrict practitioners to this type of approach. In fact, as post-construction and complete network-level diagnostics are performed, an agency will begin to understand the improvement in health, as measured by eigenvalue changes and the

related integration. Decision can then be made to maximize health while minimizing cost. Because the method is holistic and can include new systems, health will be maximized by addressing the unhealthy indicators and avoiding unnecessary work.

The advancements of the method previously described begin to approach linking the method to a utility theory approach. The analytical structure of the method should remain the same to maintain the mass-balance approach of the eigenvalue technique. However, the initial project diagnosis and dissection to indicator diagnosis, allows different weights on each indicator. Alternatively, the indicators could be combined into systems and then weights attached to those systems. Managing agencies can use various techniques to prescribe weights to the indicators or systems that best reflect the priorities of the agency. By doing so, practitioners can prioritize the work based on the goals of the agency.

Work should be done to automate this method. A platform should be created to store or locate all of the datasets so that the end users can easily produce diagnoses. As GIS applications continue to evolve, the computerized methodology should include a GIS mapping component.

At a more fundamental level, the correlation and relationship between roadside features, soils, and pavement distress should be explored in more detail. The strength of the diagnostic method was the ability to disaggregate the health of multiple indicators so that they could be reorganized into various project related systems. The assignment of indicators into systems could be modified or improved as the relationships between different indicators are known in more detail. As the method becomes used in practice, interactions between the indicators should be researched. Understanding the interaction between indicators and using

the diagnostic technique could provide researchers and practitioners with a better understanding of how different roadway attribute affect the health of other attributes. This understanding will lead to better decision making.

The diagnostic method should be expanded to include other decision making elements as data become available. For example, the method could easily accommodate a traffic related system with health indicators such as daily traffic, percent trucks, and others. Also, the selection of additional elements should be guided by asset management plan legislation. Within the United States, this legislation revolves around the Moving Ahead for Progress in the 21st Century Act (MAP-21) and the Fixing America's Surface Transportation (FAST) Act. The final rule making for the FAST Act requires performance assessment in 12 areas. As it relates to the diagnostic method, the first four areas include serious injuries per vehicle miles traveled (VMT), fatalities per VMT, number of serious injuries, and number of fatalities. These four areas fit within the user safety system of the diagnostic method and the method is flexible enough to include these indicators. Two other areas in the legislation that pertain to the diagnostic method include performance of the interstate and non-interstate system. Pavement condition metrics include roughness, cracking, and faulting. The diagnostic method currently includes three indicators fed with roughness data. Fatigue cracking was included in the diagnostic method, but the method could be expanded to include longitudinal and transverse cracking. Lastly, faulting should be included as the diagnostic method is expanded to include concrete pavements.

The activation of the data within each indicator should be reviewed to determine if more robust techniques could advance the diagnostic method. Extensive analytical

techniques were used to activate alligator cracking measurements into deterioration rate. Other extensive techniques were used to convert and activate basic surface geometry measurements into hydroplaning potential. However, expansion of the other indicators might be warranted. For example, the soil indicator consists only of American Association of State Highway Transportation Officials (AASHTO) soil classification. Much more data exists within the soils reports, such as plasticity index (PI), coefficient of linear expansion, hydraulic conductivity, and many more. It is possible these properties could be exploited to improve and better delineate the soil indicator because of its detail coarseness in the current method. Also, depending on the confidence in distress models such as rutting or ride quality, process control techniques similar to those used for alligator cracking could also be used.

The process control technique used to mine alligator cracking has potential to be a standalone offshoot of this work. During the mining of alligator cracking data, the techniques showed the ability to determine the number of work actions that occurred over an analysis period. Further use of these techniques could generate additional useful information from existing network-level datasets.

The exploitation of mobile LiDAR measurements at the network-level should be investigated by managing agencies. While mobile LiDAR is a powerful tool that generates vast amounts of data, processing and storing that data can become cumbersome, eventually leading back to a data rich, but information poor scenario. An agency should consider what geometric components can help make better decisions and focus on capturing those components with mobile LiDAR and avoid getting inundated with data that might not be helpful.

Finally, the expansion of the method to other infrastructure networks and civil functions should be evaluated. For example, expansion into pipeline networks appears fairly obvious. Pipeline networks are similar to roadway networks in that they carry a good through a fixed route that requires maintenance and improvements. This, or any other network, can be structured as a directed acyclic graph (DAG) with the overall health at the center of the graph. The overall health of the network or portion of the network is defined by the health of the individual indicators. Indicators can be identified by experts or assigned based on fundamental components associated with a particular network. The robustness and agility of the method should be tested on various infrastructure networks with readily available or attainable network-level data.

REFERENCES

Aggarwal, C. C. (2013). *Data clustering: Algorithms and applications.* CRC Press, Boca Raton, FL.

Amador-Jiménez, L., and Reza Amin, M. S. (2013). "Simulating freight traffic between Atlantic Canada and Québec to support pavement management on New Brunswick's regional highways." *J Infrastruct Syst,* 19(3), 343-350.

American Association of State Highway and Transportation Officials (AASHTO). (2011). *Roadside design guide. 4th ed.* AASHTO, Washington, D.C.

American Association of State Highway and Transportation Officials (AASHTO). (2007). *Highway drainage guidelines. 4th ed.* AASHTO, Washington, D.C.

American Association of State Highway and Transportation Officials (AASHTO). (1990). *AASHTO guidelines for pavement management systems.* AASHTO, Washington, D.C.

Anderson, D. A., Huebner, R. S., Reed, J. R., Warner, J. C., and Henry, J. J. (1998). "Improved surface drainage of pavements." *Rep. No. PTI 9825,* National Cooperative Highway Research Program Transportation Research Board, Washington D.C.

Anderson, S. D., Quiroga, C. A., Overman, J. H., Choi, K., Sahu, J., Kermanshachi, S., Goodrum, P., Taylor, T. R. B., and Li, Y. (2016). "Effective project scoping practices to improve on-time and on-budget delivery of highway budgets." *Rep. No. 821,* Transportation Research Board, Washington, D.C.

Asquith, W. H., and Roussel, M. C. (2004). *Atlas of depth-duration frequency of precipitation annual maxima for Texas.* U.S. Dept. of the Interior, U.S. Geological Survey, Water Resources Division, Austin, TX.

Bayrak, T. (2015). "A review of business analytics: A business enabler or another passing fad." *Procedia: Social & Behavioral Sciences,* 195, 230-239.

Belkin, M., and Niyogi, P. (2003). "Laplacian eigenmaps for dimensionality reduction and data representation." *Neural Comput.,* 15(6), 1373.

Bilodeau, J., Gagnon, L., and Doré, G. (2017). "Assessment of the relationship between the international roughness index and dynamic loading of heavy vehicles." *The International Journal of Pavement Engineering,* 18(8), 693-701.

Birgisson, B., and Ruth, B. E. (2002). "Improving performance through consideration of terrain conditions: Soils, drainage, and climate." *Transp.Res.Rec.*, 2(1819), 369-377.

Biyikoglu, T., Leydold, J., and Stadler, P. F. (2007). *Laplacian eigenvectors of graphs : Perron-Frobenius and Faber-Krahn type theorems.* Springer, Berlin and New York.

Bryce, J., Flintsch, G., Katicha, S., and Diefenderfer, B. (2013). "Developing a network-level structural capacity index for asphalt pavements." *J.Transp.Eng.*, 139(2), 123-129.

Budhu, M. (2015). *Soil mechanics fundamentals (Imperial Version).* John Wiley & Sons, Incorporated, Hoboken, NJ.

Cazorzi, F., Dalla Fontana, G., De Luca, A., Sofia, G., and Tarolli, P. (2013). "Drainage network detection and assessment of network storage capacity in agrarian landscape." *Hydrol.Process.*, 27(4), 541-553.

Cedergren, H. R. (1987). *Drainage of highway and airfield pavements.* R.E. Krieger Pub., Malabar, FL.

Chang, J. C., Findley, D. J., Cunningham, C. M., and Tsai, M. K. (2014). "Considerations for effective lidar deployment by transportation agencies." *Transp.Res.Rec.*, 2440, 1-8.

Chelvam, T., Somasundaram, S., and Kala, R. (2010). *Algebra, graph theory and their applications.* Narosa Publishing House, New Delhi.

Chen, D., Asaolu, B., and Qin, C. (2016). "Big data analytics in the public sector: A case study of needs analysis for the London boroughs." *IADIS International Journal on Computer Science & Information Systems*, 11(2), 171-178.

Chen, D. (2016). "Sigmoidal models for predicting pavement performance conditions." *J.Perform.Constr.Facil.*, 30(4), 1-8.

Chi, S., Murphy, M., and Zhang, Z. (2014). "Sustainable road management in Texas: Network-level flexible pavement structural condition analysis using data-mining techniques." *J.Comput.Civ.Eng.*, 28(1), 156-165.

Chi, S., Hwang, J., Arellano, M., Zhang, Z., and Murphy, M. (2013). "Development of network-level project screening methods supporting the 4-year pavement management plan in Texas." *J.Manage.Eng.*, 29(4), 482-494.

Choi, Y., Yi, H., and Park, H. (2011). "A new algorithm for grid-based hydrologic analysis by incorporating stormwater infrastructure." *Computers and Geosciences*, (37), 1035-1044.

Cioaba, S. M., and Murty, M. R. (2009). *A first course in graph theory and combinatorics.* Hindustan Book Agency, New Delhi.

Cook, A. A., Saito, M., and Schultz, G. G. (2015). "Heuristic approach to identifying horizontal curves and their parameters given lidar point cloud data." *Transportation Research Record,* 2521, 22-30.

Covar, A. P., and Lytton, R. L. (2001). "Estimating soil swelling behavior using soil classification properties." *Shallow Foundation and Soil Properties Committee Sessions at ASCE Civil Engineering Conference 2001,* ASCE, 44-63.

Cvetkovic, D. M., Rowlinson, P., and Simic, S. (1997). *Eigenspaces of graphs.* Cambridge University Press, Cambridge, England and New York.

Daoulas, J., Elfino, M., Nair, H., and Nelson, S. (2011). "Forensic investigation and remediation of pavement performance affected by groundwater seepage." *Transportation Research Record,* 2212, 65-73.

Dingess, R. (2014). "Better reporting: Utah DOT's data and planning tools provide a guide to the future and power of network-level asset data." *Roads & Bridges,* 52(1), 42-46.

Dong, Q., Huang, B., and Richards, S. H. (2015). "Calibration and application of treatment performance models in a pavement management system in Tennessee." *J.Transp.Eng.,* 141(2), 1-9.

El-Akruti, K., Dwight, R., and Zhang, T. (2013). "The strategic role of engineering asset management." *Int J Prod Econ,* 146, 227-239.

Federal Highway Administration (FHWA). (2017). "National performance management measures; assessing pavement condition for the national highway performance program and bridge condition for the national highway performance program." *MAP-21 Final Rule Making,* 82 FR 5886(112th United States Congress).

Federal Highway Administration (FHWA). (2007). *Asset management overview.* Federal Highway Administration, Office of Asset Management, Washington, DC.

Findley, D., Cunningham, C., and Hummer, J. (2011). "Comparison of mobile and manual data collection for roadway components." *Transportation Research.Part C, Emerging Technologies,* 19(3), 521-540.

Gallaway, B. M., Ivey, D. L., Hayes, G., Ledbetter, W. B., Olson, R. M., Woods, D. L., and Schiller Jr., R. F. (1979). "Pavement and geometric design criteria for minimizing hydroplaning." *Rep. No. FHWA-RD-79-31,* Texas Transportation Institute, College Station, TX.

Gallaway, B. M., and Rose, J. G. (1970). *Macro-texture, friction, cross slope and wheel track depression measurements on 41 typical Texas highway pavements.* Texas Transportation Institute, College Station, TX.

Gallaway, B. M., Schiller, R. E., and Rose, J. G. (1971). *The effects of rainfall intensity, pavement cross slope, surface texture, and drainage length on pavement water depths.* Texas Transportation Institute, College Station, TX.

Gharaibeh, N. G., Freeman, T., Saliminejad, S., Wimsatt, A., Chang-Albitres, C., Nazarian, S., Abdallah, I., Weissmann, J., Weissmann, A. J., Papagiannakis, A., and Gurganus, C. F. (2012). *Evaluation and development of pavement scores, performance models and needs estimates for the TxDOT pavement management information system : final report.* Texas A&M Transportation Institute, College Station, TX.

Gharaibeh, N. G., and Lindholm, D. (2014). "A condition assessment method for roadside assets." *Structure & Infrastructure Engineering: Maintenance, Management, Life-Cycle Design & Performance,* 10(3), 409-418.

Gharaibeh, N. G., Wimsatt, A., Saliminejad, S., Menedez, J. R., Weissmann, A. J., Weissmann, J., and Chang-Albitres, C. (2012). "Implementation of New Pavement Performance Prediction Models in PMIS." *Rep. No. FHWA/TX-12/5-6386-01-1,* Texas A&M Transportation Institute, College Station, TX.

Guharay, S. K., Thakur, G. S., Goodman, F. J., Rosen, S. L., and Houser, D. (2016). "Integrated data-driven analytics to identify instability signatures in nonstationary financial time series." *Appl.Econ.,* 48(16-18), 1678-1694.

Gurganus, C. F., Gharaibeh, N. G., and Scullion, T. (2017). "Case study on the use of mobile lidar to produce a preliminary drainage design." *Transportation Research Record: Journal of the Transportation Research Board,* 2655, 82-90.

Gurganus, C.F., and Gharaibeh, N. (2012). "Project selection and prioritization of pavement preservation." *Transp.Res.Rec.,* 2292, 36-44.

Haque, W., Urquhart, B., Berg, E., and Dhanoa, R. (2014). "Using business intelligence to analyze and share health system infrastructure data in a rural health authority." *Journal of Medical Internet Research,* 16(8), 1-16.

Hawkins, N. (2013). "Use of transportation asset management principles in state highway agencies." *Rep. No. NCHRP Synthesis 439,* Transportation Research Board, Washington, DC.

Hoffmann, M. (2016). "Introduction of a new continuous time and state space stochastic process in condition prediction." *The International Journal of Pavement Engineering,* 1-16.

Huang, Y. H. (2004). *Pavement analysis and design. 2nd ed.* Pearson/Prentice Hall, Upper Saddle River, NJ.

Huebner, R. S., Anderson, D. A., Warner, J. C., and Reed, J. R. (1997). "PAVDRN computer model for predicting water film thickness and potential for hydroplaning on new and reconditioned pavements." *Transportation Research Record,* 1599(1), 128-131.

Illinois Department of Transportation. (2006). *Drainage design.* Bureau of Local Roads and Streets, Springfield, IL.

Iowa Department of Transportation. (2012). *Design manual.* Iowa Department of Transportation, Des Moines, Iowa.

Jones, S., Cournane, S., Sheehy, N., and Hederman, L. (2016). "A business analytics software tool for monitoring and predicting radiology throughput performance." *J.Digit.Imaging,* 29(6), 645-653.

Khalifa, M., and Zabani, I. (2016). "Utilizing health analytics in improving the performance of healthcare services: A case study on a tertiary care hospital." *Journal of Infection and Public Health,* 9(6), 757-765.

King Jr., W., Mata, D., and Cooper III, S. B. (2015). "Evaluation of rutting distresses on I-20 near Minden, LA." *Rep. No. FHWA/LA.14/14-02TA-B,* Louisiana Transportation Research Center, Baton Rouge, LA.

Kokina, J., Pachamanova, D., and Corbett, A. (2017). "The role of data visualization and analytics in performance management: Guiding entrepreneurial growth decisions." *Journal of Accounting Education,* 38, 50-62.

Kyte, C. A., Perfater, M. A., Haynes, S., and Lee, H. W. (2004). "Developing and validating a tool to estimate highway construction project costs." *Transportation Management and Public Policy 2004,* (1885), 35-41.

Laiou, A., Papadimitriou, E., Yannis, G., and Milotti, A. (2017). "Road safety data and information availability and priorities in South-East European regions." *Transportation Research Procedia,* 25, 3703-3714.

Lantieri, C. (2015). "Mobile laser scanning system for assessment of the rainwater runoff and drainage conditions on road pavements." *International Journal of Pavement Research and Technology,* 8(1), 1-9.

Liebowitz, J. (2014). *Business analytics : an introduction.* CRC Press, Boca Raton, FL.

Luo, W., Wang, K. C. P., and Li, L. (2016). "Hydroplaning on sloping pavements based on Inertial Measurement Unit (IMU) and 1mm 3D laser imaging data." *Periodica Polytechnica.Transportation Engineering,* 44(1), 42-49.

Luo, W., Wang, K. C. P., Li, L., Li, Q. J., and Moravec, M. (2014). "Surface drainage evaluation for rigid pavements using an inertial measurement unit and 1-mm three-dimensional texture data." *Transp.Res.Rec.,* 2457, 121-128.

Maceda-Veiga, A., Baselga, A., Sousa, R., Vilà, M., Doadrio, I., and de Sostoa, A. (2017). "Fine-scale determinants of conservation value of river reaches in a hotspot of native and non-native species diversity." *Sci.Total Environ.,* 574, 455-466.

Matintupa, A., and Saarenketo, T. (2012). "New survey techniques in drainage evaluation: Laser scanner and thermal camera." *Rep. No. Task D1,* Roadex Network, Rovaniemi, Finland.

Melchers, R. E. (2015). "Using models to interpret data for monitoring and life prediction of deteriorating infrastructure systems." *Structure & Infrastructure Engineering: Maintenance, Management, Life-Cycle Design & Performance,* 11(1), 63-72.

Miller, J. S., and Lantz, J.,Kenneth E. (2010). "Options for improving transportation project scoping." *Public Works Manage.Policy,* 14(4), 332-350.

Mraz, A., and Nazef, A. (2008). "Innovative techniques with a multipurpose survey vehicle for automated analysis of cross-slope data." *Transportation Research Record,* 2068, 32-38.

Natural Resources Conservation Service (NRCS). "Web Soil Survey (WSS)." https://websoilsurvey.sc.egov.usda.gov/App/HomePage.htm (February 6, 2017).

New York State Department of Transportation. (2016). *Highway design manual.* Albany, NY.

Newman, M. E. J. (2010). *Networks : an introduction.* Oxford University Press, Oxford and New York.

O'Callaghan, J. F., and Mark, D. M. (1984). "The extraction of drainage networks from digital elevation data." *Computer Vision, Graphics and Image Processing,* 28, 323-344.

Olsen, M. J., Roe, G. V., Glennis, C., Persi, F., Reedy, M., Hurwitz, D., Williams, K., Tuss, H., Squellati, A., and Knodler, M. (2013). "Guidelines for the use of mobile LIDAR in transportation applications." *Rep. No. NCHRP Report 748,* Transportation Research Board, Washington, DC.

Ong, G. P., and Fwa, T. F. (2007). "Prediction of wet-pavement skid resistance and hydroplaning potential." *Transportation Research Record*, 2005, 160-171.

Pozarycki, A. (2016). "Condition assessment of lower roadway layers for pavement management systems." *Journal of Civil Engineering and Management*, 22(3), 311-321.

Roadscanners. "Roadscanners - Beyond the Surface." http://www.roadscanners.fi/company/ (March 16, 2016).

Schraven, D. (2011). "Effectiveness of infrastructure asset management: challenges for public agencies." *Built Environment Project and Asset Management*, 1(1), 61-74.

Schwanghart, W. (2014). "Short communication: TopoToolbox 2-MATLAB-based software for topographic analysis and modeling in Earth surface sciences." *Earth Surface Dynamics*, 2(1), 1-7.

Schwanghart, W. (2010). "TopoToolbox: A set of Matlab functions for topographic analysis." *Environmental Modelling & Software*, 25(6), 770-781.

Seret, A., Maldonado, S., and Baesens, B. (2015). "Identifying next relevant variables for segmentation by using feature selection approaches." *Expert Syst.Appl.*, 42(15-16), 6255-6266.

Shi, L., Zhang, L., Zhao, L., Yang, J., Li, P., and Zhang, L. (2013). "The potential of linear discriminative Laplacian eigenmaps dimensionality reduction in polarimetric SAR classification for agricultural areas." *ISPRS Journal of Photogrammetry and Remote Sensing*, 86, 124-135.

SICK: Sensor Intelligence. (2011). *Detection and ranging solutions laser measurment technology - components and application packages.* SICK, Waldkirch, Germany.

Sinha, K. C., and Labi, S. (2007). *Transportation decision making : principles of project evaluation and programming.* John Wiley & Sons, Hoboken, N.J.

Smith, R. E., and Fallaha, K. M. (1992). "Developing an interface between network-and project-level pavement management systems for local agencies." *Transp.Res.Rec.*, 1344, 14-21.

Stoklasa, J., Talasek, T., Kubatova, J., and Seitlova, K. (2017). "Likert scales in group multiple-criteria evaluation." *Journal of Multiple-Valued Logic & Soft Computing*, 29(5), 425-440.

Taheri, A., OBrien, E. J., and Collop, A. C. (2012). "Pavement damage model incorporating vehicle dynamics and a 3D pavement surface." *International Journal of Pavement Engineering*, 13(4), 374-383.

Taylor, T. R. B. (2012). "Change orders and lessons learned: Knowledge from statistical analyses of engineering change orders on Kentucky highway projects." *J.Constr.Eng.Manage.*, 138(12), 1360-1369.

Texas Department of Transportation (TxDOT). (2016). *FY 2016 PMIS rater's manual.* TxDOT Maintenance Division - Pavement Preservation Section, Austin, TX.

Texas Department of Transportation (TxDOT). (2014 (Rev. 2015)). *Hydrualic design manual.* TxDOT, Austin, TX.

Texas Department of Transportation (TxDOT). (2014a). *Condition of Texas pavements: PMIS annual report FY 2011-2014*. TxDOT Maintenance Division - Pavement Preservation Branch, Austin, TX.

Texas Department of Transportation (TxDOT). (2014b). *Project development process manual.* TxDOT, Austin, TX.

Texas Department of Transportation (TxDOT). (2014c). *Roadway design manual.* TxDOT, Austin, TX.

Texas Department of Transportation (TxDOT). (2014d). *Standard specifications for construction and maintenance of highways, streets, and bridges*. TxDOT, Austin, TX.

Texas Department of Transportation (TxDOT). (2003). *Managing Texas pavements*. TxDOT Construction Division - Materials and Pavements Section, Austin, TX.

TireRack. (a). "Tire Tech Air Pressure, Time Fluctations." https://www.tirerack.com/tires/tiretech/techpage.jsp?techid=74 (October 5, 2017).

TireRack. (b). "Tire Tech Tire Specs Explained: Tread Depth." https://www.tirerack.com/tires/tiretech/techpage.jsp?techid=197 (October 5, 2017).

Tsai, Y. C., and Li, F. (2012). "Critical assessment of detecting asphalt pavement cracks under different lighting and low intensity contrast conditions using emerging 3D laser technology." *J.Transp.Eng.*, 138(5), 649-656.

Tsai, Y. C., Ai, C. B., Wang, Z. H., and Pitts, E. (2013). "Mobile cross-slope measurement method using lidar echnology." *Transp.Res.Rec.*, 2367, 53-59.

Tufte, E. R. (2006). *Beautiful evidence.* Graphics Press, Cheshire, Conn.

Tufte, E. R. (2001). *The visual display of quantitative information. 2nd ed.* Graphics Press, Cheshire, Conn.

Umer, A., Hewage, K., Haider, H., and Sadiq, R. (2016). "Sustainability assessment of roadway projects under uncertainty using Green Proforma: An index-based approach." *International Journal of Sustainable Built Environment,* 5(2), 604-619.

Villa-Forte, A. "Merck Manual Organ Systems." http://www.merckmanuals.com/home/fundamentals/the-human-body/organ-systems (October 23, 2017).

Wang, L., and Wu, C. (2017). "Business failure prediction based on two-stage selective ensemble with manifold learning algorithm and kernel-based fuzzy self-organizing map." *Knowledge-Based Syst.,* 121, 99-110.

Wiegmann, J., and Yelchuru, B. (2012). "Resource allocation logic framework to meet highway asset preservation." *Rep. No. 736,* Transportation Research Board, Washington, D.C.

Winterkorn, H. F., and Fang, H. (1975). *Foundation engineering handbook.* Van Nostrand Reinhold, New York.

Woldesenbet, A., Jeong, H. D., and Park, H. (2016). "Framework for integrating and assessing highway infrastructure data." *J.Manage.Eng.,* 32(1), 1-14.

Wolf, R. (2016). "Dashboard design." *Strategic Finance,* 98(6), 20-27.

Yassin, M., Jayasooriya, W., and Gunaratne, M. (2013). "Assessment of the Reliability of Predicting Hydroplaning Risk Based on Past Hydroplaning Accident Data on the Florida Interstate System." *Transportation Research Record,* 2369, 104-113.

Zaghloul, S., He, Z., Kerr, J. B., and Vitillo, N. (1998). "Project scoping using falling weight deflectometer testing: New Jersey experience." *Transportation Research Record,* 1643, 34-43.

Zhang, H., Keoleian, G., and Lepech, M. (2013). "Network-level pavement asset management system integrated with life-cycle analysis and life-cycle optimization." *J Infrastruct Syst,* 19(1), 99-107.

Zhang, T. (2010). "Discriminative orthogonal neighborhood-preserving projections for classification." *IEEE Transactions on Systems, Man, and Cybernetics, Part B: Cybernetics,* 40(1), 253-263.

APPENDIX A

MOBILE LIDAR ACCURACY

A.1 PROCESSING MOBILE LIDAR DATA INTO A GRIDDED FORMAT

For this study, LiDAR points are organized in a surface grid for reduction and hydraulic analysis purposes. Three factors can affect the data orientation and data density of the roadway surface grid for mobile LiDAR data. These factors are:

- Skew created in collecting data from a mobile apparatus
- Longitudinal spacing between cross sections
- Transverse spacing within cross sections

A.1.1 **Longitudinal Skew**

Longitudinal skew, that is the difference between creating a perfectly perpendicular cross section to the centerline and one that crosses the centerline at an angle, is created by collecting data from a mobile device. Because the laser scans through the horizon and the data collection vehicle is moving, each point within a cross section is in a different longitudinal location with respect to the centerline. Table 11 shows the longitudinal skew at various data collection speeds (i.e., speed of the MLS vehicle) across the field of view, the data collection lane and from pavement edge to pavement edge of a typical two-lane roadway.

Table 11. Longitudinal skew associated with mobile LiDAR data (English units)

Vehicle Speed (mph)	Max Longitudinal Skew (in.)	Longitudinal Skew across Collection Lane (in.)	Longitudinal Skew from Edge of Pavement to Edge of Pavement (in.)
5	0.47	0.20	0.29
10	0.93	0.39	0.59
15	1.39	0.59	0.88
20	1.86	0.78	1.17
25	2.32	0.98	1.47
30	2.79	1.17	1.76
35	3.25	1.37	2.05
40	3.72	1.56	2.35
45	4.18	1.76	2.34
50	4.64	1.96	2.93
55	5.11	2.15	3.23
60	5.57	2.35	3.52
65	6.04	2.54	3.81
70	6.50	2.74	4.11
75	6.97	2.93	4.40
80	7.43	3.13	4.69

The maximum longitudinal difference represents the laser reading 190° apart, or 5° above the horizon created by the laser. This distance is often of no interest because the laser is likely reading leaves on trees or a target object far in the distance. For practical purposes,

the skew created by collecting the data from a mobile apparatus will often be less than 7.62 cm (3 in.) and will almost always be less than 15.24 cm (6 in.).

A.1.2 **Longitudinal Spacing**

Longitudinal spacing represents the spacing between cross section measurements and must be accounted for during data reduction. Using mobile LiDAR, transverse cross sections are taken on small intervals, typically less than 30 cm (1 ft.). Fig. 34 displays transverse cross section spacing for a 10.5 km (6.5 mi.) section of rural highway. On this roadway, 54,621 transverse strings of data were created. The average spacing between these strings is 19.2 cm (less than 8 in.) apart. Data were collected on this roadway section at an average vehicle speed of 69 kph (42.9 mph).

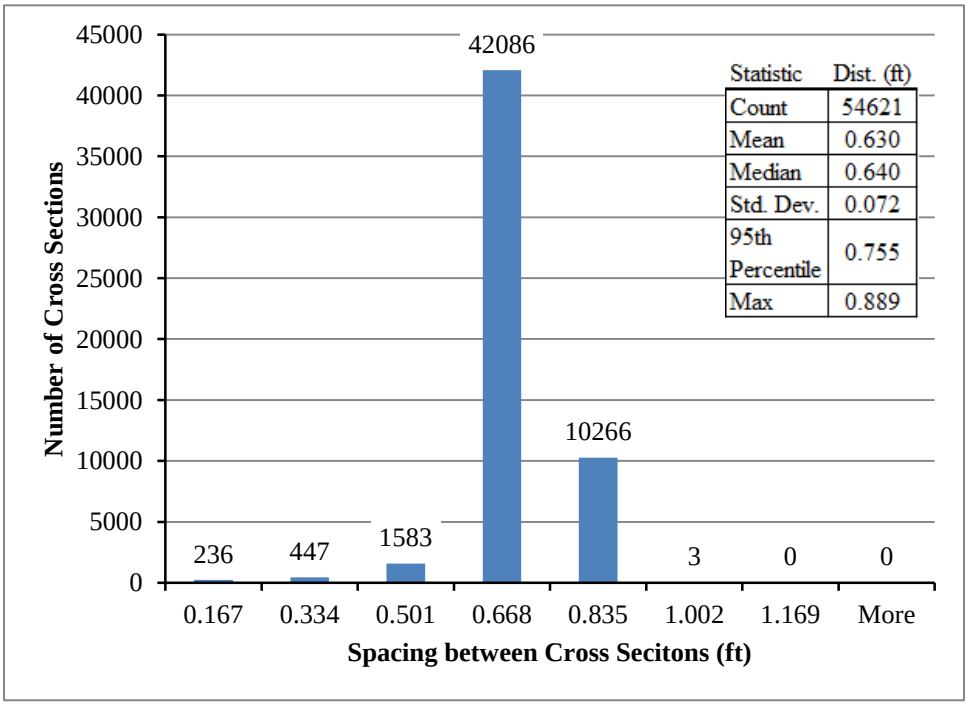

Fig. 34. Transverse cross section spacing over multiple miles traveling at approximately 43 mph (English Units)

A.1.3 **Transverse Spacing within a Cross Section**

Skew and cross section spacing deal with measurements moving in the direction of the data collection vehicle, but transverse spacing deals with the distance between measurements within a cross section. Transverse spacing (i.e., spacing within a cross section) is a function of the following four variables:

- Laser frequency
- Angular resolution
- Distance from laser source
- Slope of target surface

The laser dictates the first two variables, while surface geometry controls the latter two. Because the angular resolution does not change, if a target surface moves steeply away from the laser, measurements become farther apart. Fig. 35 displays the spacing across a typical two lane roadway with varying front slopes. Fig. 35 also displays the approximate location of the paved surface and roadside clear zones. For most paved surfaces, the spacing between points will not exceed 25.4 cm (10 in.). For large metro freeways with four, six, or eight lanes in each direction this will not be the case, but for most of the network it can be assumed that transverse spacing between points will not exceed 30.5 cm (1 ft.) and within the data collection lane points will often be within 5.08 cm (2 in.) of each other.

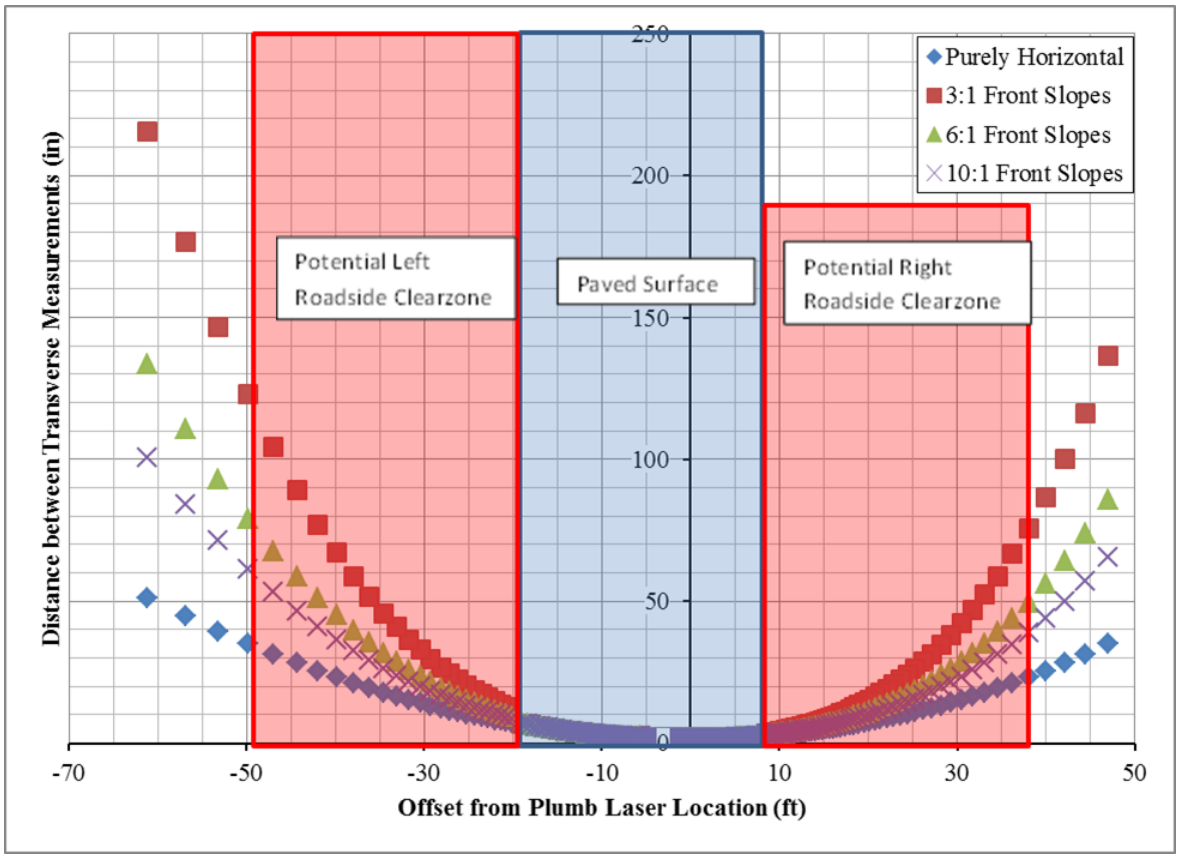

Fig. 35. Transverse spacing for a two-lane roadway (English Units)

The grid size for pavements must be small enough so that no interpolation is required. For example, if the transverse spacing is 0.36 m (14 in.), then the grid size should not be smaller than 0.36 m^2 (14 in^2) to avoid interpolation. The largest spacing between skew, longitudinal spacing and transverse spacing dictates the grid size for pavements. For a paved surface only analysis, a 0.3048 m x 0.3048 m (1 ft. x 1 ft.) grid can be used on most sections with no interpolation between points. Grid size is a function of the following variables:

- Number of lanes
- Data collection lane

- Width of paved surface
- Slope of the target surface.

Roadside geometry varies greatly depending on the topography of the site. Thus, the distance from the laser to the target surface requires a change in grid size. The clear zone concept often dictates the horizontal offset area of concern. Because roadside geometry is not typical, knowledge of the potential clear zone widths can help define the appropriate roadside grid size. The clear zone is based off of the edge of the traveled way, not the edge of pavement, and can be much smaller than 9.14 m (30 ft.) depending on posted speed and traffic volume. Because motorists do not directly interact with the roadside, interpolation between points was allowed, thus a 0.9144 m x 0.9144 m (3 ft. x 3 ft.) grid size is used for roadsides. At this grid size, along the right roadside of a rural roadway with a shoulder, no interpolation is required between the edge of pavement and 4.57 m (15 ft.) away. If no shoulder exists, this distance increases to 7.32 m (24 ft.). For a left roadside with a shoulder, interpolation begins approximately 2.44 m (8 ft.) from the edge of pavement. If no shoulder exists, it begins 5.18 m (17 ft.) from the edge of pavement. In summary, for typical rural two lane facilities, one data collection run in either travel lane can be used for network level analysis. A 0.3048 m x 0.3048 m (1 ft. x 1 ft.) grid size is used for pavement analysis and a 0.9144 m x 0.9144 m (3 ft. x 3 ft.) grid size is used for roadside analysis.

A.2 MOBILE LIDAR LENGTH ANALYSIS

A precisely measured test track of known length, stratified on 3.05 m (10 ft.) increments exists at the Texas A&M University RELLIS campus. This track has a long history of use

with inertial profiler certifications as specified in TxDOT's Standard Specifications. A piece of reflective tape was placed at 0 m (0 ft.) and another at 499.872 m (1640 ft.). Mobile LiDAR data repeatedly measured this length to within 0.15%. Table 12 displays the results of the length analysis.

Table 12. Mobile LiDAR measured length analysis

Run Number	Field Measured Distance (ft)	Field Measured Distance (m)	LiDAR Measured Distance (ft)	LiDAR Measured Distance (m)	Difference (ft)	Difference (m)	% Difference
1			1639.15	499.61	0.85	0.259	0.05%
2			1638.15	499.31	1.85	0.564	0.11%
3	1640	499.872	1637.57	499.13	2.43	0.741	0.15%
4			1638.62	499.45	1.38	0.421	0.08%
5			1638.62	499.45	1.38	0.421	0.08%

A.3 Cross Slope between Data Collection Vehicle Wheel Paths

A 1.83 m (6 ft.) straight edge and digital protractor were used to precisely measure the cross slope on 15.24 m (50 ft.) increments along the same track used for the known length measurements. MLS data was processed into cross sections of 0.1524 m (6 in.) spacing with transverse measurements within the cross sections spaced 0.0762 m (3 in.) apart. MLS data is collected dynamically and processed into predefined grids, thus accuracy analyses consider a window around the discretely measured point. A 0.6096 m (2 ft.) window around the discretely measured locations was used to compare the accuracy of the MLS cross slope. Table 13shows these results. The top portion of Table 13 compares the

field measurement with the average of the four cross slopes generated by the MLS in the 0.6096 m (2 ft.) window. The bottom portion of Table 13 compares the accuracy of the cross section most similar to the field measured location. In summary, a single cross section within a small window around a discretely measured location will likely be within 0.05% and will at times identically match. If the average value is used, the accuracy between the MLS and the finite location is near 0.15%.

Table 13. Mobile LiDAR cross slope analysis (English units)

Location	Field Measured Cross Slope (%) (1)	Mobile LiDAR Run 1		Mobile LiDAR Run 2		Mobile LiDAR Run 3	
		2-ft Average (%) (2)	Difference (1) – (2)	2-ft Average (%) (2)	Difference (1) – (2)	2-ft Average (%) (2)	Difference (1) – (2)
1 (0-ft)	1.75%	1.71%	0.04%	1.92%	-0.17%	2.18%	-0.43%
2 (50-ft)	2.09%	1.94%	0.15%	1.95%	0.14%	1.83%	0.26%
3 (100-ft)	2.27%	2.06%	0.21%	2.34%	-0.07%	2.00%	0.27%
4 (150-ft)	2.44%	2.62%	-0.18%	1.95%	0.49%	2.34%	0.10%
5 (200-ft)	2.44%	2.42%	0.02%	2.12%	0.32%	2.33%	0.11%
6 (250-ft)	2.27%	1.90%	0.37%	1.73%	0.54%	2.15%	0.12%
7 (300-ft)	2.09%	2.07%	0.02%	2.20%	-0.11%	2.14%	-0.05%
8 (350-ft)	2.27%	2.05%	0.22%	1.95%	0.32%	2.01%	0.26%
9 (400-ft)	1.92%	1.75%	0.17%	1.80%	0.12%	1.65%	0.27%
10 (450-ft)	2.44%	2.18%	0.26%	2.04%	0.40%	2.27%	0.17%
11 (500-ft)	2.27%	2.03%	0.24%	1.97%	0.30%	2.18%	0.09%

Location	Field Measured Cross Slope (%) (1)	Mobile LiDAR Run 1		Mobile LiDAR Run 2		Mobile LiDAR Run 3	
		2-ft Average (%) (2)	Difference (1) – (2)	2-ft Average (%) (2)	Difference (1) – (2)	2-ft Average (%) (2)	Difference (1) – (2)
1 (0-ft)	1.75%	1.74%	0.01%	1.85%	-0.10%	1.82%	-0.07%
2 (50-ft)	2.09%	2.09%	0.00%	2.09%	0.00%	2.08%	0.01%
3 (100-ft)	2.27%	2.23%	0.04%	2.30%	-0.03%	2.10%	0.17%
4 (150-ft)	2.44%	2.52%	-0.08%	2.13%	0.31%	2.44%	0.00%
5 (200-ft)	2.44%	2.47%	-0.03%	2.43%	0.01%	2.46%	-0.02%

A.4 CROSS SLOPE ACROSS DATA COLLECTION LANE

To expand the accuracy analysis of the MLS, the cross slope measured and processed across the entire data collection lane was compared with professionally surveyed locations. The lane used for analysis was the outside inbound lane of New Main Dr., entering the Texas A&M University campus. This lane consists of both a travel lane and bicycle lane with concrete curb on the outside. Over approximately a 161 m (0.1 mi.) section, professionally surveyed cross sections were acquired on 3.05 m (10 ft.) spacing. The cross slope evaluated for accuracy begins in the middle of the white lane striping to the left of the data collection vehicle and proceeds to the base of the curb at the outside edge. MLS data was processed into cross sections spaced on 0.3048 m (1 ft.) increments with 0.0762 m (3 in.) transverse spacing between points within a cross section. Once again, because of the dynamic nature of MLS data collection and because the precise location of the survey point is only as accurate as the survey equipment used, both a 0.3048 m (1 ft.) longitudinal and transverse window are used for accuracy comparison. Three repeat runs and 39 cross sections were used for comparison. The histogram in Fig. 36 consolidates the 39 cross sections from each of the three repeat runs. The population count in Fig. 36 is 117 with 103 cross sections, or 88% of cross sections, within an accuracy of ±0.1%. Approximately 92% of all cross slopes are within ±0.15% and more than 95% of cross sections are within ±0.2%.

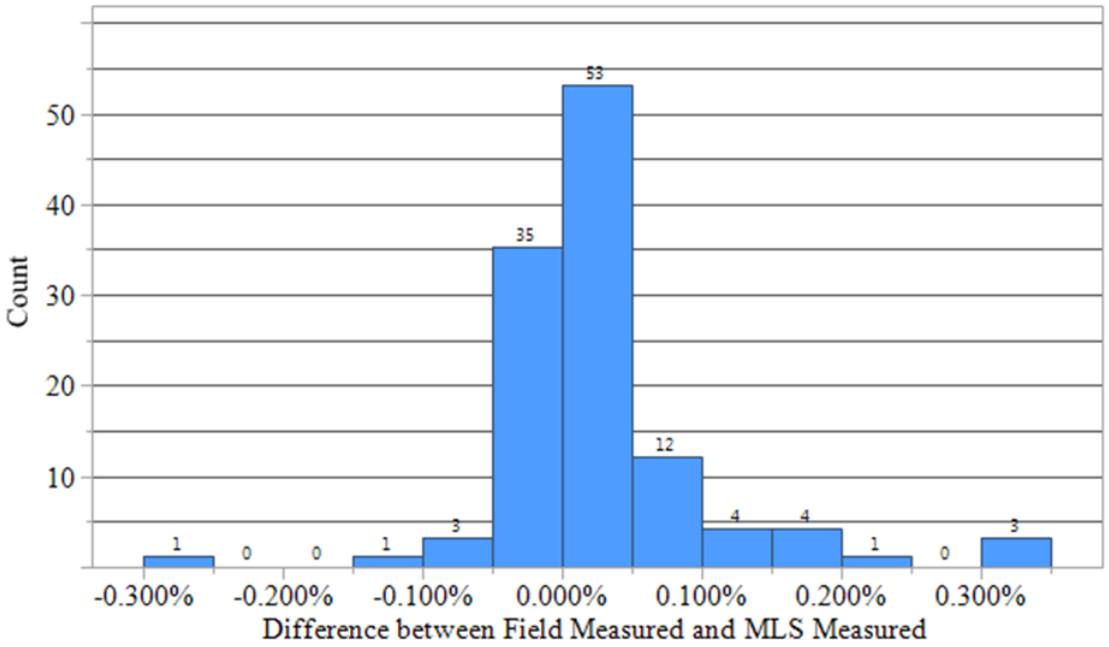

Fig. 36. Histogram of data collection lane cross slope accuracy

The multiple runs associated with this accuracy analysis allows for a comparison of the repeatability of the cross slope measurement. Fig. 37 shows that 83% of cross sections have cross slope repeatability within 0.10% and 91% within 0.15%.

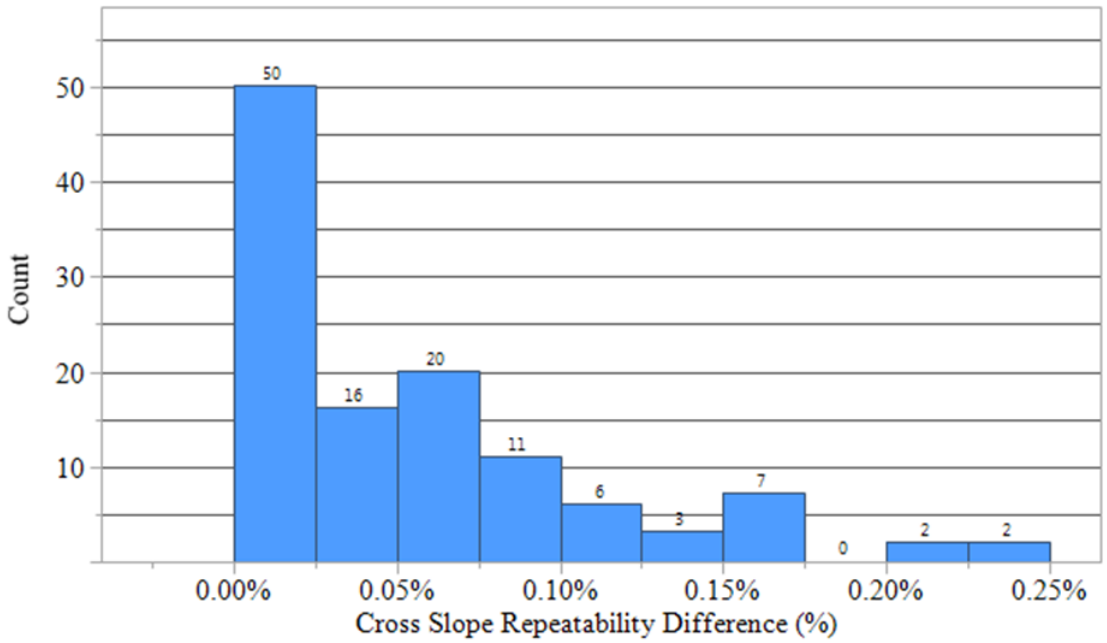

Fig. 37. Histogram of cross slope repeatability between MLS runs

A.5 Ditch Analysis

Data was collected on SH 30 in a single direction to compare actual roadside conditions with LiDAR processed measurements. Using a single data collection run in one direction, both the left and right roadsides are analyzed. Due to the increase in spacing as the target moves away from the laser, a 0.9144 m (3 ft.) x 0.9144 m (3 ft.) grid is used to process the data on the roadsides. Along a 45.72 m (150 ft.) longitudinal section of SH 30, 16 cross sections are available on 3.05 m (10 ft.) increments for right and left ditch analysis.

Table 14 shows the comparison of the MLS generated ditch offset within the 0.9144 m (3 ft.) x 0.9144 m (3 ft.) grid to the surveyed offset. Along the right side of the roadway, adjacent to the data collection lane, all ditch offsets are within 0.9144 m (3 ft.). As the laser has to travel farther to the target surface on the left side of the roadway, the accuracy

remains within 0.9144 m (3 ft.). Data are not available for cross sections 4 through 11 on the left side because a driveway exists in this location. Table 15 compares the ditch depth from the processed data with the survey data. In Table 15, it is clear that the surveyed ditch depth is deeper than that measured by the MLS. This is most likely because of the vegetation along the right-of-way. The laser returns to the source after striking a surface, therefore when it encounters grass, it returns a measurement without completely reaching the ground. The area along SH 30 was finish mowed during MLS collection. Fig. 38 is a screenshot from the MLS software on the day of data collection showing how tightly the ROW is mowed along with the driveway on the left side of the screen reference with the omitted data.

Table 14. Ditch flowline offset accuracy comparison (English units)

Cross Section No.	Right Side Ditch Flowline			Left Side Ditch Flowline		
	Surveyed Offset (ft)	MLS Processed Offset (ft)	Difference (ft)	Surveyed Offset (ft)	MLS Processed Offset (ft)	Difference (ft)
1	30.21	28.784	1.426	42.63	43.2126	-0.5826
2	30.05	28.784	1.266	41.57	40.2126	1.3574
3	30.1	28.784	1.316	40.43	40.2126	0.2174
4	29.98	28.784	1.196	49.9		
5	30.21	28.784	1.426	40.22		
6	29.99	28.784	1.206	50.22		
7	30.44	28.784	1.656	39.87		
8	30.38	28.784	1.596	49.65		
9	30.18	28.784	1.396	49.67		
10	30.75	28.784	1.966	50.43		
11	31.24	28.784	2.456	40.37	40.2126	0.1574
12	30.16	28.784	1.376	40.37	40.2126	0.1574
13	29.92	28.784	1.136	39.24	40.2126	-0.9726
14	30.07	28.784	1.286	38.56	40.2126	-1.6526
15	30.34	28.784	1.556	38.08	40.2126	-2.1326
16	30.71	28.784	1.926	38.29	40.2126	-1.9226

Table 15. Ditch flowline depth comparison (English units)

Cross Section No.	Right Side Ditch Flowline			Left Side Ditch Flowline		
	Surveyed Depth (ft)	MLS Processed Depth (ft)	Difference (ft)	Surveyed Depth (ft)	MLS Processed Depth (ft)	Difference (ft)
1	2.19	2.09	0.10	2.77	2.45	0.32
2	2.20	1.99	0.21	2.78	2.57	0.21
3	2.19	1.97	0.22	2.83	2.54	0.29
4	2.14	1.89	0.25			
5	2.04	1.94	0.10			
6	2.09	1.94	0.15	0.66		
7	2.04	1.92	0.12	0.65		
8	2.08	1.93	0.15	0.62		
9	2.08	1.95	0.13	0.55		
10	2.13	1.95	0.18	0.61		
11	1.87	1.85	0.02	2.28	1.89	0.39
12	2.04	2.00	0.04	2.07	1.88	0.19
13	2.15	2.07	0.08	1.86	1.62	0.24
14	2.12	2.04	0.08	1.84	1.60	0.24
15	2.12	1.96	0.16	1.96	1.65	0.31
16	2.02	1.92	0.10	2.09	1.72	0.37

Fig. 38. SH 30 on the day of MLS data collection

Along the right roadside, a finished mowed surface creates a ditch or roadside surface between one inch and three inches higher than the actual ground surface. Vegetation also affects the measured slopes of the roadside. For rural areas, vegetation is expected to be higher. Ideally, data collection will occur immediately following the TXDOT mowing cycle. Under Item 730 in TxDOT's Standard Specifications, roadside mowers should be set to between 12.7 cm (5 in.) and 17.78 cm (7 in.) (Texas Department of Transportation (TxDOT) 2014d).

A.6 Roadside Slope(s) Analysis

Using 0.9144 m (3 ft.) x 0.9144 m (3 ft.) grids, the LiDAR processed roadside slopes are compared against ground truth surveyed slopes. Along SH 30, 26 cross sections are used for the analysis. Data was collected in a single direction, but both the left and right roadsides were processed for comparison. Entering this analysis, it was expected that the accuracy of the left side would be lower than the right side because the laser travels farther to reach left

roadside slopes. Fig. 39 shows the absolute value of the difference between the MLS processed right front and back slopes compared with survey measured values. Fig. 40 shows the same information using the same scaling for the left roadside. For both the right front and back slope, 26 cross sections are used for analysis, but on the left side only 18 cross sections are used for the front slope and 16 for the back slope. The availability of more sections on the right side (i.e. the side adjacent to the data collection vehicle) indicates cleaner data. In this case, cleanliness of data speaks to the ability of the laser to reach the target surface. This becomes more difficult on the left side because the laser must cross opposing traffic or the laser encounters an obstruction rather than reaching the target surface. Encountering an obstruction can take place on the right side as well, but it can easier to deal with in post processing because multiple points can be available near the obstruction because the laser is closer to its source. On the left side, spacing between laser readings can be far enough apart that the reading on the obstruction is the only value to use in post processing.

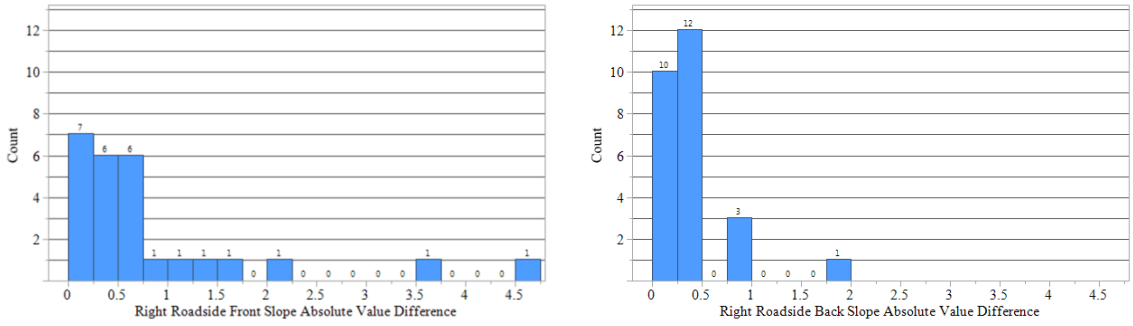

Fig. 39. Right roadside slope comparison

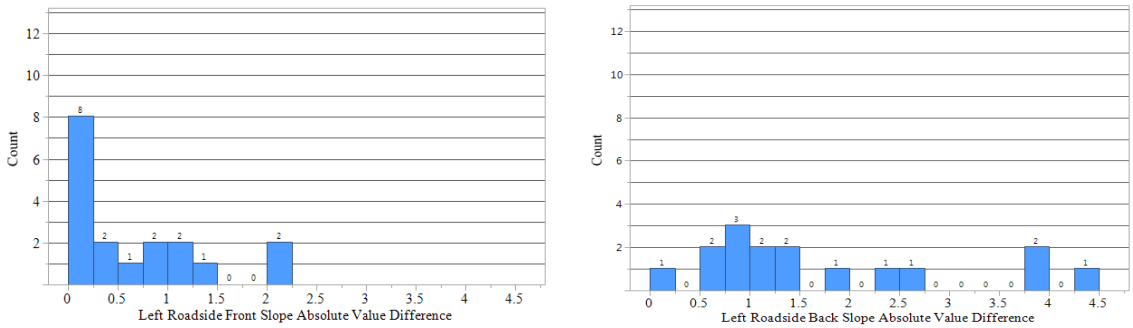

Fig. 40. Left roadside slope comparison

Fig. 39 shows that the difference between the survey measured front slope and MLS processed front slope is typically less than 0.75. For the back slope, values are typically within 0.5, more accurate than the front slope. Initially, this appears counterintuitive because the back slope is farther from the laser source than the front slope. However, front slope surfaces, by definition, are moving away from the laser source. Essentially, the laser chases the front slope downward to reach the surface. The back slope however moves upward and more easily back into the laser trajectory. For this reason, when the back slope is not significantly far from the laser source, it has the potential to be more accurate than the front slope. Moving to the left side of the roadway, the front slope is accurate on almost half of its readings to within 0.25. The accuracy of the left roadside back slope is much more variable as the laser begins to exceed 22.86 m (75 ft.) from source to target surface. Table 16 shows the average, median, and standard deviation for the histograms referenced in Fig. 39 and Fig. 40. Analysis of the median value helps minimize the effect of outliers and shows that the right roadside accuracy, regardless of front or back slope is within 0.5. More often than not, the MLS processed front slope is flatter than the surveyed front slope. This result is

expected as vegetation in the ditch flowline raises the elevation of the target surface. When using the pavement as the tie-point, with a raised flowline the flatter slope is generated.

Table 17 shows the direct comparison for 16 cross sections on the right roadside along SH 30. A larger number associated with the horizontal measurement indicates a flatter slope. In every instance in Table 17, the MLS processed slope is flatter than the surveyed slope.

Table 16. Roadside difference statistics

Roadside Attribute	Number of Cross Sections	Mean	Median	Standard Deviation
Right Front Slope	26	0.835	0.481	1.101
Right Back Slope	26	0.394	0.331	0.379
Left Front Slope	18	0.698	0.439	0.707
Left Back Slope	16	1.729	1.297	1.277

Table 17. Direct right roadside slope comparison

Cross Section Number	Surveyed Front Slope	MLS Processed Front Slope	Surveyed Back Slope	MLS Processed Back Slope
1	7.53(H):1(V)	7.59(H):1(V)	8.80(H):1(V)	8.51(H):1(V)
2	7.46(H):1(V)	8.04(H):1(V)	8.38(H):1(V)	8.27(H):1(V)
3	8.18(H):1(V)	7.97(H):1(V)	7.90(H):1(V)	7.68(H):1(V)
4	7.59(H):1(V)	8.47(H):1(V)	7.76(H):1(V)	7.68(H):1(V)
5	8.18(H):1(V)	8.49(H):1(V)	7.67(H):1(V)	7.36(H):1(V)
6	8.04(H):1(V)	8.60(H):1(V)	7.29(H):1(V)	6.88(H):1(V)
7	8.77(H):1(V)	9.11(H):1(V)	7.01(H):1(V)	6.94(H):1(V)
8	8.48(H):1(V)	8.91(H):1(V)	6.75(H):1(V)	6.59(H):1(V)
9	8.44(H):1(V)	8.86(H):1(V)	6.74(H):1(V)	6.80(H):1(V)
10	8.40(H):1(V)	8.94(H):1(V)	6.44(H):1(V)	6.73(H):1(V)
11	10.23(H):1(V)	10.22(H):1(V)	6.86(H):1(V)	7.73(H):1(V)
12	8.72(H):1(V)	9.02(H):1(V)	6.73(H):1(V)	7.15(H):1(V)
13	7.77(H):1(V)	8.27(H):1(V)	6.55(H):1(V)	6.93(H):1(V)
14	8.41(H):1(V)	8.58(H):1(V)	6.43(H):1(V)	6.86(H):1(V)
15	8.05(H):1(V)	8.61(H):1(V)	6.26(H):1(V)	6.65(H):1(V)
16	8.41(H):1(V)	8.46(H):1(V)	6.24(H):1(V)	6.68(H):1(V)

A.7 Rut Depth Measurements

Using the inverted rut track located at the Texas A&M University RELLIS campus, the ability of the MLS device to measure rut depth was analyzed. Using 7.62 cm (3 in.), 2.54 cm (1 in.), 1.27 cm (0.5 in.), and 0.635 cm (0.25 in.) inverted rut plates of approximately 12.19 m (40 ft.), three measurements MLS measurements along each plate were compared

with the known height. Fig. 41 displays the reflection data and cross section for the 2.54 cm (1 in.) rut plates. The rut plates are easily visible in the cross section view. Below Fig. 41 is Table 18 showing the MLS measurements of the rut plates. To develop the measurements in Table 18, 7.62 cm (3 in.) transverse spacing was used in processing. Each measurement dot in Fig. 41 is spaced 7.62 cm (3 in.) apart.

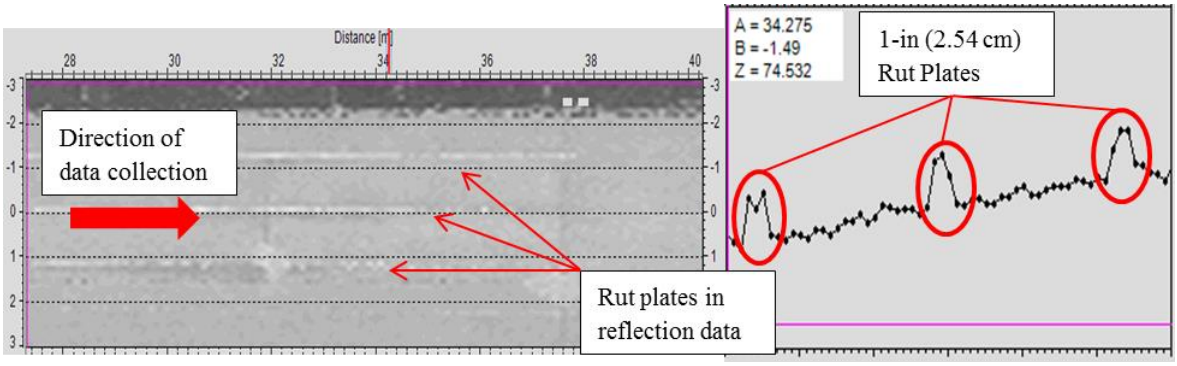

Fig. 41. 2.54 cm (1 in.) rut plate display

Table 18. MLS rut height measurement comparison (English units)

3-in (7.62 cm) Rut Plate Measurements						
Location No.	MLS Measurements (in)			Difference (in) (Actual – MLS)		
	Left Plate	Middle Plate	Right Plate	Left Plate	Middle Plate	Right Plate
1	3.11	2.91	3.15	-0.11	0.09	-0.15
2	2.95	2.83	3.07	0.05	0.17	-0.07
3	2.95	3.07	2.87	0.05	-0.07	0.13
1-in (2.54 cm) Rut Plate Measurements						
Location No.	MLS Measurements (in)			Difference (in) (Actual – MLS)		
	Left Plate	Middle Plate	Right Plate	Left Plate	Middle Plate	Right Plate
1	0.98	0.98	1.02	0.02	0.02	-0.02
2	0.94	1.02	1.18	0.06	-0.02	-0.18
3	0.87	0.98	1.06	0.13	0.02	-0.06
0.5-in (1.27 cm) Rut Plate Measurements						
Location No.	MLS Measurements (in)			Difference (in) (Actual – MLS)		
	Left Plate	Middle Plate	Right Plate	Left Plate	Middle Plate	Right Plate
1	0.55	0.51	0.79	-0.05	-0.01	-0.29
2	0.67	0.47	0.63	-0.17	0.03	-0.13
3	0.59	0.51	0.47	-0.09	-0.01	0.03
0.25-in (0.635 cm) Rut Plate Measurements						
Location No.	MLS Measurements (in)			Difference (in) (Actual – MLS)		
	Left Plate	Middle Plate	Right Plate	Left Plate	Middle Plate	Right Plate

APPENDIX B

DATA ACTIVATION SUPPLEMENTAL MATERIAL

B.1 FATIGUE CRACKING DATA MINING METHODOLOGY AND FIGURES

B.1.1 Skew of Fatigue Cracking Data and Stability of the Median

Pavement distress data does not follow a normal distribution. Fig. 42 shows histograms for percent alligator cracking from the TxDOT Austin District across four fiscal years. The data is highly right skewed with standard deviations higher than the mean value.

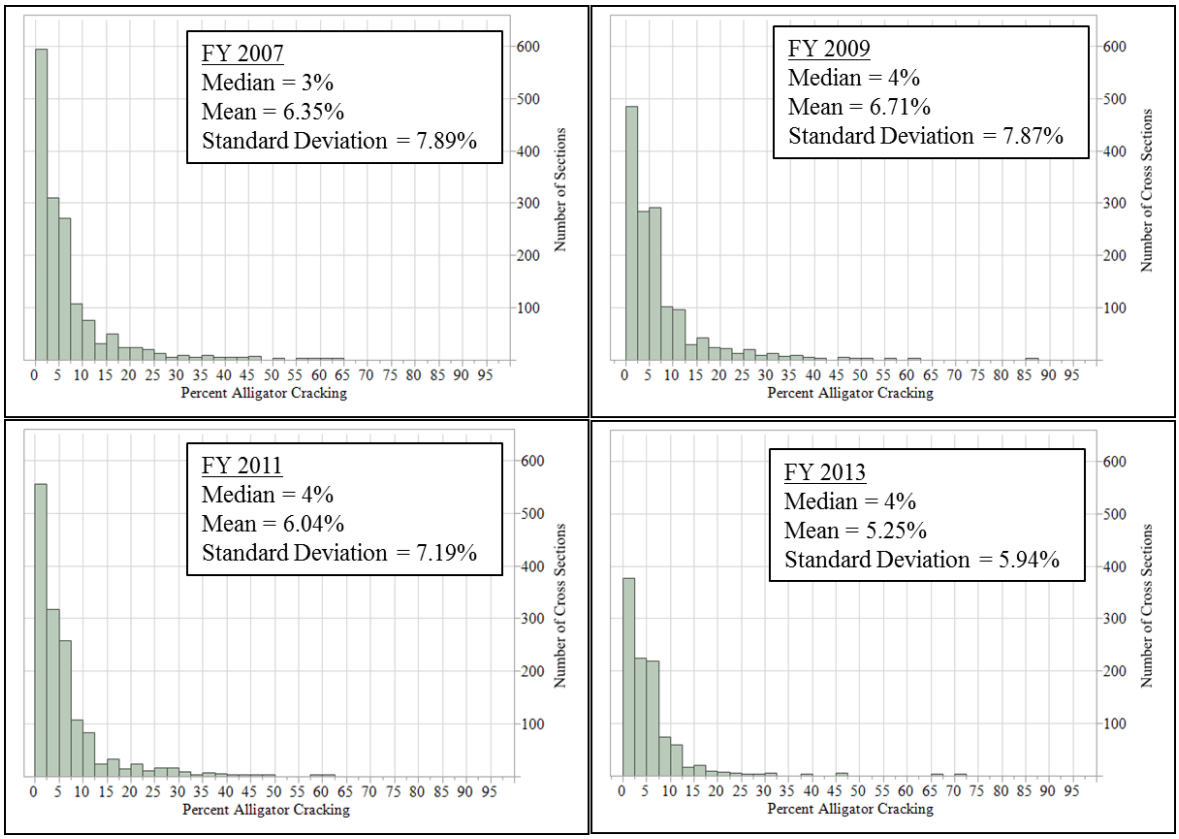

Fig. 42. Percent alligator cracking histograms for Austin District pavement sections in FY 2007, 2009, 2011, and 2013

Table 19, Table 20, and Table 21 present percent alligator statistics for the Austin, Bryan, and Tyler districts from FY 2007 thru FY 2016.

Table 19. Austin district 10-year alligator cracking statistics

Fiscal Year	Austin District (All sections)					Austin District (Only sections with alligator cracking)				
	N	Median	Mean	Std. Dev.	90th Percentile	N	Median	Mean	Std. Dev.	90th Percentile
2007	6803	0	1.33	4.38	4	1456	3	6.35	7.89	15
2008	6962	0	1.74	4.86	5	1794	4	6.87	7.69	15
2009	7069	0	1.32	4.38	4	1396	4	6.71	7.87	15
2010	7140	0	1.53	4.61	5	1480	5	7.36	7.72	17
2011	7189	0	1.20	3.94	4	1435	4	6.04	7.19	13
2012	7177	0	1.69	5.06	5	1587	5	7.57	8.34	17
2013	7219	0	0.69	2.73	2	970	4	5.25	5.94	11
2014	7494	0	0.76	2.75	2	1172	3	4.94	5.60	11
2015	7442	0	0.75	2.98	2	1034	3	5.42	6.23	12
2016	7218	0	0.57	2.46	1	893	3	4.63	5.94	10

Table 20. Bryan district 10-year alligator cracking statistics

Fiscal Year	Bryan District (All sections)					Bryan District (Only sections with alligator cracking)				
	N	Median	Mean	Std. Dev.	90th Percentile	N	Median	Mean	Std. Dev.	90th Percentile
2007	6809	0	0.33	1.99	0	469	3	4.72	6.09	11
2008	6830	0	0.26	1.64	0	462	2	3.91	5.06	9
2009	6907	0	0.25	1.68	0	430	2	4.08	5.44	9
2010	6970	0	0.33	2.17	0	469	3	4.94	6.88	11
2011	6916	0	0.27	1.75	0	435	3	4.33	5.56	9
2012	7194	0	0.60	2.22	2	1239	2	3.49	4.32	8
2013	7181	0	0.47	2.80	1	901	2	3.76	7.07	7
2014	7234	0	0.42	2.11	1	885	2	3.47	5.07	8
2015	7268	0	0.72	3.03	2	1173	2	4.49	6.34	10
2016	6974	0	0.81	3.11	2	1183	3	4.75	6.20	11

Table 21. Tyler district 10-year alligator cracking statistics

Fiscal Year	Tyler District (All sections)					Tyler District (Only sections with alligator cracking)				
	N	Median	Mean	Std. Dev.	90th Percentile	N	Median	Mean	Std. Dev.	90th Percentile
2007	8118	0	0.40	2.20	0	756	2	4.28	5.96	10
2008	8028	0	0.63	3.41	1	893	2	5.68	8.73	13
2009	8104	0	0.48	2.58	1	873	2	4.50	6.63	11
2010	8212	0	0.48	2.56	1	909	2	4.38	6.50	10
2011	8211	0	0.40	2.21	0	820	2	4.04	5.87	10
2012	8299	0	0.38	1.84	1	903	2	3.49	4.50	9
2013	8331	0	0.42	2.22	1	851	2	4.13	5.75	11
2014	8327	0	0.45	2.49	1	856	2	4.36	6.58	11
2015	6984	0	0.51	2.80	1	743	2	4.79	7.31	11
2016	7897	0	1.23	4.63	3	1524	3	6.39	8.86	16

Table 19 shows that for sections within the Austin district with alligator cracking, the median value varies between 3% and 5% over the 10-year period. Within this study, 4% was used as the target value for the Austin district. A district specific value was chosen to better represent information within a decision making unit, such as a district. Also, using district specific measurements acknowledges that different districts manage pavements differently and have different thresholds within their expectations, regardless of whether or not these thresholds formally exist. Alligator cracking with the Bryan district had a median value of either 2% or 3%, with 2% used as the target value within the study. Tyler district had an alligator cracking median of 2% in each year except the final year where it increased to 3%. For Tyler district projects, 2% was used as the target value.

Table 19, Table 20, and Table 21 also contain statistics on percent alligator cracking for all sections within the respective districts. The median alligator cracking value across each of the district was zero, an expected result because between 80% and 90% of sections within a district have no alligator cracking. For this reason and also because the use of zero

as the target value can cause problems for the CUSUM technique, the median value for sections with alligator cracking was chosen as the appropriate target value.

B.1.2 **Data Mining Methodology**

The initial step in determining deterioration rate for a project was to determine the age of each data collection section and subsequently the age of the entire project. Age was determined using calibrated distress models. The curves within the model behave according to the following equation:

$$L_i = \alpha e^{-\left(\frac{A}{age}\right)^{\beta}} \tag{26}$$

Where, L_i = distress density, α = maximum loss factor, age = no. of years since last construction, A = prolongation factor, and β = slope factor.

The coefficients α, A, and β correspond to one of four climate and subgrade zones in Texas and one of three traffic volumes. The age variable allows the model to predict the amount of distress present after a particular type of work action over a given time period. The different work actions include preventative maintenance, light rehabilitation, medium rehabilitation, or heavy rehabilitation.

For a pavement project composed of I total sections analyzed over a total of J years, the cumulative sum calculation follows the vector logic presented below:

- $\vec{d}$ represents the distress vector, populated with d_{ij}, where d_{ij} = the distress present in section i during year j.
- $\vec{t}$ represents the target vector, populated with t_j, where t_j = the target distress during year j. For age determination in this study, a constant value near or equal to the

median for a particular district was used. The value does not have to remain constant from year to year, hence the use of the vector format to represent the target value rather than a scalar.

- $\vec{s} = \vec{d} - \vec{t} = \langle d_{i,j} - t_j, d_{i,j+1} - t_{j+1}, d_{i,j+2} - t_{j+2}, \cdots, d_{i,k} - t_k \rangle$ and represents the vector created by subtracting the target vector from the distress vector for each section within a pavement project. The k value represents the number of years within the analysis. The researcher has chosen to use 10 years for the analysis period.
- Q is the cumulative sum of $\vec{s}$, calculated by

$$Q = \sum_{j=1}^{k} s_{i,j} \quad (27)$$

Where, Q applies to individual sections within a project and can be used to determine the behavioral age of a particular section. The researcher defined the behavioral age of a section by minimizing the difference between Q for a section and Q for a deterioration rate at a given age.

Using the pavement prediction equation described above, expected distress manifestation within each year of a 10 year analysis was calculated. For a given zone and pavement type, a predicted distress vector was created for a design life of 30 years. The vector logic for these calculations is presented below:

- $\vec{p}$ = the predicted distress vector for a given zone and pavement type
- $\vec{p}$ is populated with $d_{p,a}$, or the predicted distress at age a.
- $\overrightarrow{sp} = \vec{p} - \vec{t} = \langle d_{p,a} - t_j, d_{p,a+1} - t_{j+1}, d_{p,a+2} - t_{j+2}, \cdots, d_{p,k} - t_k \rangle$ and represents the vector created by subtracting the target vector from the predicted distress vector. The k value continues to represent the 10 years within the analysis.

Within a consecutively moving 10 year analysis period, the subtraction of the target vector from the predicted distress creates a matrix that develops from the calculations below:

$$\begin{bmatrix} d_{p1} \\ d_{p2} \\ d_{p3} \\ \vdots \\ d_{p28} \\ d_{p29} \\ d_{p30} \end{bmatrix} - \begin{bmatrix} t_j \\ t_{j+1} \\ t_{j+2} \\ \vdots \\ t_{j+27} \\ t_{j+28} \\ t_{j+29} \end{bmatrix} = [sp] = \begin{bmatrix} d_{p1} - t_j & NA & NA & NA & NA \\ d_{p2} - t_{j+1} & d_{p2} - t_{j+1} & NA & NA & NA \\ \text{M} & d_{p3} - t_{j+2} & d_{p3} - t_{j+2} & NA & NA \\ d_{p9} - t_{j+8} & \text{M} & d_{p4} - t_{j+3} & \text{O} & NA \\ d_{p10} - t_{j+9} & d_{p10} - t_{j+9} & \text{M} & \text{O} & NA \\ NA & d_{p11} - t_{j+10} & d_{p11} - t_{j+10} & \text{O} & NA \\ NA & NA & d_{p12} - t_{j+11} & \text{O} & NA \\ NA & NA & NA & \text{O} & NA \\ NA & NA & NA & \text{O} & d_{p21} - t_{j+20} \\ NA & NA & NA & \text{O} & d_{p22} - t_{j+21} \\ NA & NA & NA & \text{O} & \text{M} \\ NA & NA & NA & \text{O} & d_{p29} - t_{j+28} \\ NA & NA & NA & NA & d_{p30} - t_{j+29} \end{bmatrix} \quad (28)$$

Using a 30 year design life, matrix $[sp]$ contains 30 rows and 20 columns. Each column can be summed to create a cumulative sum of the predicted distress for a given pavement age. The cumulative sum of each column can be represented with the following equation:

$$Q_{p,j} = \sum_{a=j}^{k} sp_a \quad (29)$$

where j represents the age of the pavement at the beginning of a 10 year analysis period, which corresponds to the column number, and k represents the age of the pavement 10 years beyond j, which is also the pavements current age when the difference between Q_p and Q was minimized.

B.1.3 **Fatigue Cracking Data Mining Example**

The following example of this technique came from FM 1696, a pavement related project in the Bryan District. FM 1696 consisted of 18 data collection sections within the project limits. Table 22 displays the distress for each section over the 10 year analysis period. Table 22 provides 18 $\vec{\boldsymbol{d}}$ vectors displayed as $\mathbf{1}\boldsymbol{x}\boldsymbol{k}$ row vectors. Table 23 also contains 18 $1xk$ row vectors, but these vectors are the result of the vector subtraction of the target vector from the vectors in Table 22. The target vector for FM 1696, and all subsequent Bryan District projects, was a $1x10$ row vector entirely populated with the value 2. The only change in the target value comes when changing districts, not from year to year. If the median value for alligator cracking had been highly unstable, there would have been a need to modify the target value from year to year, but this was not the case.

Table 22. FM 1696 10-year alligator cracking

Section No.	FY 2007	FY 2008	FY 2009	FY 2010	FY 2011	FY 2012	FY 2013	FY 2014	FY 2015	FY 2016
1	0	0	0	3	0	0	0	1	1	4
2	0	0	0	0	0	10	0	1	0	0
3	0	0	0	0	0	11	0	0	0	0
4	0	0	0	0	0	0	0	0	0	0
5	0	0	0	0	0	3	0	0	0	0
6	0	0	0	0	0	11	0	0	0	0
7	0	0	0	0	0	5	0	0	0	0
8	0	0	0	0	0	7	0	0	0	0
9	0	0	0	0	2	6	0	0	0	0
10	0	0	0	0	0	2	0	0	0	0
11	0	0	0	0	0	0	0	0	0	0
12	0	0	0	0	0	0	0	0	0	0
13	0	0	0	0	0	0	0	1	0	0
14	0	0	0	0	0	0	0	0	1	0
15	0	0	0	0	1	0	0	0	0	0
16	0	0	0	0	0	3	0	1	0	0
17	0	0	0	0	0	1	0	0	0	0
18	0	0	0	1	0	0	0	0	3	1

Table 23. FM 1696 $\vec{s}$ vectors for each section

Section No.	FY 2007	FY 2008	FY 2009	FY 2010	FY 2011	FY 2012	FY 2013	FY 2014	FY 2015	FY 2016
1	-2	-2	-2	1	-2	-2	-2	-1	-1	2
2	-2	-2	-2	-2	-2	8	-2	-1	-2	-2
3	-2	-2	-2	-2	-2	9	-2	-2	-2	-2
4	-2	-2	-2	-2	-2	-2	-2	-2	-2	-2
5	-2	-2	-2	-2	-2	1	-2	-2	-2	-2
6	-2	-2	-2	-2	-2	9	-2	-2	-2	-2
7	-2	-2	-2	-2	-2	3	-2	-2	-2	-2
8	-2	-2	-2	-2	-2	5	-2	-2	-2	-2
9	-2	-2	-2	-2	0	4	-2	-2	-2	-2
10	-2	-2	-2	-2	-2	0	-2	-2	-2	-2
11	-2	-2	-2	-2	-2	-2	-2	-2	-2	-2
12	-2	-2	-2	-2	-2	-2	-2	-2	-2	-2
13	-2	-2	-2	-2	-2	-2	-2	-1	-2	-2
14	-2	-2	-2	-2	-2	-2	-2	-2	-1	-2
15	-2	-2	-2	-2	-1	-2	-2	-2	-2	-2
16	-2	-2	-2	-2	-2	1	-2	-1	-2	-2
17	-2	-2	-2	-2	-2	-1	-2	-2	-2	-2
18	-2	-2	-2	-1	-2	-2	-2	-2	1	-1

Table 24 represents the cumulative sum for each section within the FM 1696 project. The values in Table 24 come from cumulatively summing each row in Table 23. The values in Table 24 were iteratively compared with the CUSUM values using the pavement prediction curve to determine at what age the data collection section was behaving. The minimum difference between the predicted CUSUM and the actual CUSUM was selected as the age for a data collection section. Table 25shows these results.

Table 24. Cumulative sum vector for FM 1696

Section No.	Cumulative Sum
1	-11
2	-9
3	-9
4	-20
5	-17
6	-9
7	-15
8	-13
9	-12
10	-18
11	-20
12	-20
13	-19
14	-19
15	-19
16	-16
17	-19
18	-15

Table 25. FM 1696 data collection section age determination

Highway	BRM	ERM	Min. CUSUM Diff	Assigned Beginning Year Analysis	Current Pavement Age
FM1696	642.0	642.5	-5	3	13
FM1696	642.5	643.0	4	4	14
FM1696	643.0	643.5	6	4	14
FM1696	643.5	644.0	-16	1	11
FM1696	644.0	644.5	0	6	16
FM1696	644.5	645.0	6	4	14
FM1696	645.0	645.5	1	2	12
FM1696	645.5	646.0	0	3	13
FM1696	646.0	646.5	7	3	13
FM1696	646.5	647.0	-6	1	11
FM1696	647.0	647.5	-16	1	11
FM1696	647.5	648.0	-16	1	11
FM1696	648.0	648.5	-13	1	11
FM1696	648.5	649.0	-14	1	11
FM1696	649.0	649.5	-10	1	11
FM1696	649.5	650.0	2	1	11
FM1696	650.0	650.5	-11	1	11
FM1696	650.5	651.1	-2	1	11
Mean				2.17	12.17
Std Dev				1.5	
Median				1	11

Table 25 clearly indicates that data collection sections behave at different ages. Because of the stability of the median value at the network-level, the researcher determined the age of the entire project as the median age determined through the CUSUM process control technique. For FM 1696, the age of the project as defined by alligator cracking was

determined to be 11 years old. Using this age, the pavement prediction curves were used to develop control charts for the deterioration rate.

B.1.4 **Project Age Tables, Deterioration Rate Control Charts, and Activated Data**

B.1.4.1 FM 1660 Project

The same calculations were performed for the FM 1660 project. Table 26 shows the age calculation for each section within the project and the median value assigned as the project age. The FM 1660 project behaves as old as possible. Fig. 43 shows the deterioration rate curves used to analyze each section and Table 27 shows the activated data for each section. For the FM 1660 project, every section was deteriorating very rapidly, thus the unhealthiest activated value was used for each section.

Table 26. FM 1660 age determination

Highway	BRM	ERM	Min. CUSUM Diff	Assigned Beginning Year Analysis	Current Pavement Age
FM1660	429.0	429.5	7	19	29
FM1660	429.5	430.0	151	20	30
FM1660	430.0	430.5	143	20	30
FM1660	430.5	431.0	-4	19	29
FM1660	431.0	431.5	299	20	30
FM1660	431.5	432.0	193	20	30
FM1660	432.0	432.5	547	20	30
FM1660	432.5	432.7	15	18	28
Mean				19.5	29.5
Std Dev				0.756	
Median				20	30

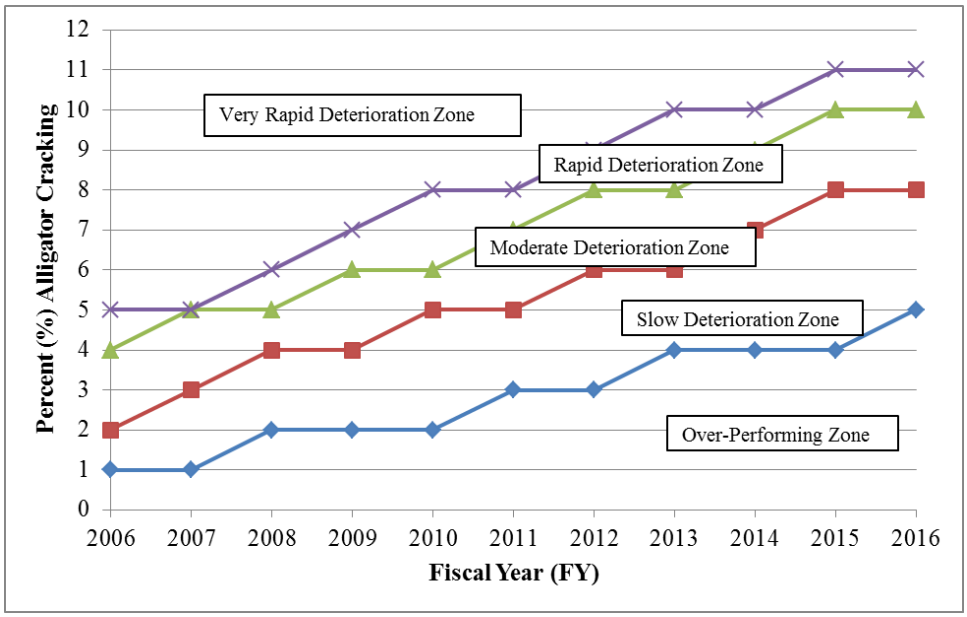

Fig. 43. FM 1660 deterioration control chart

Table 27. FM 1660 activated deterioration rate data

Sect. No.	BRM	ERM	Deterioration Rate	Indexed Deterioration Rate
1	429	429.5	Very Rapid	5
2	429.5	430	Very Rapid	5
3	430	430.5	Very Rapid	5
4	430.5	431	Very Rapid	5
5	431	431.5	Very Rapid	5
6	431.5	432	Very Rapid	5
7	432	432.5	Very Rapid	5
8	432.5	432.7	Very Rapid	5

B.1.4.2 FM 908 Project

Table 28 shows the age determination for the FM 908 project. This project only consisted of three sections, all behaving at different ages. Fig. 44 has the deterioration rate

curves and Table 29 has the activated indicator data. Table 29 shows that that middle section within the project has deteriorated much more rapidly that the other two sections.

Table 28. FM 908 age determination

Highway	BRM	ERM	Min. CUSUM Diff	Assigned Beginning Year Analysis	Current Pavement Age
FM 908	581.0	581.5	1	6	16
FM 908	581.5	582.0	0	11	21
FM 908	582.0	582.5	0	1	11
Mean				6.00	16.00
Std Dev				4.08	
Median				6	16

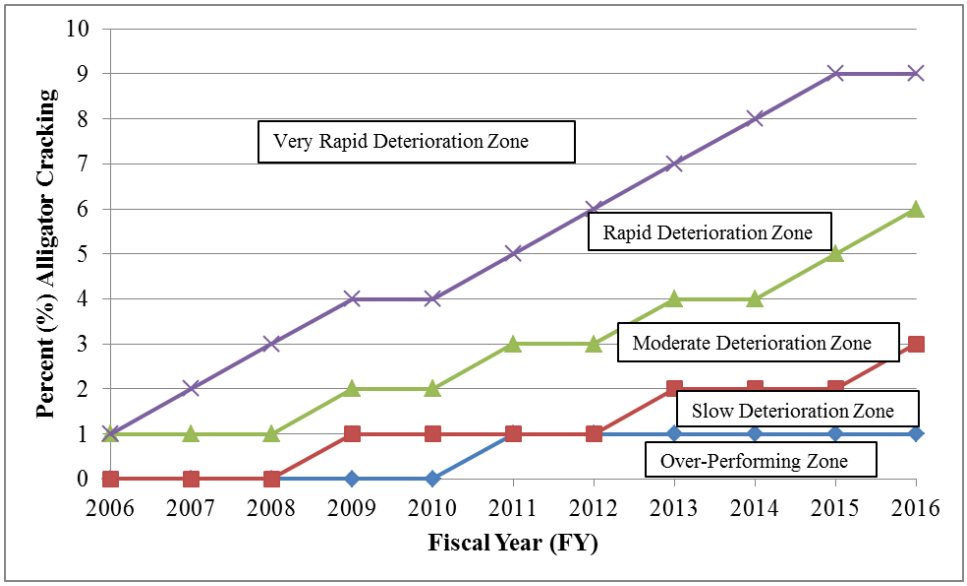

Fig. 44. FM 908 deterioration control chart

Table 29. FM 908 activated deterioration rate data

Sect. No.	BRM	ERM	Deterioration Rate	Indexed Deterioration Rate
1	581	581.5	Slow	2
2	581.5	582	Very Rapid	5
3	582	582.5	Over Perf.	1

B.1.4.3 OSR Project

While the OSR project was eventually divided into two separate analysis sections, the age of the entire length was originally determined. Table 30 is the age determination table, Fig. 45 has the deterioration rate curves, and Table 31 has the activated data for the project. Table 31clearly shows that the section of the project from reference marker 641.5 to reference marker 643.5 has deteriorated more rapidly than the rest of the project.

Table 30. OSR age determination

Highway	BRM	ERM	Min. CUSUM Diff	Assigned Beginning Year Analysis	Current Pavement Age
OSR	634	634.5	-16	1	11
OSR	634.5	635	-14	1	11
OSR	635	635.5	-16	1	11
OSR	635.5	636	-11	1	11
OSR	636	636.5	-16	1	11
OSR	636.5	637	-14	1	11
OSR	637	637.5	-16	1	11
OSR	637.5	638	-13	1	11
OSR	638	638.5	-13	1	11
OSR	638.5	639	-16	1	11
OSR	639	639.5	-6	1	11
OSR	639.5	640	-16	1	11
OSR	640	640.5	-16	1	11
OSR	640.5	641	-16	1	11
OSR	641	641.5	-16	1	11
OSR	641.5	642	4	1	11
OSR	642	642.5	-16	1	11
OSR	642.5	643	0	10	20
OSR	643	643.5	0	6	16
OSR	643.5	644	0	2	12
OSR	644	644.5	-1	1	11
OSR	644.5	645	-16	1	11
OSR	645	645.5	-3	1	11
OSR	645.5	646	-1	2	12
OSR	646	646.5	-10	1	11
OSR	646.5	647	-16	1	11
OSR	647	647.5	-12	1	11
OSR	647.5	648	-14	1	11
OSR	648	648.5	-9	1	11
OSR	648.5	649	-10	1	11
Mean				1.53	11.53
Std Dev				1.82	
Median				1	11

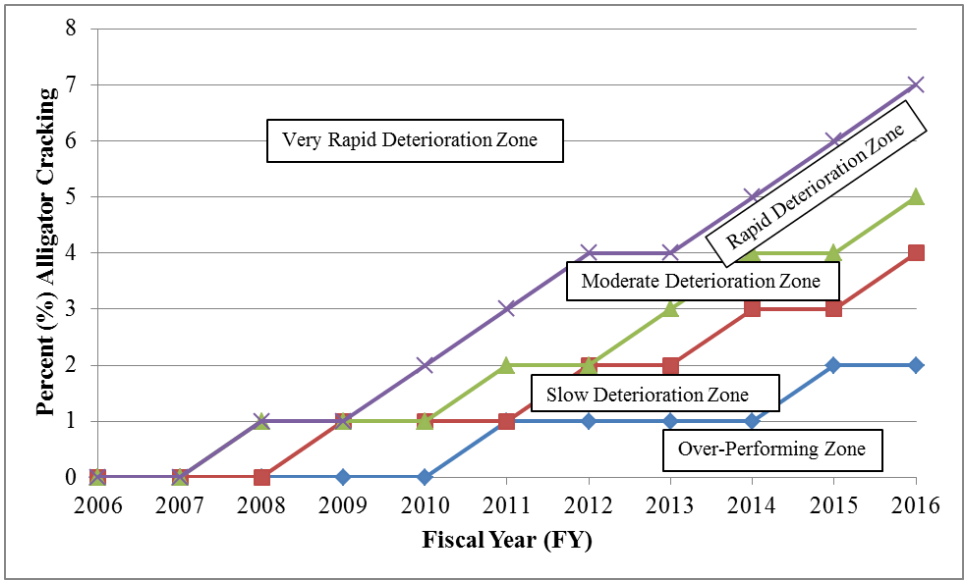

Fig. 45. OSR deterioration control chart

Table 31. OSR activated deterioration rate data

Sect. No.	BRM	ERM	Deterioration Rate	Indexed Deterioration Rate
1	634.0	634.5	Over Perf.	1
2	634.5	635.0	Over Perf.	1
3	635.0	635.5	Over Perf.	1
4	635.5	636.0	Over Perf.	1
5	636.0	636.5	Over Perf.	1
6	636.5	637.0	Over Perf.	1
7	637.0	637.5	Over Perf.	1
8	637.5	638.0	Over Perf.	1
9	638.0	638.5	Over Perf.	1
10	638.5	639.0	Over Perf.	1
11	639.0	639.5	Slow	2
12	639.5	640.0	Over Perf.	1
13	640.0	640.5	Over Perf.	1
14	640.5	641.0	Over Perf.	1
15	641.0	641.5	Over Perf.	1
16	641.5	642.0	Rapid	4
17	642.0	642.5	Over Perf.	1
18	642.5	643.0	Very Rapid	5
19	643.0	643.5	Very Rapid	5
20	643.5	644.0	Rapid	4
21	644.0	644.5	Slow	2
22	644.5	645.0	Over Perf.	1
23	645.0	645.5	Slow	2
24	645.5	646.0	Moderate	3
25	646.0	646.5	Over Perf.	1
26	646.5	647.0	Over Perf.	1
27	647.0	647.5	Over Perf.	1
28	647.5	648.0	Over Perf.	1
29	648.0	648.5	Over Perf.	1
30	648.5	649.0	Over Perf.	1

B.1.4.4 FM 50 Project

Table 32 is the age determination table for the FM 50 project and indicates each section within the project behaves as young as possible. Fig. 46 has the deterioration rate curves used for FM 50 and Table 33 has the activated data. Table 33 reflects the youth of FM 50 by showing that nine of the 10 sections receive the healthiest activated value.

Table 32. FM 50 age determination

Highway	BRM	ERM	Min. CUSUM Diff	Assigned Beginning Year Analysis	Current Pavement Age
FM 50	447	447.5	-27	1	11
FM 50	447.5	448.0	-31	1	11
FM 50	448	448.5	-31	1	11
FM 50	448.5	449.0	-25	1	11
FM 50	449	449.5	-28	1	11
FM 50	449.5	450.0	-17	1	11
FM 50	450	450.5	-23	1	11
FM 50	450.5	451.0	-27	1	11
FM 50	451	451.5	-26	1	11
FM 50	451.5	452.0	-26	1	11
Mean				1.00	11.00
Std Dev				0.00	
Median				1	11

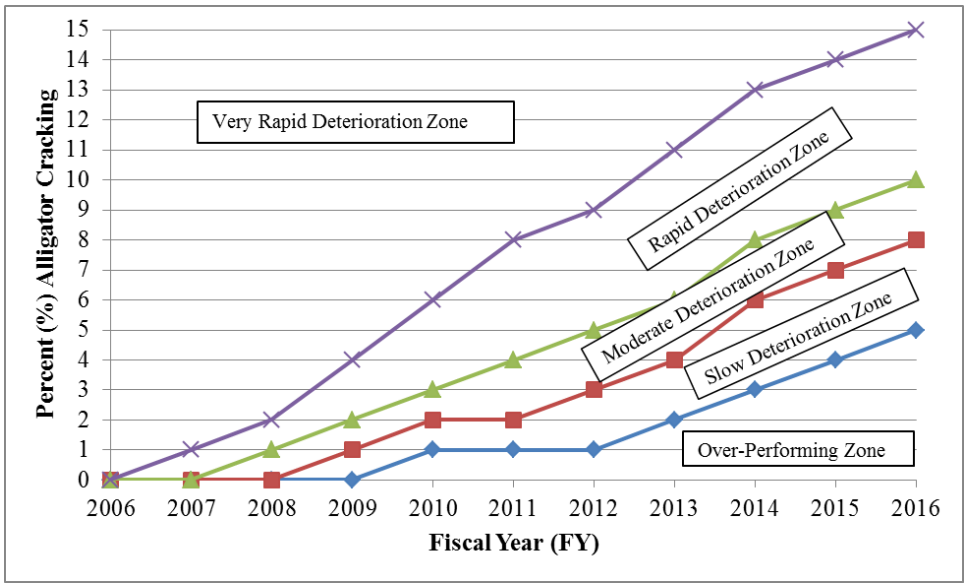

Fig. 46. FM 50 deterioration control chart

Table 33. FM 50 activated deterioration date data

Sect. No.	BRM	ERM	Deterioration Rate	Indexed Deterioration Rate
1	447	447.5	Over Perf.	1
2	447.5	448.0	Over Perf.	1
3	448	448.5	Over Perf.	1
4	448.5	449.0	Over Perf.	1
5	449	449.5	Over Perf.	1
6	449.5	450.0	Slow	2
7	450	450.5	Over Perf.	1
8	450.5	451.0	Over Perf.	1
9	451	451.5	Over Perf.	1
10	451.5	452.0	Over Perf.	1

B.1.4.5 FM 1844 Project

The FM 1844 project was unhealthy as it relates to deterioration rate. Table 34, Fig. 47, and Table 35 summarize the deterioration rate health of FM 1844. All but the second section had either rapid or very rapid deterioration.

Table 34. FM 1844 age determination

Highway	BRM	ERM	Min. CUSUM Diff	Assigned Beginning Year Analysis	Current Pavement Age
FM 1844	702.0	702.5	3	11	21
FM 1844	702.5	703.0	-2	9	19
FM 1844	703.0	703.5	5	17	27
FM 1844	703.5	704.0	1	13	23
FM 1844	704.0	704.5	-9	13	23
FM 1844	704.5	705.0	-7	13	23
FM 1844	705.0	705.5	7	11	21
FM 1844	705.5	706.0	1	15	25
Mean				12.75	22.75
Std Dev				2.33	
Median				13	23

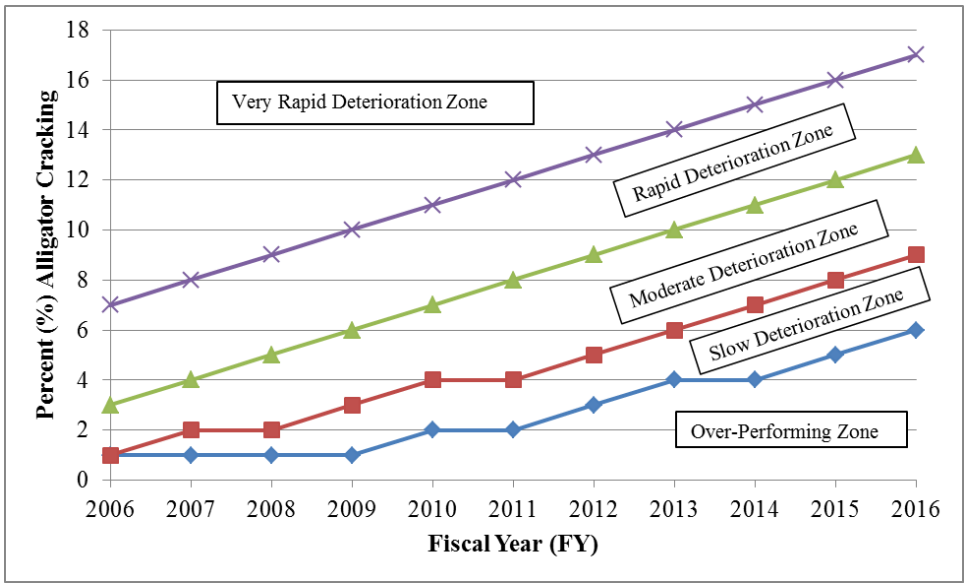

Fig. 47. FM 1844 deterioration control chart

Table 35. FM 1844 activated deterioration rate data

Sect. No.	BRM	ERM	Deterioration Rate	Indexed Deterioration Rate
1	702.0	702.5	Rapid	4
2	702.5	703.0	Over Perf.	1
3	703.0	703.5	Very Rapid	5
4	703.5	704.0	Very Rapid	5
5	704.0	704.5	Rapid	4
6	704.5	705.0	Very Rapid	5
7	705.0	705.5	Rapid	4
8	705.5	706.0	Very Rapid	5

B.1.4.6 FM 2661 Project

The FM 2661 project was described as a widening project that was easily identified within the diagnostic method. Table 36, Fig. 48, and Table 37 contain the required information and data to activate deterioration rate health. The deterioration rate was

diagnosed as potentially unhealthy. The potential unhealthy comes from the two sections that have rapid deterioration, while all others sections have over-performed.

Table 36. FM 2661 age determination

Highway	BRM	ERM	Min. CUSUM Diff	Assigned Beginning Year Analysis	Current Pavement Age
FM 2661	290	290.5	0	1	11
FM 2661	290.5	291	0	1	11
FM 2661	291	291.5	0	1	11
FM 2661	291.5	292	-1	6	16
FM 2661	292	292.5	-1	7	17
FM 2661	292.5	293	0	1	11
Mean				2.83	12.83
Std Dev				2.61	
Median				1	11

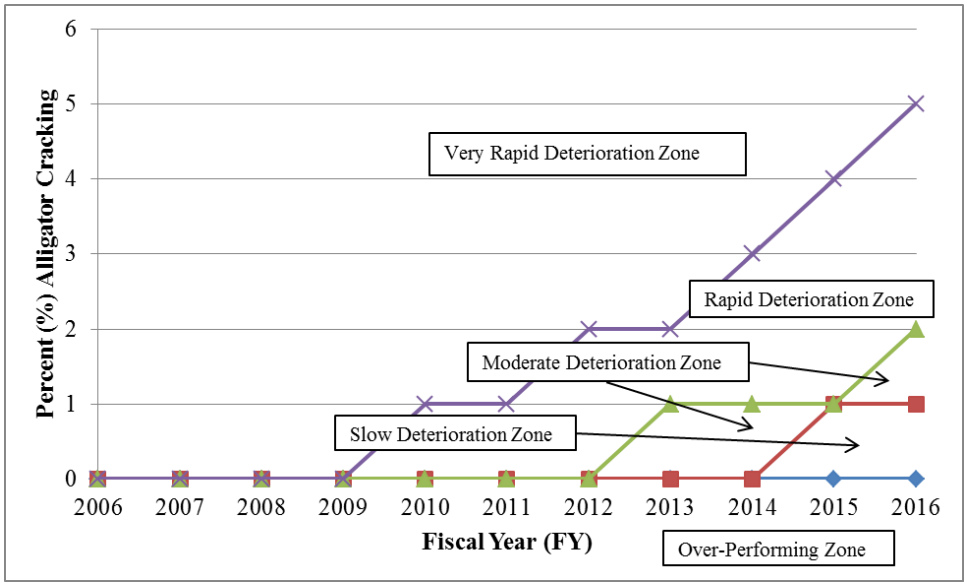

Fig. 48. FM 2661 deterioration control chart

Table 37. FM 2661 activated deterioration rate data

Sect. No.	BRM	ERM	Deterioration Rate	Indexed Deterioration Rate
1	290	290.5	Over Perf.	1
2	290.5	291	Over Perf.	1
3	291	291.5	Over Perf.	1
4	291.5	292	Rapid	4
5	292	292.5	Rapid	4
6	292.5	293	Over Perf.	1

B.1.4.7 FM 2054 Project

The FM 2054 project behaved similarly to the FM 2661 project. Both projects were assigned a widening construction activity. Table 38, Fig. 49, and Table 39 have the deterioration rate activation information. The information shows that the first section of the project has experienced deterioration, while all other sections have over-performed.

Table 38. FM 2054 age determination

Highway	BRM	ERM	Min. CUSUM Diff	Assigned Beginning Year Analysis	Current Pavement Age
FM 2054	328	328.5	-1	7	17
FM 2054	328.5	329	0	1	11
FM 2054	329	329.5	0	1	11
FM 2054	329.5	330	0	1	11
FM 2054	330	330.5	0	1	11
FM 2054	330.5	331	0	1	11
FM 2054	331	331.4	0	1	11
Mean				1.86	11.86
Std Dev				2.10	
Median				1	11

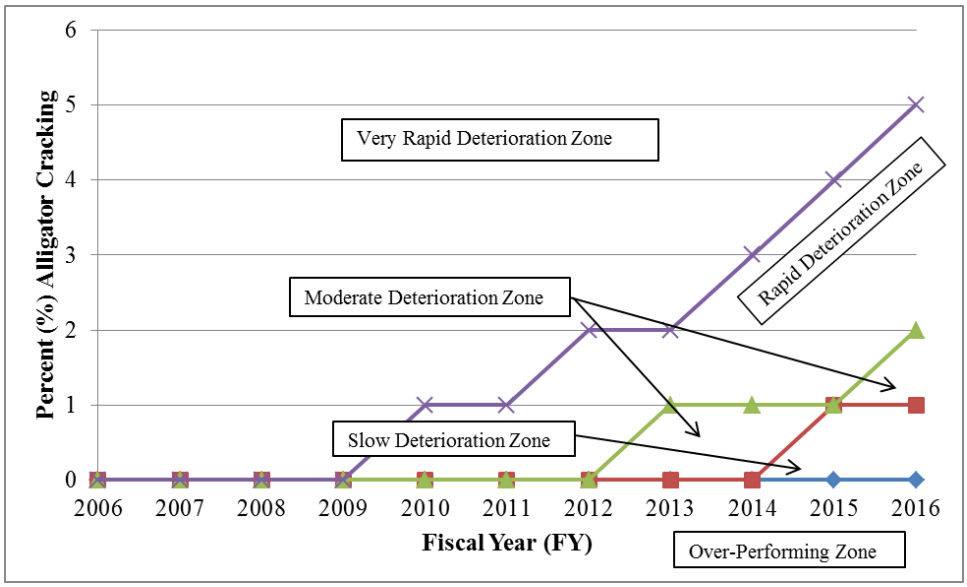

Fig. 49. FM 2054 deterioration control chart

Table 39. FM 2054 activated deterioration rate data

Sect. No.	BRM	ERM	Deterioration Rate	Indexed Deterioration Rate
1	328.0	328.5	Very Rapid	5
2	328.5	329.0	Over Perf.	1
3	329.0	329.5	Over Perf.	1
4	329.5	330.0	Over Perf.	1
5	330.0	330.5	Over Perf.	1
6	330.5	331.0	Over Perf.	1
7	331.0	331.4	Over Perf.	1

B.1.4.8 RM 690 Project

Similar to FM 2661 and FM 2054, the RM 690 project was described as a widening project. The deterioration rate information presents overall as healthy, with only the first section of the project experiencing moderate deterioration. The deterioration rate information is in Table 40, Fig. 50, and Table 41.

Table 40. RM 690 age determination

Highway	BRM	ERM	Min. CUSUM Diff	Assigned Beginning Year Analysis	Current Pavement Age
FM 690	402	402.5	-57	2	12
FM 690	402.5	403	-57	2	12
FM 690	403	403.5	-57	2	12
FM 690	403.5	404	-57	2	12
FM 690	404	404.5	-57	2	12
FM 690	404.5	405	-57	2	12
FM 690	405	405.5	-48	2	12
FM 690	405.5	406	-57	2	12
FM 690	406	406.5	-41	2	12
Mean				2.00	12.00
Std Dev				0.00	
Median				2	12

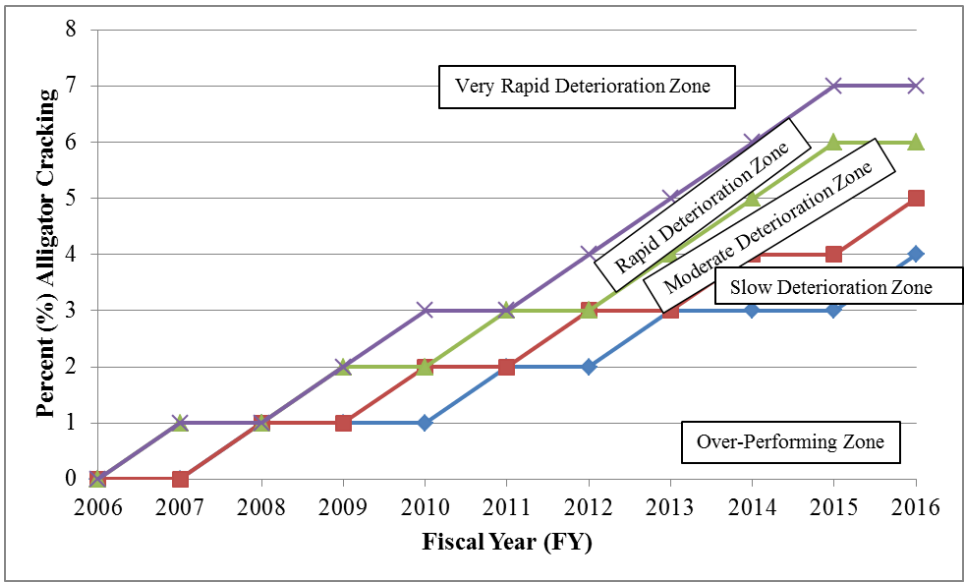

Fig. 50. RM 690 deterioration control chart

Table 41. RM 690 activated deterioration rate data

Sect. No.	BRM	ERM	Deterioration Rate	Indexed Deterioration Rate
1	402	402.5	Over Perf.	1
2	402.5	403	Over Perf.	1
3	403	403.5	Over Perf.	1
4	403.5	404	Over Perf.	1
5	404	404.5	Over Perf.	1
6	404.5	405	Over Perf.	1
7	405	405.5	Over Perf.	1
8	405.5	406	Over Perf.	1
9	406	406.5	Moderate	3

B.1.4.9 SH 138 Project

Deterioration rate information for the SH 138 project is shown in Table 42 , Fig. 51, and Table 43. The deterioration rate for this project was either over-performing or very rapid. The degree of very rapid deterioration led to an unhealthy diagnosis for the structural system and coincided with the rehabilitation construction strategy.

Table 42. SH 138 age determination

Highway	BRM	ERM	Min. CUSUM Diff	Assigned Beginning Year Analysis	Current Pavement Age
SH 138	526.0	526.5	-18	2	12
SH 138	526.0	527.0	-57	2	12
SH 138	526.0	527.5	-57	2	12
SH 138	528.0	528.0	-57	2	12
SH 138	528.0	528.5	5	9	19
SH 138	528.0	529.0	-14	11	21
SH 138	528.0	529.5	1	2	12
SH 138	530.0	530.0	5	4	14
SH 138	530.0	530.5	-47	2	12
SH 138	530.0	531.0	-57	2	12
SH 138	530.0	531.5	-57	2	12
SH 138	532.0	532.0	3	3	13
SH 138	532.0	532.4	-19	2	12
Mean				3.46	13.46
Std Dev				2.87	
Median				2	12

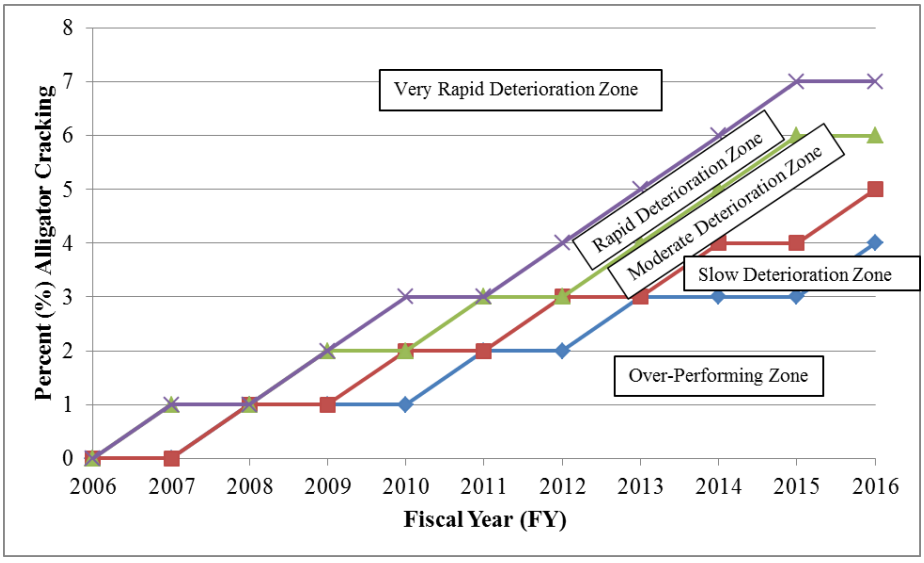

Fig. 51. SH 138 deterioration control chart

Table 43. SH 138 activated deterioration rate data

Sect. No.	BRM	ERM	Deterioration Rate	Indexed Deterioration Rate
1	526.0	526.5	Very Rapid	5
2	526.0	527.0	Over Perf.	1
3	526.0	527.5	Over Perf.	1
4	528.0	528.0	Over Perf.	1
5	528.0	528.5	Very Rapid	5
6	528.0	529.0	Very Rapid	5
7	528.0	529.5	Very Rapid	5
8	530.0	530.0	Very Rapid	5
9	530.0	530.5	Over Perf.	1
10	530.0	531.0	Over Perf.	1
11	530.0	531.5	Over Perf.	1
12	532.0	532.0	Very Rapid	5
13	532.0	532.4	Very Rapid	5

B.2 HYDROPLANING METHODOLOGY AND SUPPLEMENTAL MATERIAL

The Rational Method was chosen as the foundational formula to calculate HPS because of its historical use for small drainage areas (American Association of State Highway and Transportation Officials (AASHTO) 2007). Inputting the area generated from LiDAR data into the Rational Method allowed for the calculation of peak discharge. Using the peak discharge as an input into Manning's equation and using the assumption that for overland sheet flow the hydraulic radius equals the flow depth, water depth was solved. The kinematic wave equation can be derived by combining the Rational Method and Manning's equation with the hydraulic radius equal to water depth. The kinematic wave equation has commonly been used for overland flow calculations, including water depth on pavements

(American Association of State Highway and Transportation Officials (AASHTO) 2007; D. A. Anderson et al. 1998; Huebner et al. 1997).

The water depth calculations begin with the Rational Method and use the following steps:

$$Q = CIA \tag{30}$$

Where, $Q =$ peak discharge (ft^3/s); $C =$ runoff coefficient, assumed to be 1.0 for all non-permeable pavements; $A =$ drainage basin area (acres); and $I =$ rainfall intensity (in./hr).

To use the Rational Method, the rainfall intensity had to be selected. TxDOT's Hydraulic Design manual includes a table in Chapter 4 that details the appropriate storm to use for design calculations. For freeways and principle arterials, the 50-year storm serves as the design standard (Texas Department of Transportation (TxDOT) 2014 (Rev. 2015)). Hydroplaning potential is at its highest when the WFT is deepest. This situation occurs during a short-duration, heavy rain event when the entire drainage area contributes to the critical point. Within this study, the critical point for hydroplaning is the wheel path with the largest drainage area and therefore the largest accumulation of water.

Within the HPS calculations, the 15-minute, 50-year storm intensity was used. This value was taken from USGS depth-duration maps (Asquith and Roussel 2004). The use of a 15-minute storm implies the time of concentration within the drainage area does not exceed 15 minutes. This implication exists because the hydraulic calculations for hydroplaning assume that the entire drainage area contributes water to the critical location at the same time. When calculating the water film thickness, the researcher checked the time of

concentration to ensure it did not exceed 15 minutes. Projects were used from the Bryan, Austin, and Tyler Districts to evaluate the realism of the diagnostic method. The rainfall for these districts are 21.34 cm/hr. (8.4 in./hr.), 20.32 cm/hr. (8.0 in./hr.), and 20.32 cm/hr. (8.0 in./hr.) respectively.

Converting peak discharge to an average unit discharge required dividing Q by the average width of the drainage basin as defined using gridded LiDAR data. Because the data was processed into rows with 0.3048 m (1-ft.) spacing, the number of grids within each row belonging to the largest drainage basin could be counted to get the width of the basin at each longitudinal location. Using this method to determine average width proved more accurate than simply dividing the area of the drainage basin by the overall length.

Continuity Equation: $Q = AV = wdV$ (31)

Where, Q = peak discharge (ft^3/s); A = cross-sectional area of flow (ft^2); V = water velocity (ft/s); w = width of flow (ft); and d = water depth (ft).

Manning's Equation: $V = \frac{1.49}{n} R^{2/3} S^{1/2} = \frac{1.49}{n} d^{2/3} S^{1/2}$ (32)

Where, V = water velocity (ft/s); n = Manning's roughness number; R = hydraulic radius, which equals the depth of flow, d, when the depth is small compared with the width; S = slope of drainage basin, calculated from LiDAR data.

$$\frac{Q}{w} = q = dV = \frac{1.49}{n} d^{5/3} S^{1/2} \quad (33)$$

$$d = \left(\frac{qn}{1.49 S^{1/2}}\right)^{3/5} \quad (34)$$

The above calculations result in a water depth, not WFT. The WFT consists of water above the pavement texture depth, thus the computation of WFT requires subtracting the

MTD from the water depth found using the above equations. For hydroplaning potential calculations generated for this study, the pavement surface types were noted during data collection, and mean surface texture depths (MTDs) for various surface types were taken from literature. Average MTD values were developed based on a thorough 41-pavement study performed by Gallaway and Rose in 1970 (Gallaway and Rose 1970). That study provided multiple data points for seal-coated surfaces, dense-graded hot-mix surfaces, concrete surfaces, and flushed seal-coated surfaces. The researcher interpolated between a seal-coated surface and a flushed seal-coated surface to establish an MTD for partially flushed surfaces. These values, along with Manning's *n* values from TxDOT's *Hydraulic Design Guide* and abbreviations used in the pseudocode are shown in Table 44 (Texas Department of Transportation (TxDOT) 2014 (Rev. 2015); Gallaway and Rose 1970).

Table 44. Surface type hydroplaning variables

Surface Type	Surface Abbreviation	MTD, mm (in.)	TxDOT's Manning's *n*
Concrete	CONC	0.58 (0.023)	0.015
Dense Graded Mix	HMA	0.61 (0.024)	0.013
Open Graded Mix	OGC	3.81 (0.15)	0.02
Seal Coat	ST	1.40 (0.055)	0.016
Partially Flushed Seal Coat	PFST	0.76 (0.03)	0.012
Flushed Seal Coat	FST	0.10 (0.004)	0.01
Unknown Asphaltic Surface	ASPH	0.51 (0.02)	0.013

With WFT calculated from mobile LiDAR data, the researcher could use formulas developed by others to calculate hydroplaning speed (HPS).

Gallaway's formula is:

$$HPS = SD^{0.04} P_t^{0.3} (TD + 1)^{0.06} A \quad (35)$$

Where, HPS = hydroplaning speed (mph); SD = spindown (fixed at 0.10); P_t = tire pressure (psi); TD = tire tread depth (in 32nd inch); A is the greater of:

$$\frac{10.409}{WFT^{0.06}} + 3.507 \quad (36)$$

$$\left[\frac{28.952}{WFT^{0.06}} - 7.817\right] MTD^{0.14} \quad (37)$$

Where, WFT = water film thickness (in.); MTD = mean texture depth of pavement surface (in.).

Ong and Fwa's formula is:

$$HPS = WL^{0.2} P_t^{0.5} \left(\frac{0.82}{WFT^{0.06}} + 0.49\right) \quad (38)$$

Where, HPS = hydroplaning speed (kph); WL = wheel load (N); P_t = tire pressure (kPa); WFT = water film thickness (mm).

Within the Gallaway equation, English units are used. Tire pressure and tread depth are required within the Gallaway equation. Within the finite element method (FEM) equation, SI units are used. Tire pressure and wheel load are required in the FEM equation. To perform the Monte Carlo simulation a mean value and standard deviation was chosen for each vehicle characteristic.

For tire tread depth, 7/32 in. was selected as the mean value, with 2.4/32 in. selected as the standard deviation. Typical new tires have approximately 11/32-in. tread depth and

2/32-in. tread depth is typically considered the legal limit of tire wear (TireRack b). The average of these two values was 6.5/32, but was rounded up to 7/32 in. for this project. The researcher selected a mean tire pressure of 35 psi with a standard deviation of 7 psi. Typical passenger vehicle tire pressures range from 30 psi to 35 psi (TireRack a).

Texas has an eclectic group of vehicles that use its roadways. A compact car such as a Toyota Corolla weighs approximately 12,700 N (2850 lb), and a larger sedan such as a Toyota Camry weighs approximately 15,000 N (3400 lb). In Texas, many users drive trucks and SUVs. A Chevrolet Tahoe weighs approximately 24,500 N (5500 lb), and a Ford F-150 pick-up weighs approximately 20,500 N (4600 lb). The average of these numbers is 18,000 N (4100 lb). To account for the larger-size vehicle use in Texas, a mean vehicle weight of 19,500 N (4400 lb) was chosen with a standard deviation of 4,250 N (950 lb).

Fig. 52 is a flow chart and summary of the HPS analysis.

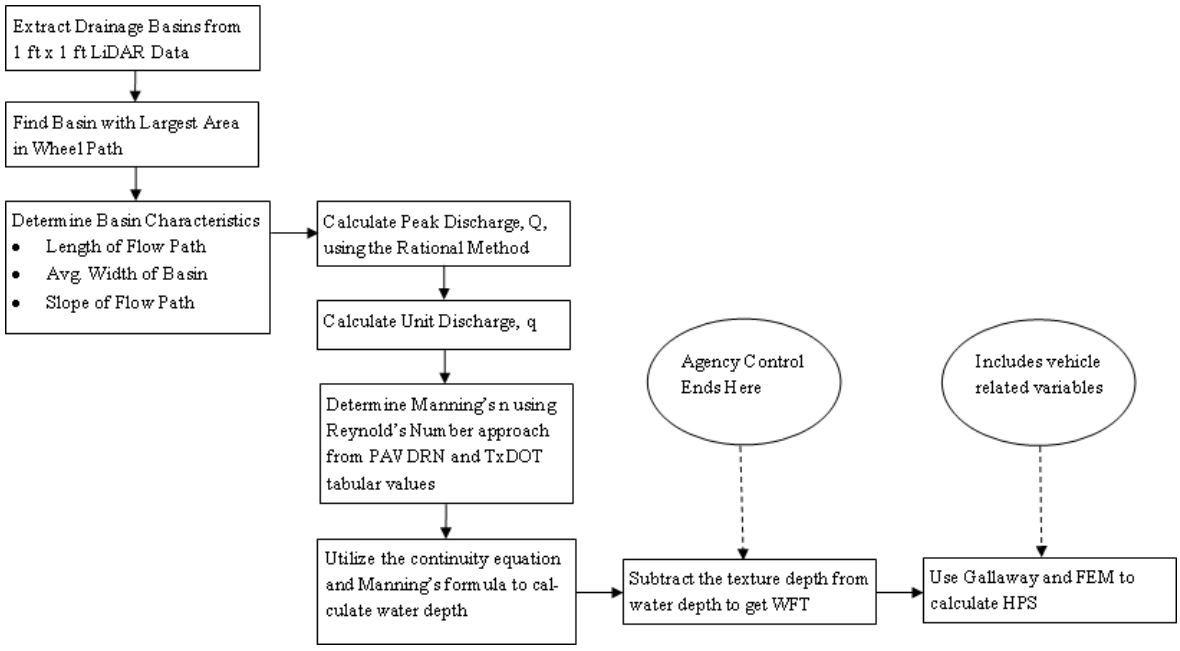

Fig. 52. Hydroplaning calculation flow chart

B.3 DITCH SLOPE VELOCOTIY CHARTS

Fig. 53 shows the relationship between depth of water and water velocity. Fig. 53 illustrates that the deeper the water, the faster it flows. Fig. 54 shows the relationship between front slope geometry and water velocity. Reviewing the front slope geometry captures the impact of the wetted perimeter. While some impact is revealed in Fig. 54, the impact of front slope geometry is much less than that of water depth. Fig. 55 shows the relationship between Manning's *n* and water velocity. As Manning's *n* goes down, water velocity increases, but the magnitude of the velocity impact is much less than the contribution of water depth.

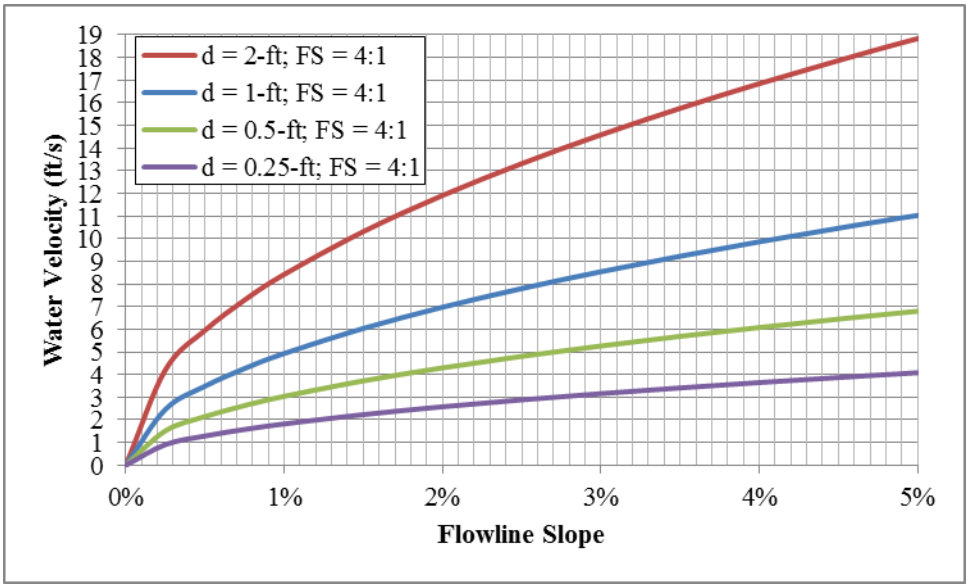

Fig. 53. Depth of water effect on water velocity

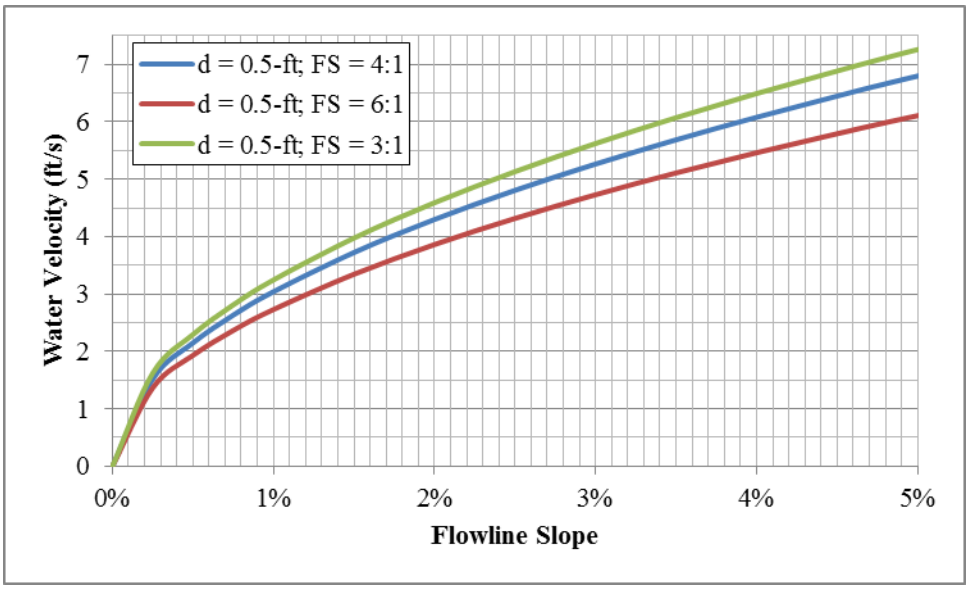

Fig. 54. Front slope geometry effect on water velocity

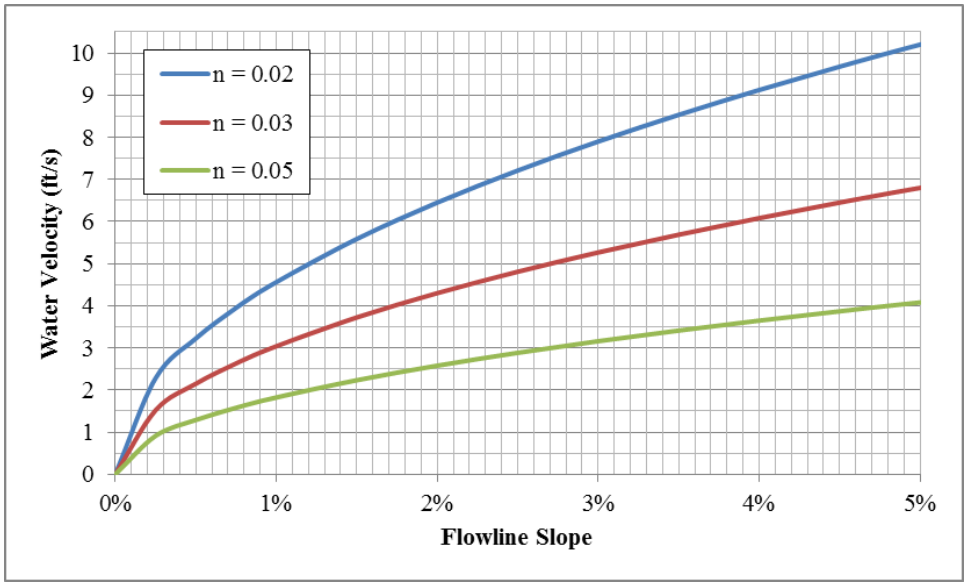

Fig. 55. Manning's *n* effect on water velocity

Regardless of the variable in question, each curve begins to rapidly descend toward zero velocity near a flowline slope of 0.3%. Based on this, researchers selected 0.3% as the absolute minimum flowline slope.

APPENDIX C

FM 1696 AND FM 908 SECTION BY SECTION DIAGNOSTIC VISUAL AIDS

The diagnostic method created by the researcher was expanded beyond project to provide an approximation of health at the network level. Fig. 56, Fig. 57, Fig. 58, Fig. 59, Fig. 60, Fig. 61, Fig. 62, and Fig. 63 provide the section by section diagnoses for the FM 1696 project. Each of these figures contains the diagnoses for two sections. The diagnoses include the system diagnoses for each section with the visual representation of the activated data below its respective gauge chart. The visualization of the activated data provides a visual tool to understand the health of each indicator at the section level. This visual aid was constructed by the researcher to visually interpret the data that populated the weighted edge incidence matrices.

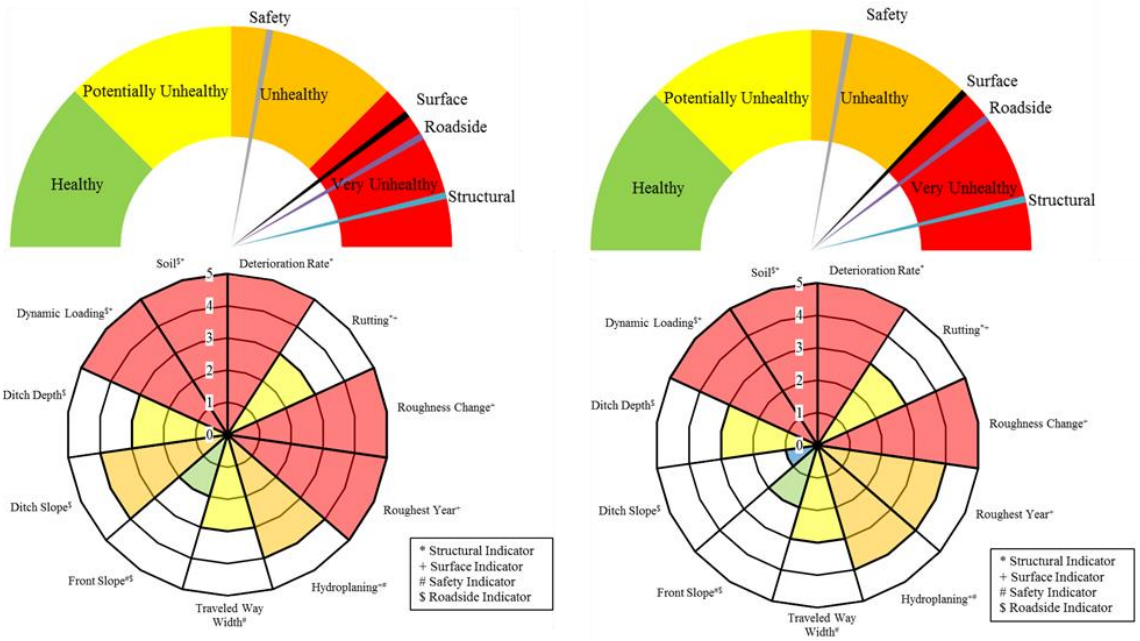

Fig. 56. FM 1696 section 642 and 642.5 diagnoses

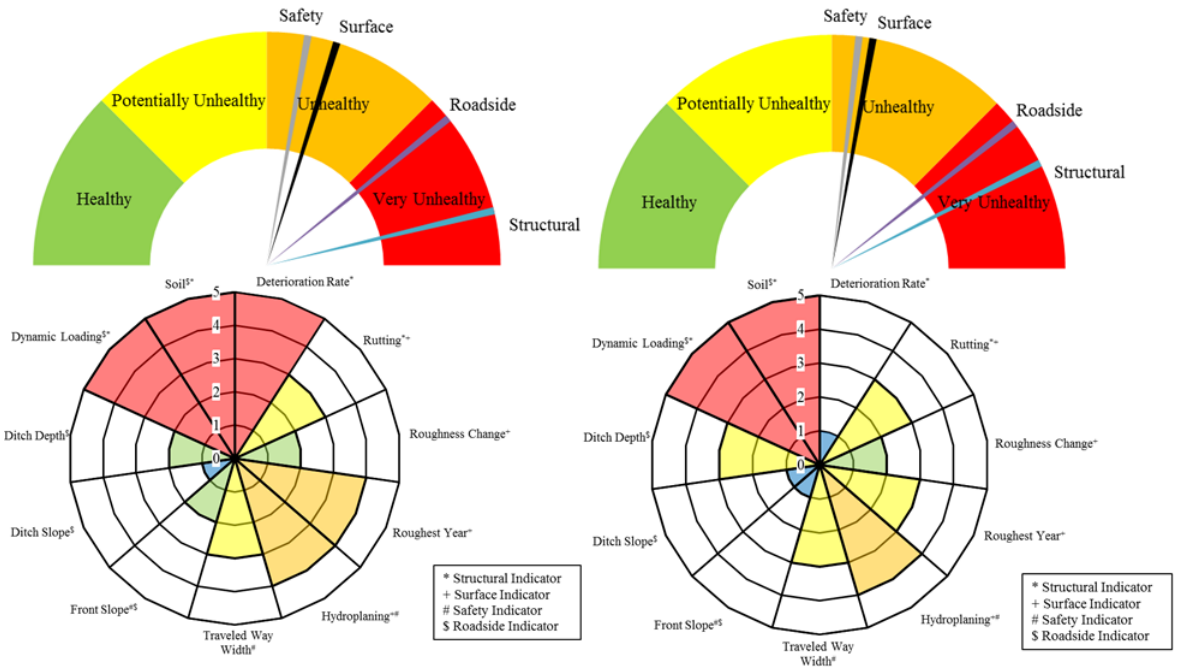

Fig. 57. FM 1696 section 643 and 643.5 diagnoses

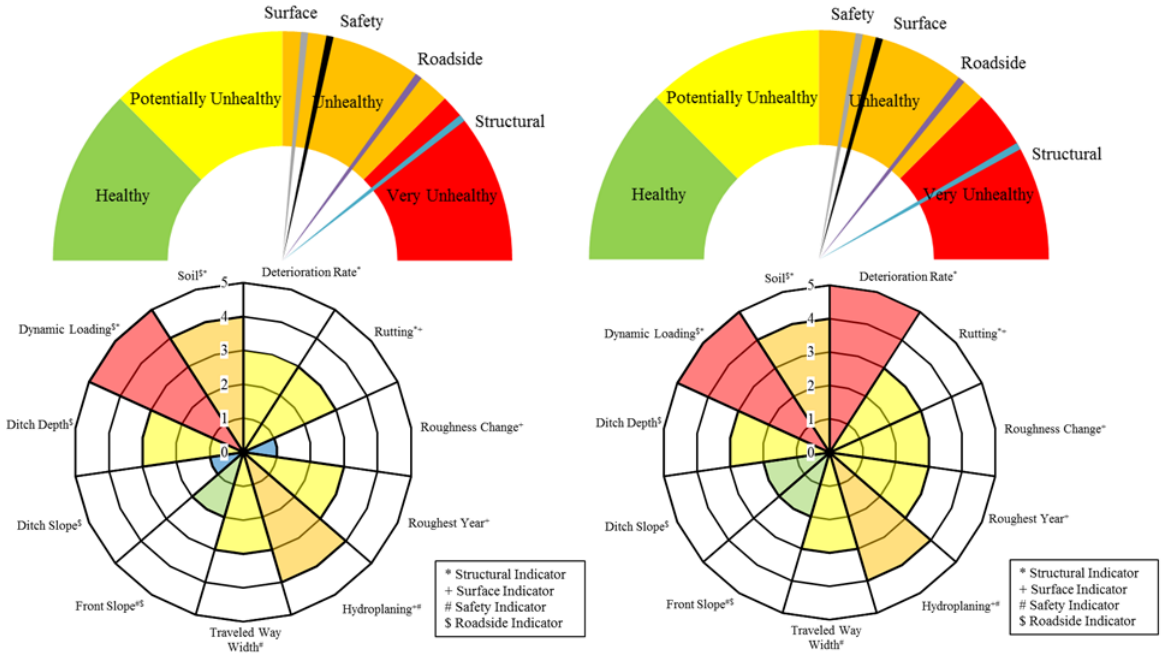

Fig. 58. FM 1696 section 644 and 644.5 diagnoses

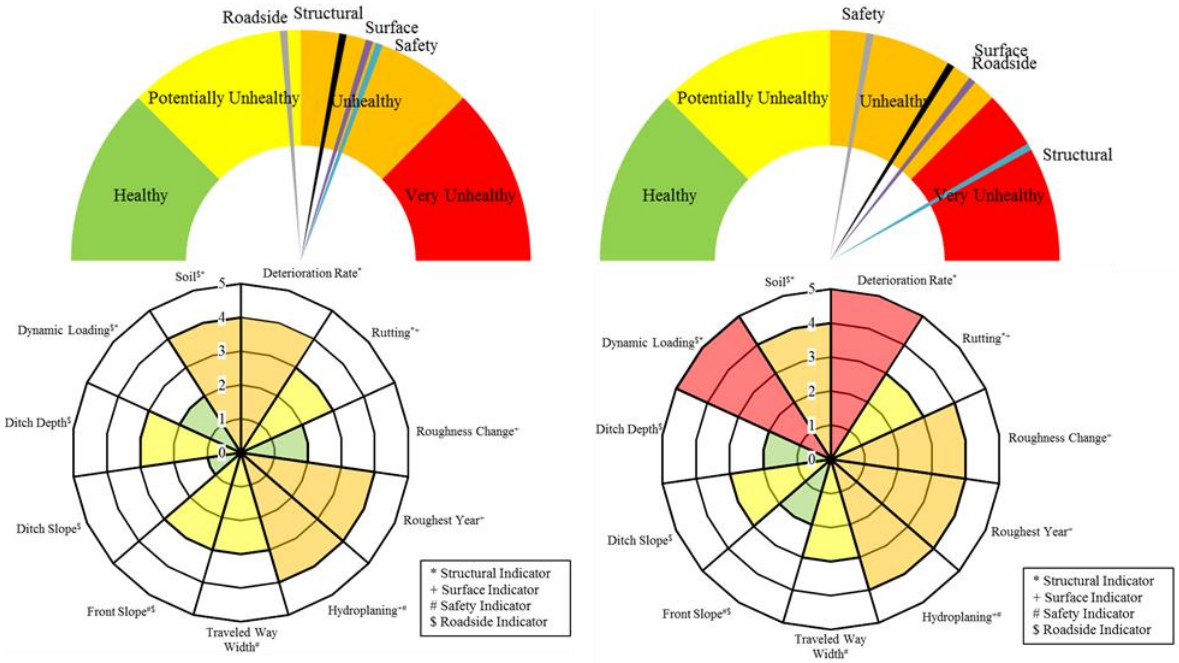

Fig. 59. FM 1696 section 645 and 645.5 diagnoses

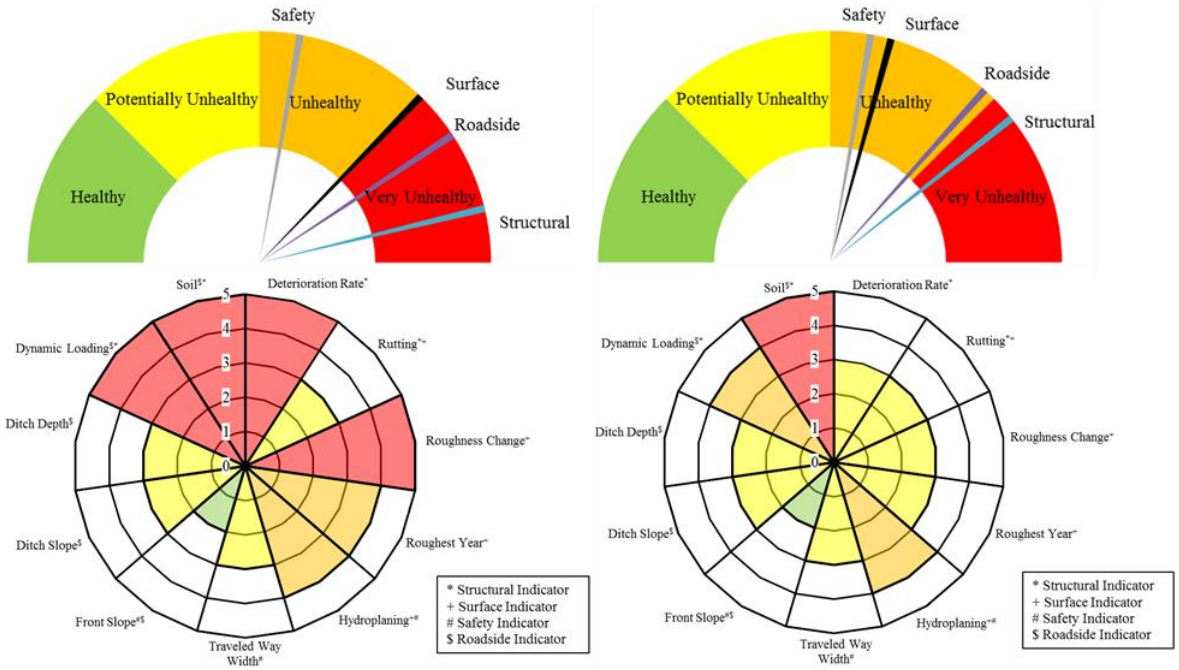

Fig. 60. FM 1696 section 646 and 646.5 diagnoses

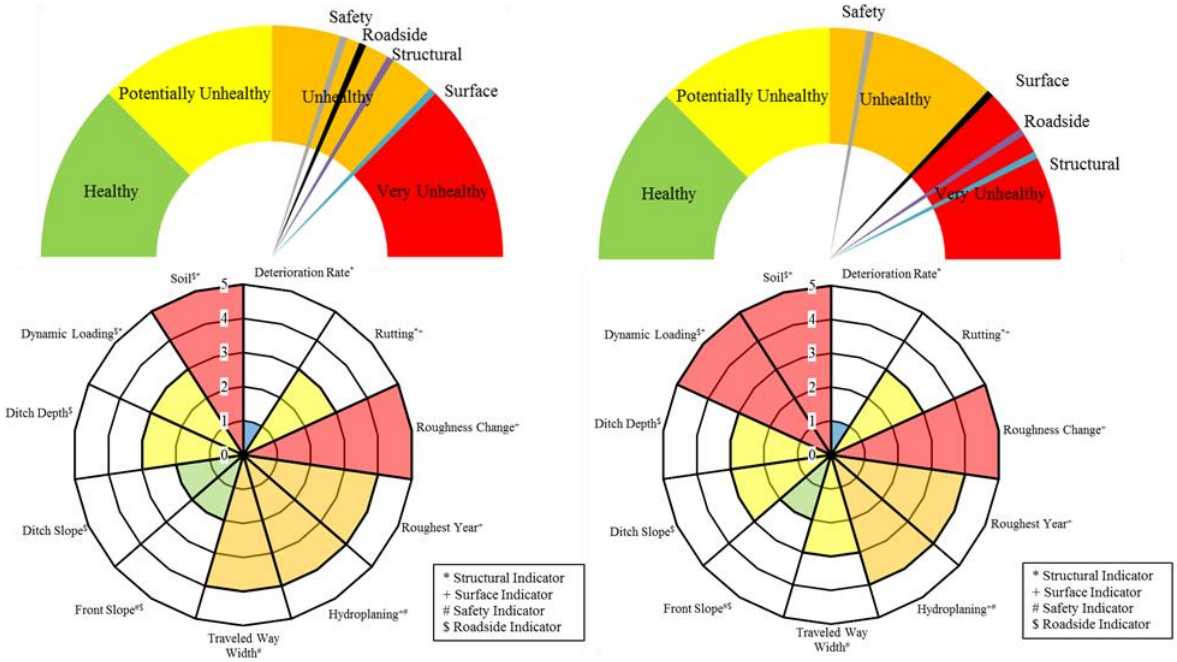

Fig. 61. FM 1696 section 647 and 647.5 diagnoses

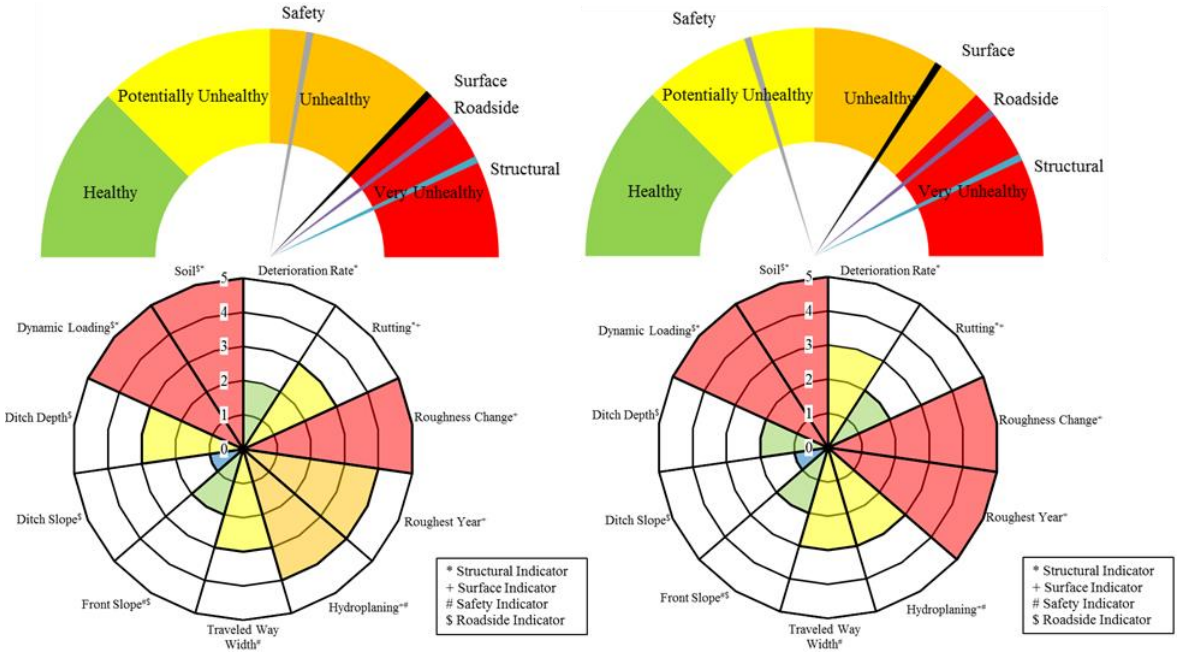

Fig. 62. FM 1696 section 649 to 649.5 diagnoses

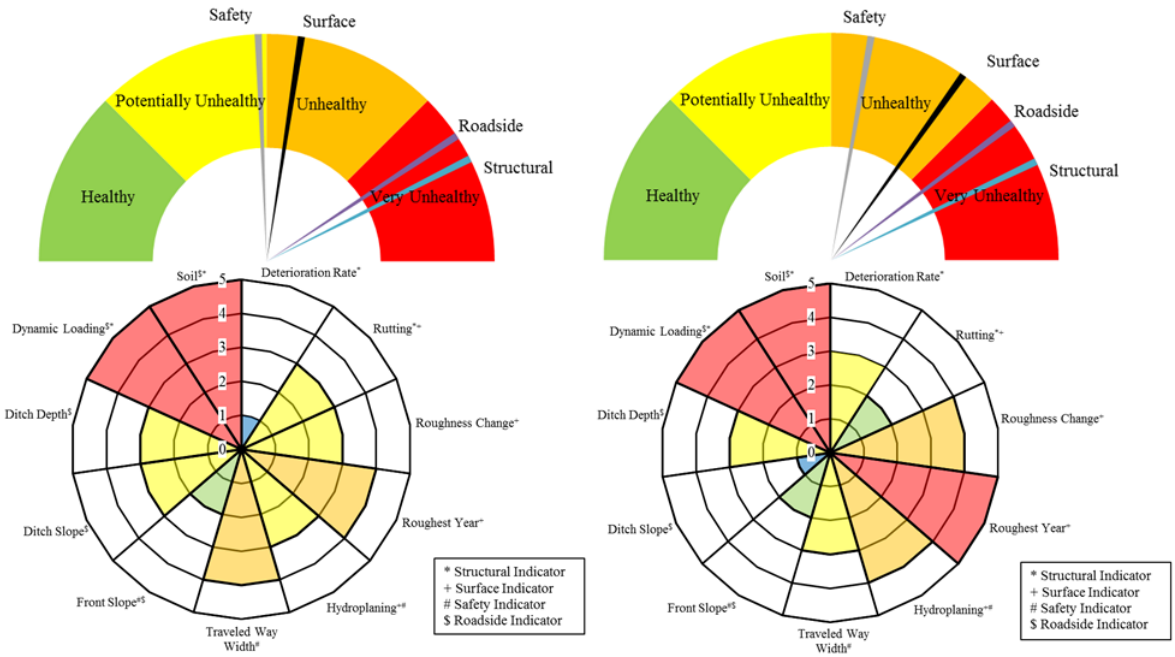

Fig. 63. FM 1696 section 650 to 650.5 diagnoses

The section by section analysis and visual aid representation was also done for the FM 908 project. Fig. 64, Fig. 65, and Fig. 66 display the diagnoses for each section within the FM 908 project. Each figure displays the system diagnoses for a section on the left and the activated indicator data on the right.

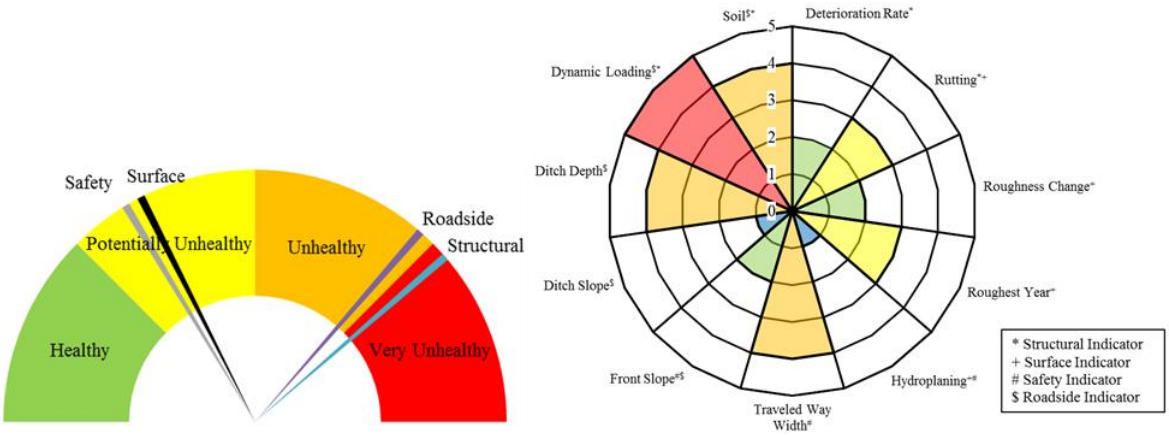

Fig. 64. FM 901 section 581 diagnosis

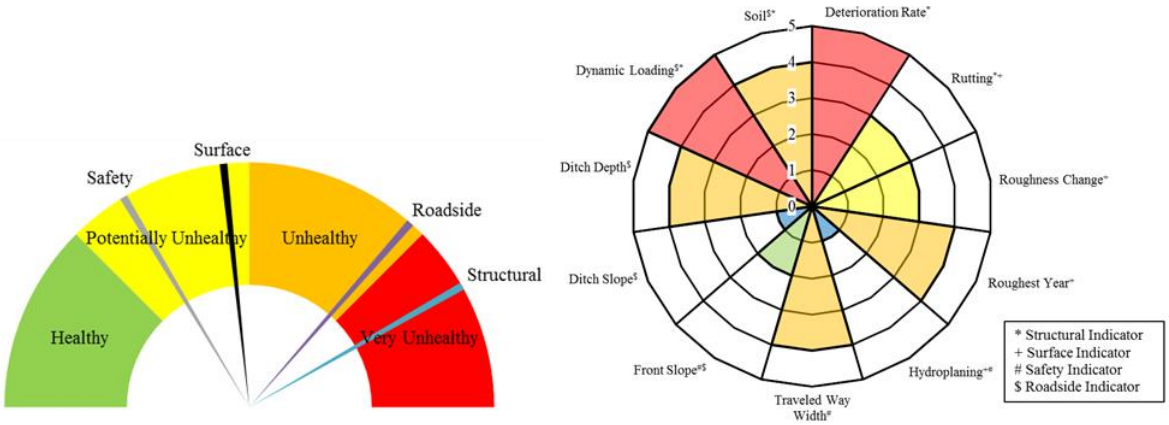

Fig. 65. FM 908 section 581.5 diagnosis

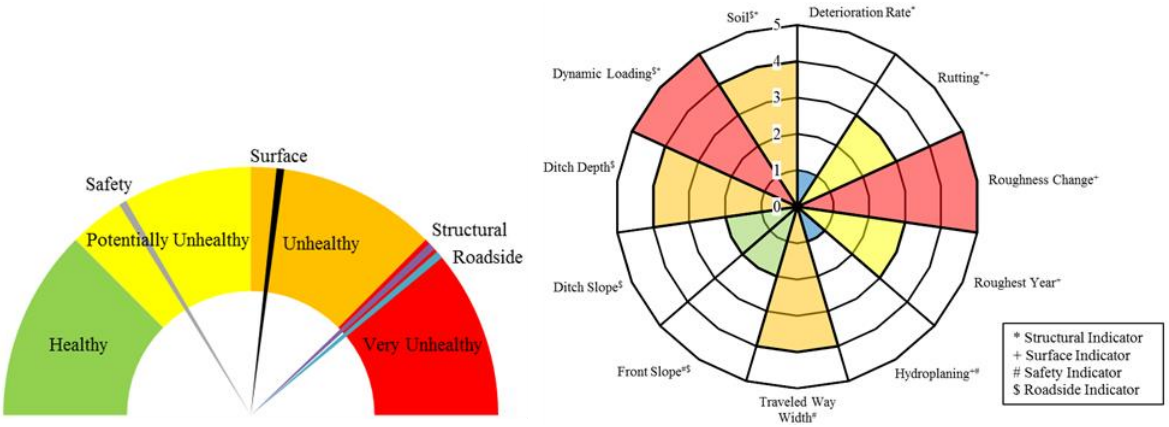

Fig. 66. FM 908 section 582 diagnosis

APPENDIX D

OTHER PROJECTS' DIAGNOSTIC VISUAL AIDS

The following diagnostic graphs provide the visual aid information associated with project diagnostics discussed in the Application of the Diagnostic Method chapter. The graphs are presented in the order in which the projects were discussed. The gauge charts include overall project diagnosis and each system diagnosis for each project.

D.1 OSR PART 1 DIAGNOSTIC GAUGE CHARTS

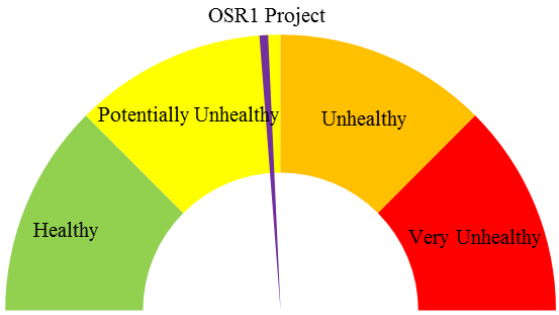

Fig. 67. OSR part 1 project diagnosis

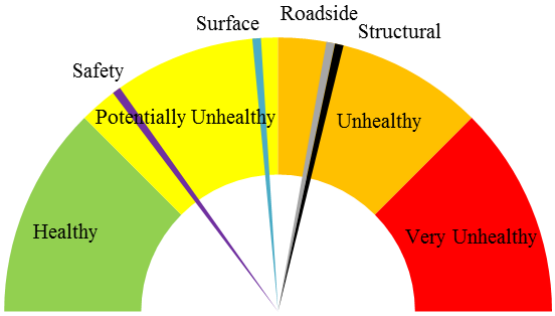

Fig. 68. OSR part 1 system diagnoses

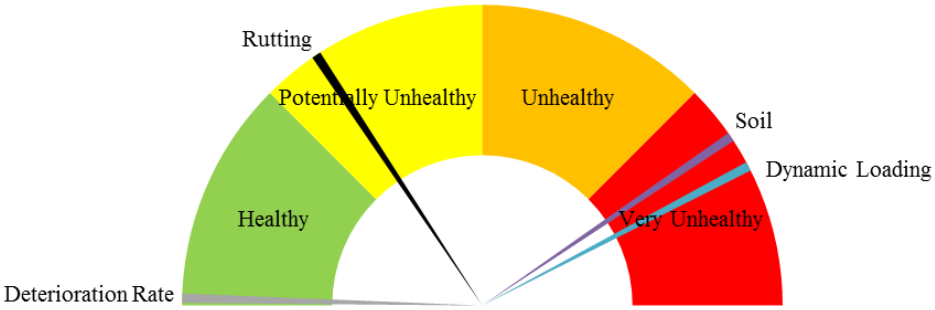

Fig. 69. OSR part 1 structural system diagnosis

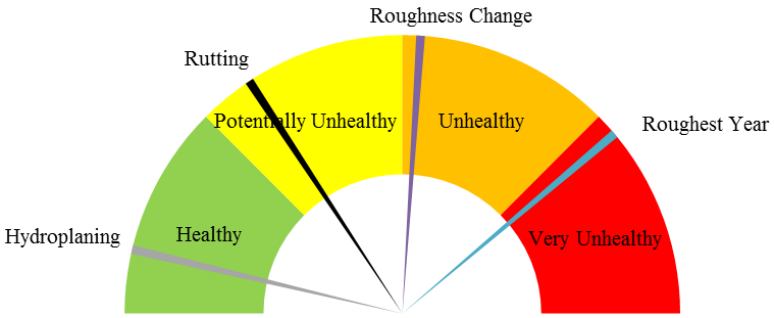

Fig. 70. OSR part 1 surface system diagnosis

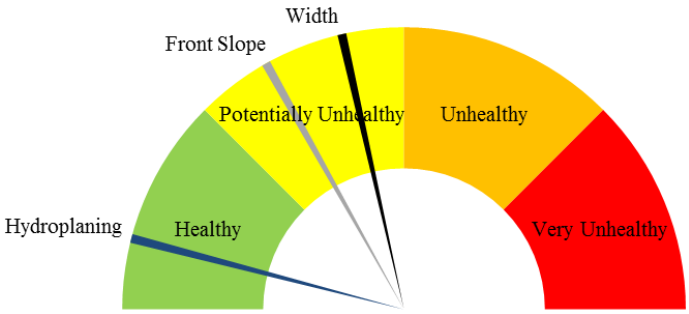

Fig. 71. OSR Part 1 safety system diagnosis

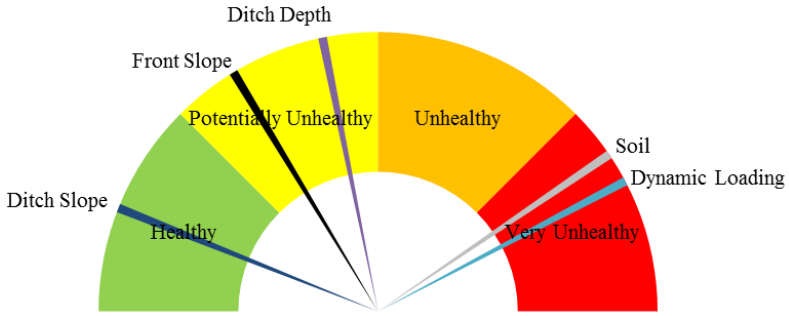

Fig. 72. OSR part 1 roadside diagnosis

D.2 OSR PART 2 DIAGNOSTIC GAUGE CHARTS

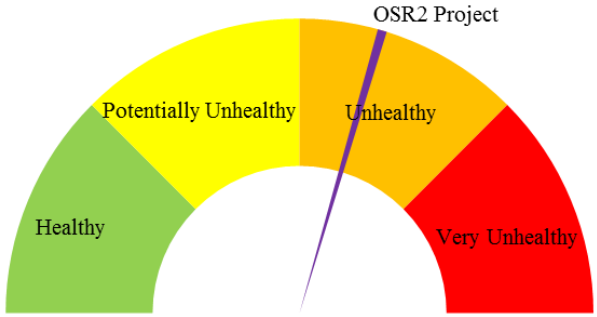

Fig. 73. OSR part 2 project diagnosis

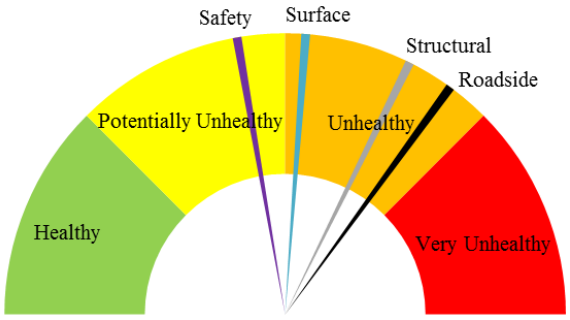

Fig. 74. OSR part 2 systems diagnoses

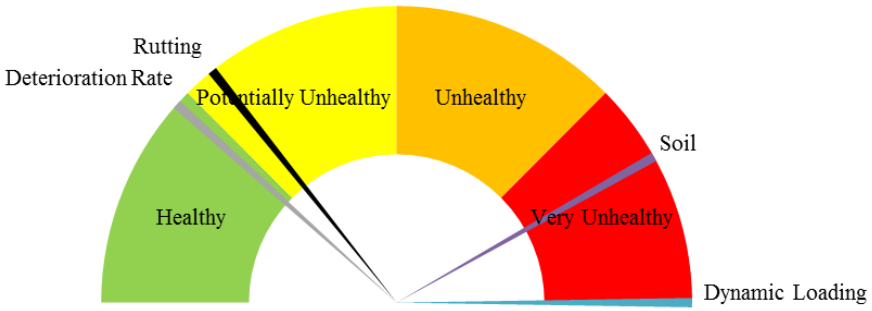

Fig. 75. OSR part 2 structural diagnosis

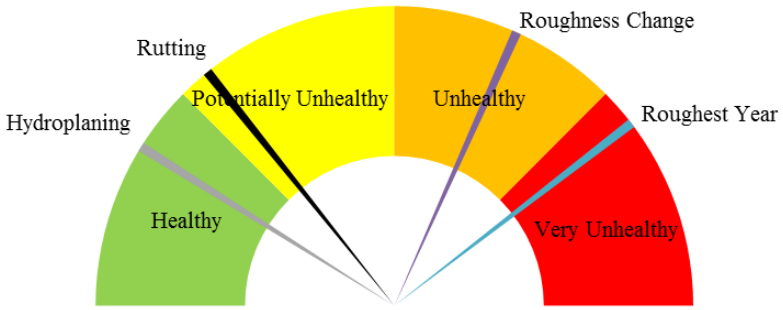

Fig. 76. OSR part 2 surface diagnosis

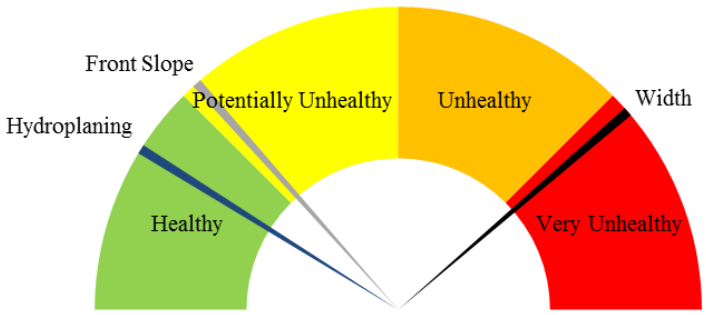

Fig. 77. OSR part 2 safety diagnosis

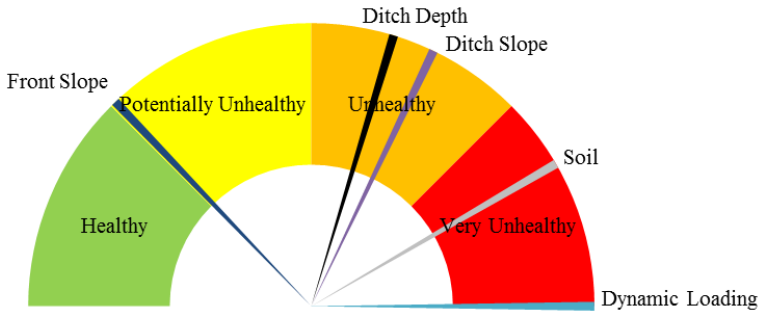

Fig. 78. OSR part 2 roadside diagnosis

D.3 FM 50 DIAGNOSTIC GAUGE CHARTS

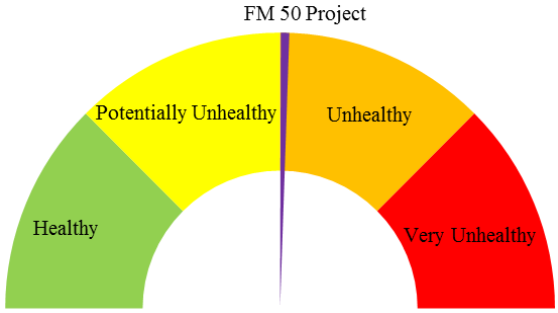

Fig.79. FM 50 project diagnosis

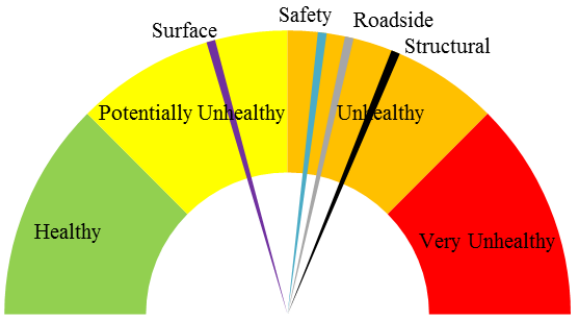

Fig. 80. FM 50 systems diagnoses

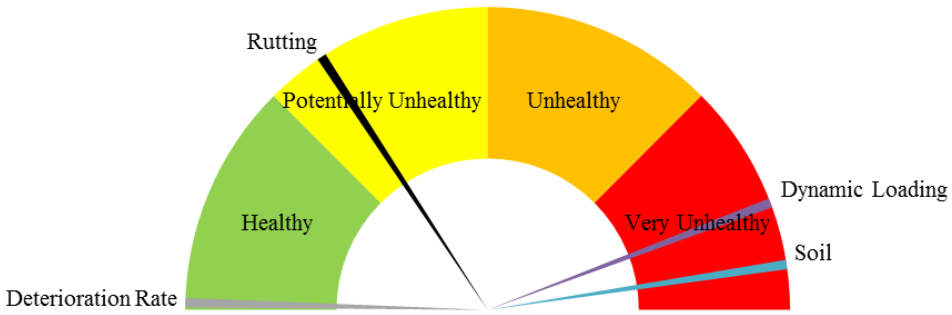

Fig. 81. FM 50 structural diagnosis

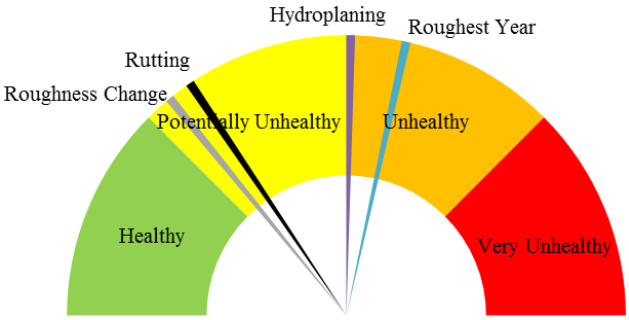

Fig. 82. FM 50 surface diagnosis

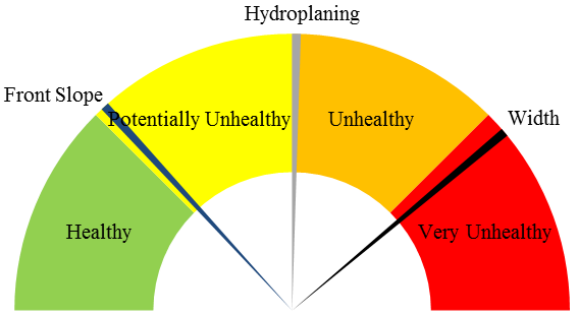

Fig. 83. FM 50 safety system diagnosis

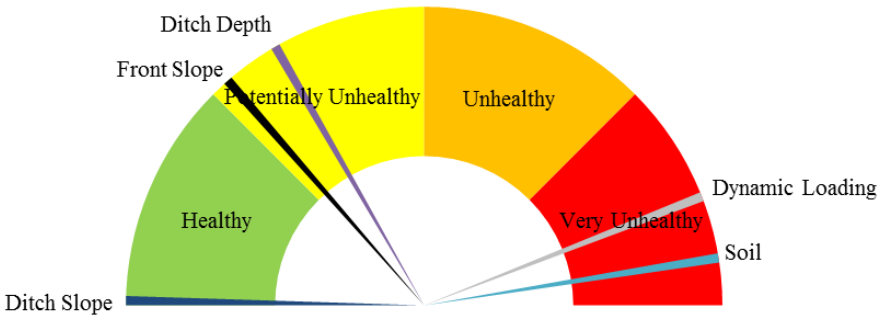

Fig. 84. FM 50 roadside system diagnosis

D.4 FM 1844 DIAGNOSTIC GAUGE CHARTS

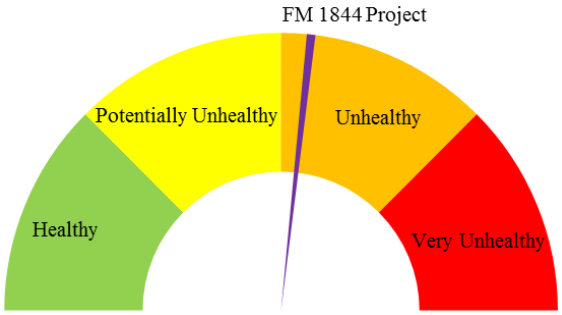

Fig. 85. FM 1844 project diagnosis

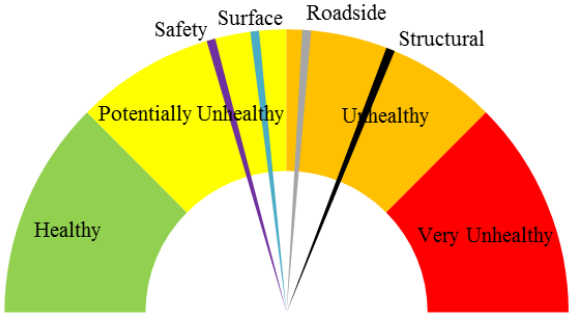

Fig. 86. FM 1844 systems diagnoses

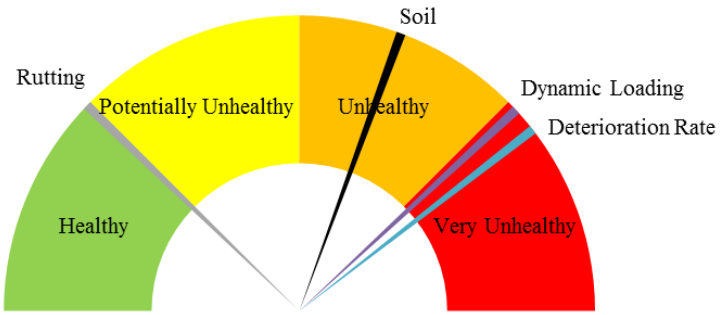

Fig. 87. FM 1844 structural system diagnosis

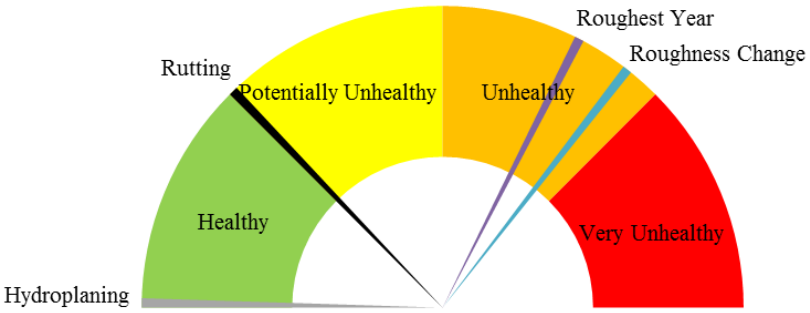

Fig. 88. FM 1844 surface system diagnosis

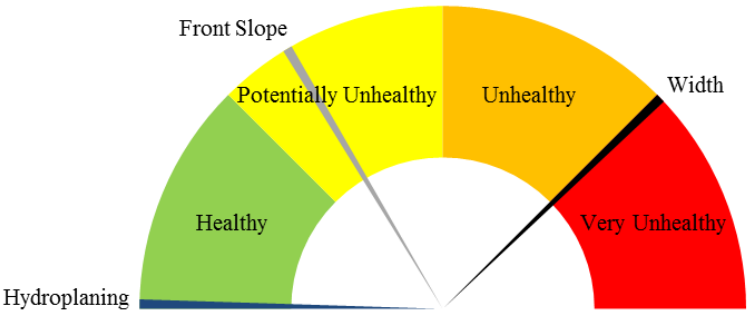

Fig. 89. FM 1844 safety system diagnosis

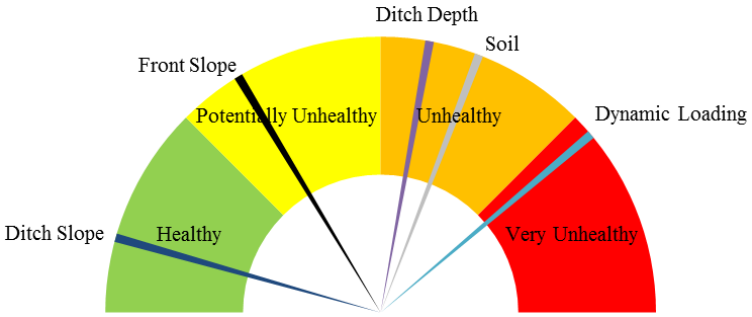

Fig. 90. FM 1844 roadside system diagnosis

D.5 FM 2661 DIAGNOSTIC GAUGE CHARTS

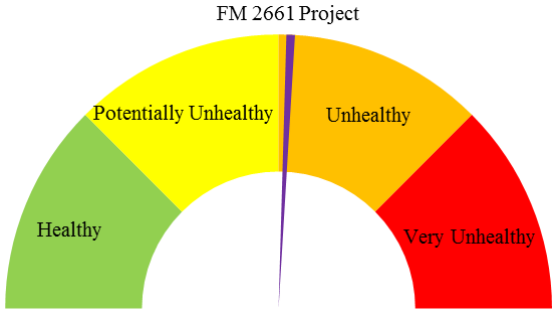

Fig. 91. FM 2661 project diagnosis

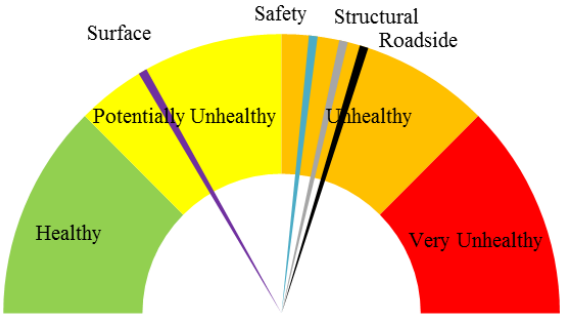

Fig. 92. FM 2661 systems diagnoses

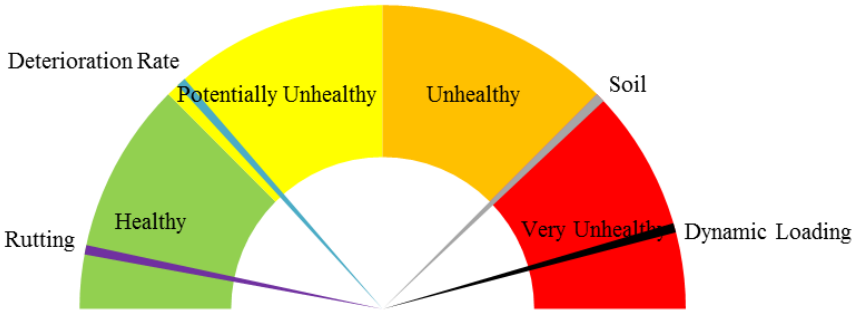

Fig. 93. FM 2661 structural system diagnosis

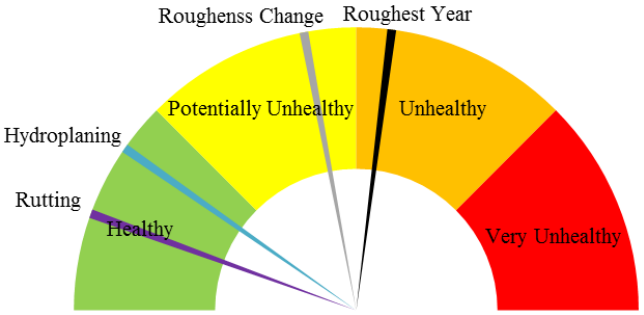

Fig. 94. FM 2661 surface system diagnosis

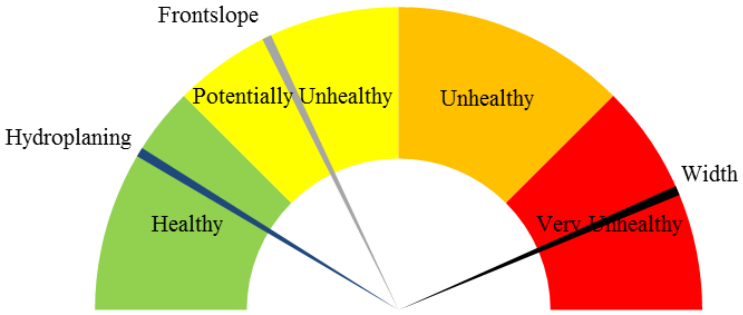

Fig. 95. FM 2661 safety system diagnosis

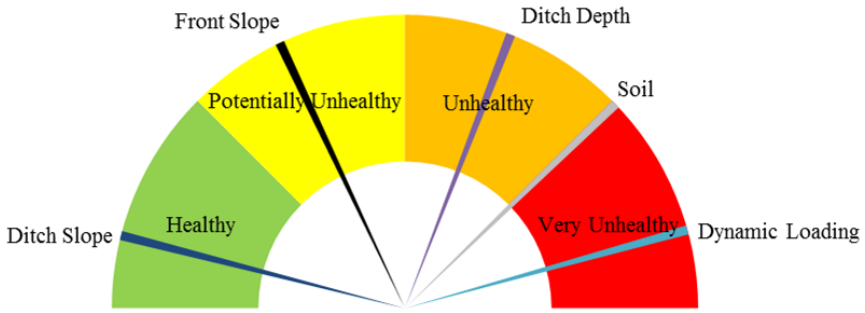

Fig. 96. FM 2661 roadside system diagnosis

D.6 FM 2054 DIAGNOSTIC GAUGE CHARTS

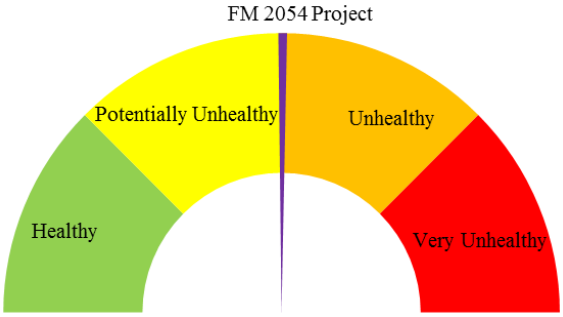

Fig. 97. FM 2054 project diagnosis

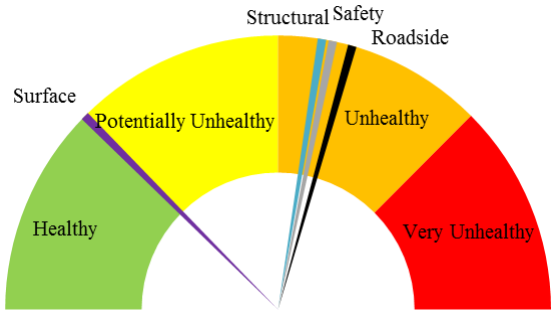

Fig. 98. FM 2054 system diagnoses

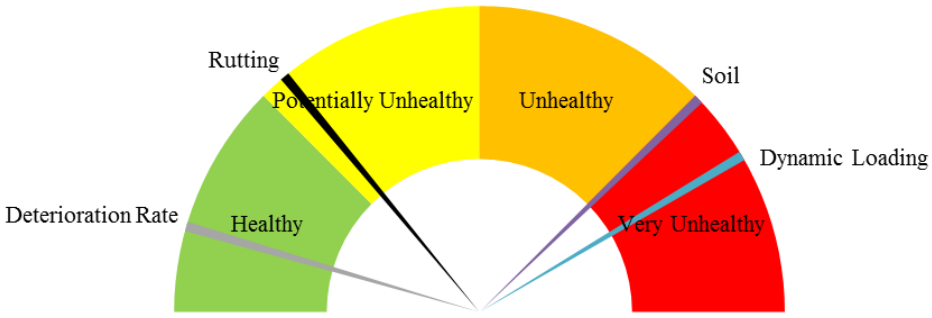

Fig. 99. FM 2054 structural system diagnosis

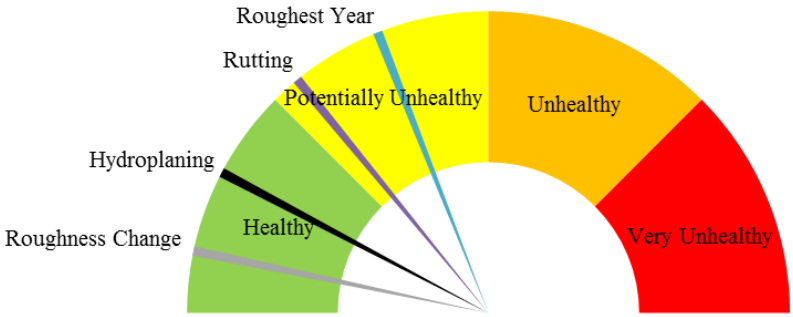

Fig. 100. FM 2054 surface system diagnosis

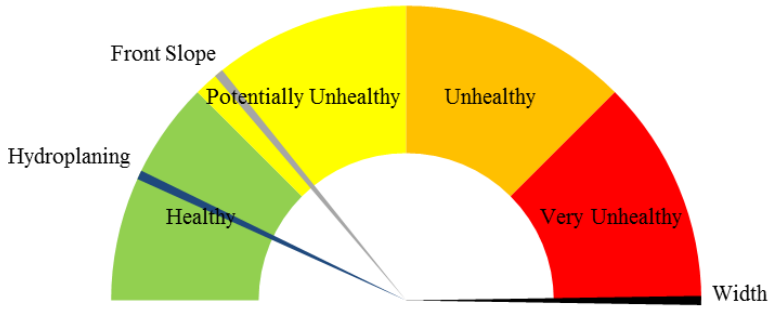

Fig. 101. FM 2054 safety system diagnosis

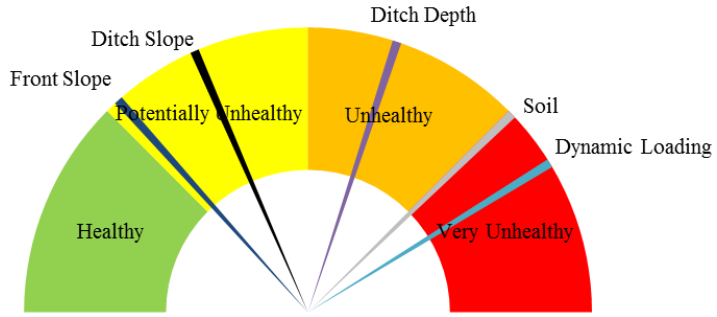

Fig. 102. FM 2054 roadside system diagnosis

D.7 RM 690 DIAGNOSTIC GAUGE CHARTS

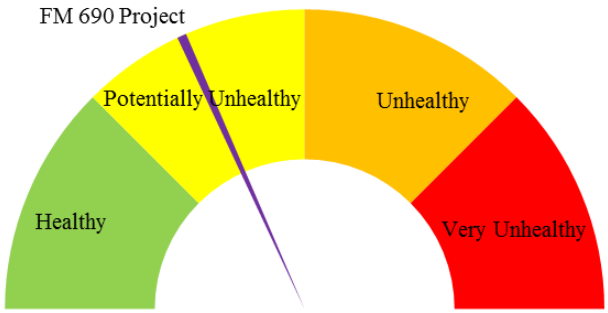

Fig. 103. FM 690 project diagnosis

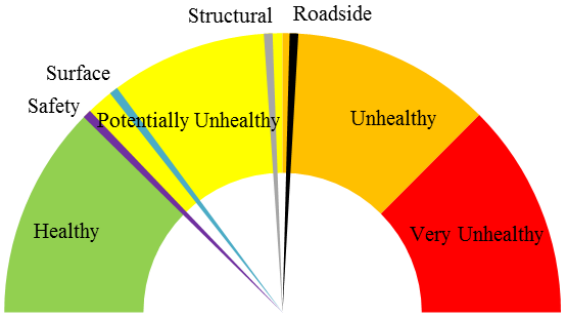

Fig. 104. FM 690 systems diagnoses

Fig. 105. FM 690 structural system diagnosis

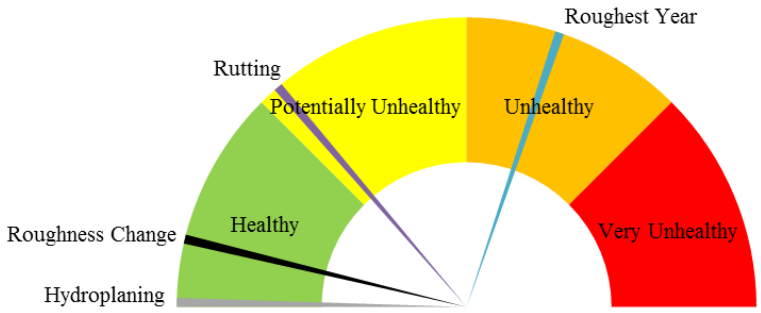

Fig. 106. FM 690 surface system diagnosis

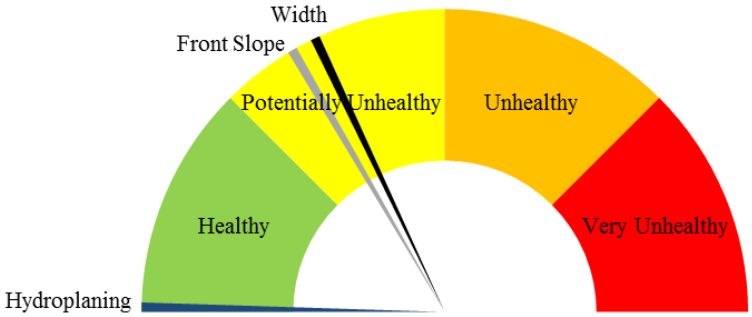

Fig. 107. FM 690 safety system diagnosis

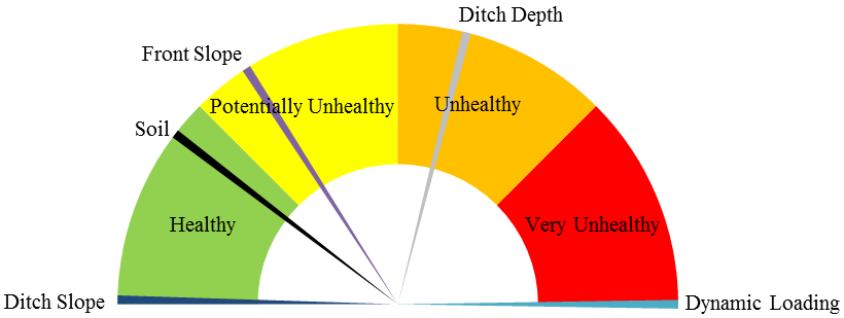

Fig. 108. FM 690 roadside system diagnosis

D.8 SH 138 DIAGNOSTIC GAUGE CHARTS

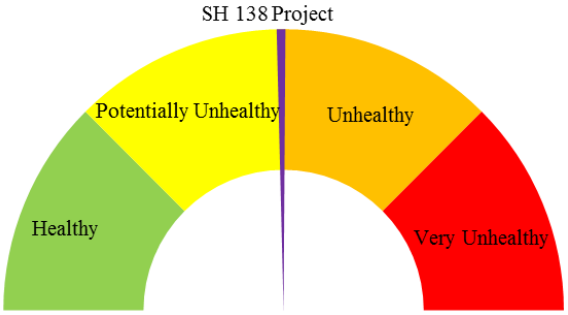

Fig. 109. SH 138 project diagnosis

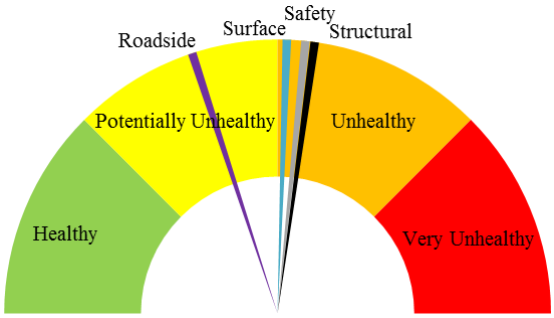

Fig. 110. SH 138 systems diagnoses

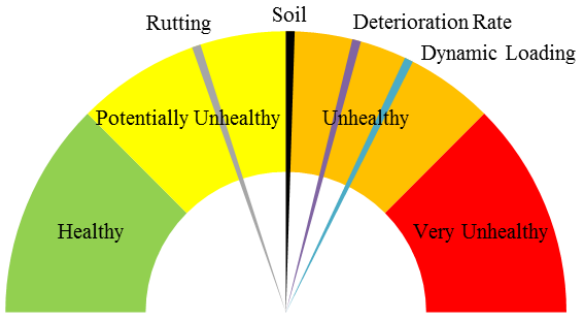

Fig. 111. SH 138 structural system diagnosis

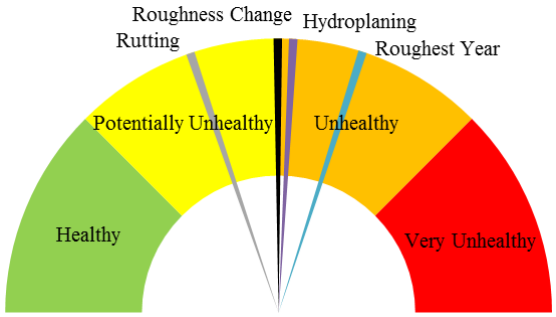

Fig. 112. SH 138 surface system diagnosis

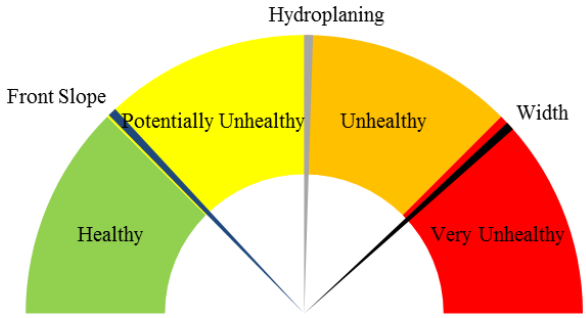

Fig. 113. SH 138 safety system diagnosis

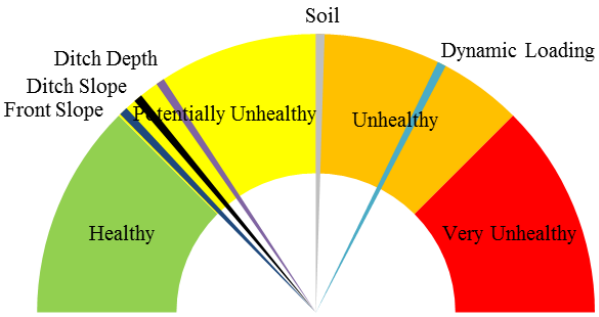

Fig. 114. SH 138 roadside system diagnosis